UNIVERSITY OF OKLAHOMA

GRADUATE COLLEGE

APPLICATION OF A NEW YIELD STRENGTH ACQUISITION METHOD TO THE CALCULATION OF COLLAPSE PRESSURE

A THESIS

SUBMITTED TO THE GRADUATE FACULTY

in partial fulfillment of the requirements for the

Degree of

MASTER OF SCIENCE

By

ZACHARY COLLINS
Norman, Oklahoma
2018

APPLICATION OF A NEW YIELD STRENGTH ACQUISITION METHOD TO THE CALCULATION OF COLLAPSE PRESSURE

A THESIS APPROVED FOR THE
MEWBOURNE SCHOOL OF PETROLEUM AND GEOLOGICAL ENGINEERING

BY

_____
Dr. Catalin Teodoriu, Chair

_____
Dr. Saeed Salehi

_____
Dr. Hamidreza Karami Mirazizi

For Stacey

Acknowledgements

I would like to thank Dr. Teodoriu for his support and good humor. He has solutions to every problem and makes the work fun. I would like to thank Dr. Salehi and Dr. Karami for their help and guidance in the classroom and throughout my OU career. I also want to thank Jeff McCaskill for all his help at the WCTC. Without him, I'm sure that facility would grind to a halt. Finally, I would like to thank my wife and family for their unwavering support. I know this has been a long time coming.

Table of Contents

Acknowledgements iv

List of Tables viii

List of Figures ix

Abstract xiv

Chapter 1: Introduction 1

1.1 Motivation and Problem Statement 1

1.2 Objectives 3

1.3 Organization of Thesis 3

Chapter 2: Pipe Manufacture and Testing Procedures 4

2.1 Pipe Manufacture 4

2.1.1 Seamless Pipe 4

2.1.2 Electrically Welded Pipe 4

2.2 Testing Procedures 6

2.2.1 Yield Strength Testing 6

2.2.2 Collapse Resistance Testing 8

Chapter 3: Classic API Collapse Equations 10

3.1 Elastic Collapse 10

3.2 Yield Strength Collapse 11

3.3 Plastic Collapse 11

3.4 Transition Collapse 12

3.5 Delineation of Collapse Mode 13

3.5.1 Yield Strength Collapse Region 13

3.5.2 Plastic Collapse Region 14
3.5.3 Transition Collapse Region 15
3.5.4 Elastic Collapse Region 16
3.6 Accounting for Axial Load and Internal Pressure 18
Chapter 4: Equations Beyond API 19
4.1 Shortcomings of API 5C3 Equations 19
4.2 New Collapse Equations 24
4.2.1 Yield Strength Collapse 24
4.2.2 Elastic Collapse 29
4.2.3 Combination Elastic/Plastic Collapse 31
4.2.4 Design Equations 35
4.2.5 Accounting for Axial Load and Internal Pressure 40
4.3 Performance of New Equations 41
4.3.1 Comparison of Models to API 41
4.3.2 Model to Model Comparison 54
Chapter 5: Yield Strength Acquisition Method 59
5.1 Experimental Setup 61
5.2 Test Procedure 70
5.3 Development of the Yield Strength Equation 72
5.4 Results 77
5.4.1 Finding Yield Strength Empirically 77
5.4.2 Comparing Empirical Method to Measured Data 96
5.4.3 Nominal vs. Empirical Yield Strength for K&T Collapse 98

Chapter 6: Conclusion and Recommendations 105

6.1 Conclusion 105

6.2 Recommendations 106

Nomenclature 107

References 112

List of Tables

Table 2.1: Specifications for strip and round bar specimens (API 5CT 2006) 8

Table 3.1: Yield collapse pressure formula range (API 5C3 1994) 14

Table 3.2: Plastic collapse pressure formula range (API 5C3 1994)..... 15

Table 3.3: Transition collapse pressure formula range (API 5C3 1994)..... 16

Table 4.1: Pipe tensile and hardness requirements (API 5CT 2006) 20

Table 4.2: Collapse mode (after Klever and Tamano 2006) 38

Table 4.3: Constants for ovality correction (after Ju et al. 1998)..... 40

Table 4.4: Down-rating factors (after Adams et al. 1998) 50

Table 4.5: Model comparison with full-scale test data (Abbassian and Parfitt 1995).... 58

Table 4.6: Model comparison of predictive accuracies (after Adams et al. 1998)..... 58

Table 5.1: Yield strength deviation from nominal, Drilling Engineering Association data set (Brechan et al. 2018)..... 59

Table 5.2: Yield strength deviation from nominal, ISO HRS data set (Brechan et al. 2018)..... 59

Table 5.3: Yield strength deviation from nominal, ISO CRS (Brechan et al. 2018)..... 60

Table 5.4: Resulting API grade for samples with MTR..... 96

Table 5.5: Empirical yield strength vs. API nominal yield strength vs. MTR yield strength 97

Table 5.6: K&T collapse pressures for nominal and empirical yield strengths 99

List of Figures

Figure 2.1: Seamless pipe manufacturing process (Bourgoyne et al. 1986) 4

Figure 2.2: Production process for seamless and welded pipes (Brechan et al. 2018)..... 5

Figure 2.3: Full-section, strip, and round bar test specimen (API 5CT 2006) 7

Figure 2.4: “Autoclave” type test frame (Teodoriu and Holzman 2010) 9

Figure 2.5: “Open” type test frame (Teodoriu and Holzman 2010)..... 9

Figure 3.1: Collapse curves for N-80 (top), J-55 vs. N-80 vs. P-110 (bottom) (Staelens et al. 2012) 17

Figure 4.1: Definition of normalization factor r_n (Ju et al 1998)..... 21

Figure 4.2: Original API database observed collapse pressures normalized by API calculated collapse pressures (Ju et al. 1998) 22

Figure 4.3: Post-1963 database observed collapse pressures normalized by API calculated collapse pressures (Ju et al. 1998) 22

Figure 4.4: Accuracy of Eq. 4.5 and Eq. 4.6 (Klever and Tamano 2006, modified) 27

Figure 4.5: Transition from initial to through-wall yield (Sun 2010) 28

Figure 4.6: Eq. 4.15 comparison given different c values (Klever and Tamano 2006, modified) 31

Figure 4.7: Elasto-plastic collapse pressure (Kuriyama and Mimaki 1994) 32

Figure 4.8: Elastic ovalization (Abbassian and Parfitt 1995)..... 33

Figure 4.9: 4-hinge mechanism (Abbassian and Parfitt 1995) 33

Figure 4.10: Elastic ovalization and plastic collapse curves define collapse pressure (Abbassian and Parfitt 1995) 35

Figure 4.11: Stress/strain curve shape and work hardening (Klever and Tamano 2006)37

Figure 4.12: Yield strength collapse equation comparison (Klever and Tamano 2006) 42
Figure 4.13: Elasto-plastic and API collapse pressure comparison (Kuriyama and Mimaki 1994) 42
Figure 4.14: Collapse pressure margins normalized by ideal pipe (Kuriyama and Mimaki 1994) 43
Figure 4.15: Effect of original ovality (a), yield strength (b), and D/t value (c) on collapse pressure (Abbassian and Parfitt 1995)..... 44
Figure 4.16: 4-hinge model versus test data (Abbassian and Parfitt 1995, modified) ... 45
Figure 4.17: API collapse prediction versus test data (Abbassian and Parfitt 1995, modified) 45
Figure 4.18: Observed collapse data normalized by the design equation (Ju et al. 1998) 46
Figure 4.19: Observed collapse data normalized by the resistance equation (Ju et al. 1998)..... 46
Figure 4.20: Probability of failure for four different pipe grades using API equations (Ju et al. 1998) 47
Figure 4.21: Probability of failure for four different pipe grades using the design equation (Ju et al. 1998) 48
Figure 4.22: Value of DF given desired failure probability, K-55 (Ju et al. 1998)..... 48
Figure 4.23: Value of DF given desired failure probability, L-80 (Ju et al. 1998) 49
Figure 4.24: Comparison of Adams et al. model and API equations (Adams et al. 1998) 49
Figure 4.25: FEA compared with model curves (Klever and Tamano 2006) 50

Figure 4.26: Effect of work hardening on collapse resistance (Klever and Tamano 2006) 51
Figure 4.27: Effect of effective axial load on pressure differential gradient (Klever and Tamano 2006)..... 52
Figure 4.28: Effect of effective axial load on collapse pressure differential (Klever and Tamano 2006)..... 53
Figure 4.29: Comparison of Sun, API, and Tamano et al. yield equations (Sun 2010) . 54
Figure 4.30: Comparison of elasto-plastic collapse with theoretical elastic, API yield, and Tamano et al. yield (Kuriyama and Mimaki 1994) 55
Figure 4.31: Comparison of four collapse pressure models for L-80 pipe (Klever and Tamano 2006)..... 56
Figure 4.32: Actual versus predicted strength for six models (Adams et al. 1998) 57
Figure 5.1: Actual/Nominal yield strength, DEA data set (Brechan et al. 2018)..... 60
Figure 5.2: Actual/nominal yield strength, ISO data set (Brechan et al. 2018) 60
Figure 5.3: Hydraulic shop press..... 62
Figure 5.4: Steel test apparatus..... 62
Figure 5.5: Steel test apparatus 3D model..... 63
Figure 5.6: Omega force gauge 63
Figure 5.7: Omega force gauge bolted to aluminum plate 64
Figure 5.8: Omega force gauge mounted to test apparatus 64
Figure 5.9: Holes drilled in hydraulic press 65
Figure 5.10: Test apparatus with alignment bars..... 65
Figure 5.11: Displacement gauge and cross bar..... 66

Figure 5.12: Scissor jack on top of the press 66
Figure 5.13: Chains attaching top plate to scissor jack 67
Figure 5.14: Band saw cutting pipe 68
Figure 5.15: Pipe divided into eight equal sections 69
Figure 5.16: Pipe divided into eight equal sections and marked 69
Figure 5.17: Using Positector ultrasonic tool to measure wall thickness 70
Figure 5.18: Pipe loaded into test apparatus 71
Figure 5.19: Ensure correct pipe orientation 71
Figure 5.20: Pump layout 72
Figure 5.21: Forces occurring at the inner and outer pipe wall 73
Figure 5.22: Cross-sectional view, pipe wall in tension (green) and compression (red) 74
Figure 5.23: Moment of F about point p 74
Figure 5.24: Forces associated with pipe crush 75
Figure 5.25: 1.5” force vs. displacement curves 80
Figure 5.26: 2 3/8” force vs. displacement curves 81
Figure 5.27: 2 7/8” force vs. displacement curves 82
Figure 5.28: 3” force vs. displacement curves 83
Figure 5.29: 3.5” force vs. displacement curves 84
Figure 5.30: New 3.5” force vs. displacement curves 85
Figure 5.31: Aluminum 3.5” force vs. displacement curves 86
Figure 5.32: 5.5” force vs. displacement curves 87
Figure 5.33: 1.5” stress vs. displacement curves 88
Figure 5.34: 2 3/8” stress vs. displacement curves 89

Figure 5.35: 2 7/8” stress vs. displacement curves 90
Figure 5.36: 3” stress vs. displacement curves 91
Figure 5.37: 3.5” stress vs. displacement curves 92
Figure 5.38: New 3.5” stress vs. displacement curves 93
Figure 5.39: Aluminum 3.5” stress vs. displacement curves 94
Figure 5.40: 5.5” stress vs. displacement curves 95
Figure 5.41: K&T collapse pressures for nominal and empirical yield strengths, grade T-95 100
Figure 5.42: K&T collapse pressures for nominal and empirical yield strengths, grade J-55 101
Figure 5.43: K&T collapse pressures for nominal and empirical yield strengths, grade H-40 102
Figure 5.44: API collapse with nominal yield strength versus K&T collapse with empirical yield strength 104

Abstract

The accuracy of a casing collapse prediction is critical to a successful casing design program. This is especially true today as the likelihood of HPHT reservoirs and difficult conditions downhole has become increasingly more prevalent. To account for these conditions, more up to date, accurate collapse resistance equations and true yield strengths should be used.

The original API collapse equations were adopted in the 1960s and reflect the quality of the pipes produced. Since that time, improvements in manufacturing procedures have increased pipe quality and improved tolerances of material properties. It is necessary to adopt new collapse resistance equations that reflect this improvement in overall quality.

Many new collapse equations have been proposed since the API equations were originally adopted. A review of a selection of these equations compares them to each other, the API equations and real collapse data. As a result, the Klever and Tamano model was shown to most accurately predict the collapse resistance of real pipes.

With a new more accurate collapse equation in place, the next largest factor in determining true pipe collapse depends on knowing the real yield strength of the pipe. The expense of testing has resulted in infrequent testing and, therefore, inherent uncertainty in the material properties of any given pipe. A new method of yield strength acquisition simplifies the testing procedure in hopes of encouraging an increase in testing frequency. Additionally, the new method finds yield strength in the hoop direction instead of the axial direction, which is directly related to collapse.

The new acquisition method was compared against the tested yield strengths given by the pipe manufacturer. Testing was performed on a variety of outer diameters, wall thicknesses, and pipe grades. The new method proved to be very accurate, yielding just a 0.5% variation from the mean yield strength values.

Chapter 1: Introduction

1.1 Motivation and Problem Statement

When making the decision of what components to put into a well, it is of utmost importance to have accurate, reliable information concerning the properties of those components. This is especially true of the collapse resistance of casing. Collapse resistance can affect the success of a drilling program as well as the economics of the design due to cost variations in casing grades and weights. The relevance of these issues is on the rise given the increasing prevalence and likelihood of HPHT conditions downhole in many of today's new wells (Teodoriu and Holzman 2010).

A successful and economical casing design must make use of a casing collapse equation to predict the collapse pressure of the selected tubulars to ensure that they will survive the expected downhole pressures. The accuracy of the collapse pressure prediction depends upon the equation selected and the value of yield strength used in that equation. Numerous equations exist for the different modes of collapse that may occur. Collapse modes may include yield strength collapse, plastic collapse, transition collapse, and elastic collapse. The mode of collapse experienced by any one pipe is dependent on the ratio of outer diameter to wall thickness (D/t) and pipe grade (J-55, N-80, P-110, etc.).

The best-known collapse equations are the widely used American Petroleum Institute (API) equations originally adopted at the 1968 API Standardization Conference. These equations, for better or worse, are still widely used in the industry today. This is hardly a surprise as these equations appear in the classic textbook,

Applied Drilling Engineering, by Bourgoyne et al. (1986), which serves as the basis of many introductory drilling engineering courses across the world.

The adoption of these equations is tied to the quality of tubulars produced more than fifty years ago. Since then, advances in manufacturing processes have tightened production tolerances and resulted in increases in both burst and collapse resistance. This increase in resistance means that for pipes with relatively large D/t ratios (>18), the API equations result in an excessively high safety margin leading to "over-engineered" designs that are more costly than necessary (Adams et al. 1998). On the other hand, the API equations tend to over-predict the collapse resistance of pipes with smaller D/t ratios (<18). This over-estimation of collapse resistance could have catastrophic consequences in a vital portion of the casing design such as the production liner (Ju et al. 1998).

Improved collapse resistance predictions can be had through the use of more up to date formulae. Additionally, using the true yield strength of the pipe will increase accuracy of predictions. In API equations, nominal yield strength based on casing grade is used for calculations, but pipes within any one particular grade will have a range of yield strengths. Also, API standard yield strength testing practice utilizes a specimen removed from a pipe and tested axially. However, collapse of the tubular is primarily influenced by the material properties in the hoop direction (Ju et al. 1998). The manufacturing process results in inherent anisotropy between axial and hoop material properties and should be taken into account.

This thesis aims to distill the currently available collapse pressure resistance formulae to determine best practice and propose a novel method for the acquisition of yield strength in the hoop direction.

1.2 Objectives

1. Explore pipe manufacturing processes and testing procedures, noting changes with time, to find areas for improvement
2. Review and compare traditional API collapse pressure equations to newly developed equations to reach a conclusion on best practice
3. Develop a new method for experimental determination of tubular yield strength in the hoop direction
4. Apply the new testing method to the best performing collapse pressure formula to create an improved system for predicting tubular collapse resistance

1.3 Organization of Thesis

The first chapter lays out motivation behind this study as well as the objectives used to fully explore the problem. The second chapter presents some background on pipe manufacturing and its advancements in the last fifty years as well as the material testing procedures currently used by the API. Chapter three explores the history and development of the classical API collapse equations. The fourth chapter reviews the shortcomings of the API equations and outlines a few new equations that have been presented in the last fifty years, as well as their performance. Chapter five details the development of the new yield strength acquisition method including experimental setup,

equation derivation, and performance. Chapter six completes the thesis with conclusions of the work completed as well as recommendations for future work and improvements.

Chapter 2: Pipe Manufacture and Testing Procedures

2.1 Pipe Manufacture

The two main types of tubulars manufactured are seamless and electrically welded (EW).

2.1.1 Seamless Pipe

Production of seamless pipe is a four-step process. First, a hot rod of steel called a billet is pierced by a mandrel in a rotary piercing mill. Then the pierced billet is processed through the plug mills where the wall thickness of the pipe is reduced. Reelers then burnish the pipe surfaces and form a more uniform wall thickness. Finally, a sizing mill produces the final pipe dimensions and roundness (Bourgoyne et al. 1986). This process can be seen in **Figure 2.1.**

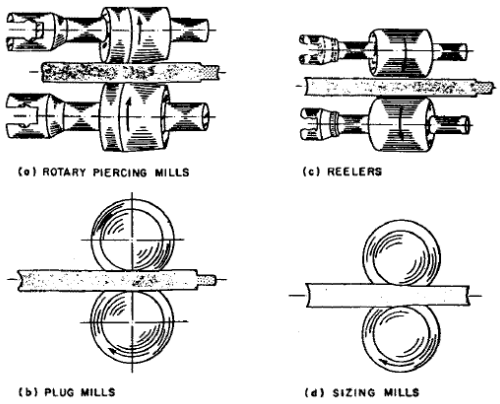

Figure 2.1: Seamless pipe manufacturing process (Bourgoyne et al. 1986)

2.1.2 Electrically Welded Pipe

EW pipe starts as flat sheet stock that is then cut, formed, and the two edges are welded together. The welding process can either be electric resistance welding using an

electrode or electric-flash welding where the two edges are flash heated and then pressed together to form the weld (Bourgoyne et al. 1986). This procedure is sometimes called the UOE process. This means the flat sheet stock is pressed into a “U” shape, formed to an “O” shape, welded, and then “E”xpanded circumferentially (Ju et al. 1998). The electrically welded pipes are then rolled and straightened to ensure uniform sizing.

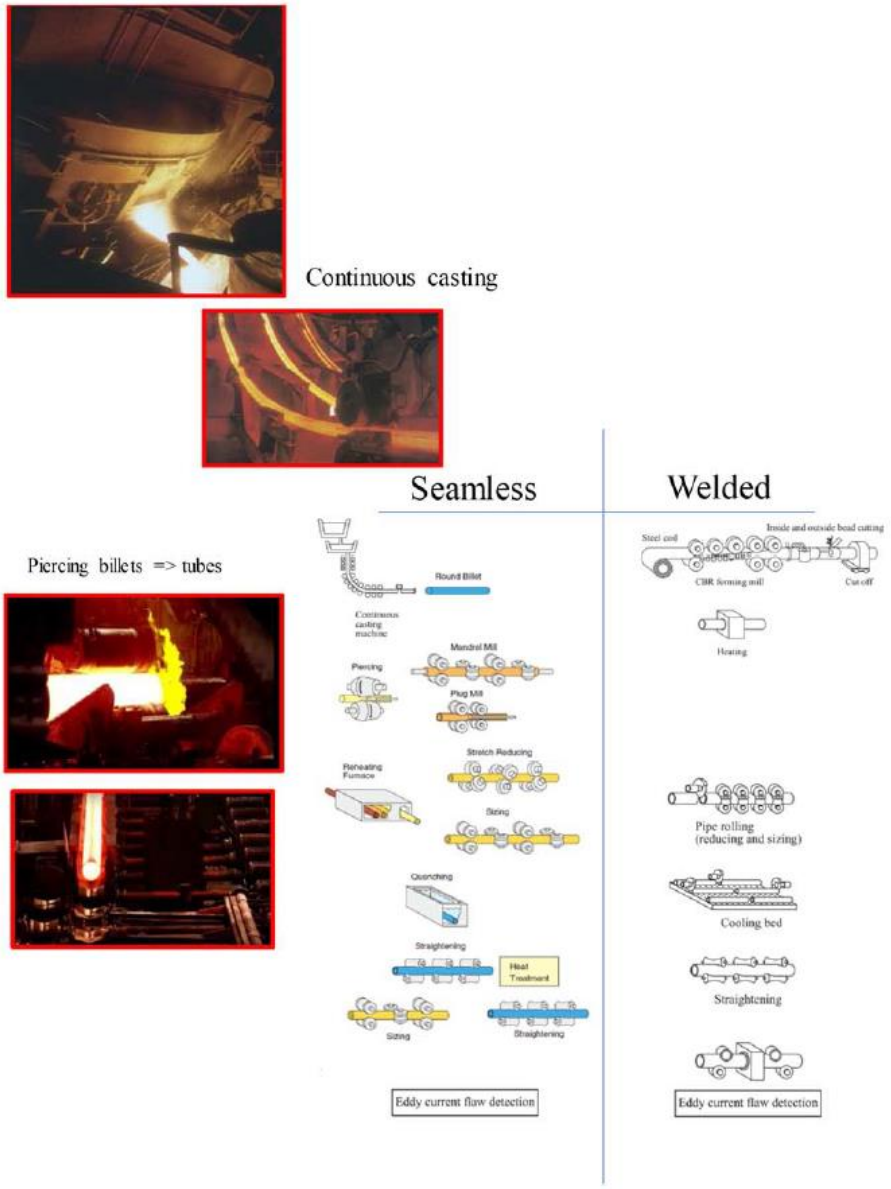

Figure 2.2: Production process for seamless and welded pipes (Brechan et al. 2018)

The increase in burst and collapse resistance in modern tubulars is a result of improvements in manufacturing processes since the adoption of the original API collapse equations in the 1960s. Today, inert gases are used to help achieve the desired chemical composition and grain structure, as well as prevent imperfections. Computer controlled heat processes help ensure consistent metallurgy and the conveyor type "continuous casting" provides a more consistent product than the "batch" processes used previously (Brechan et al. 2018). **Figure 2.2** shows the continuous casting process in the upper right corner, billet piercing for seamless pipe on the left side, and seamless and welded pipe creation side by side on the right side.

2.2 Testing Procedures

2.2.1 Yield Strength Testing

Material testing procedures are published in API 5CT – Specification for Casing and Tubing. According to 5CT, yield strength is defined as the tensile stress required to produce a specified elongation under load. The value of this elongation is specified in Table E.6 in the 5CT specification. For most pipe grades, yield strength is found at 0.5% elongation, while P-110 uses 0.6% elongation and Q-125 uses 0.65% elongation.

The testing frequency can be found in Table E.40 in 5CT. Testing frequency depends on pipe grade and size, and is defined as the number of required tests per lot. A lot is a group of pipes possessing the same properties and the size of the lot varies from 100 to 400. This means testing frequency can vary from 0.25% of pipes in a lot tested on the low side, to 1% of pipes tested in a lot on the high side.

Test specimens can be full-section pieces, strip specimens, or round bar specimens as seen in **Figure 2.3**. The ideal 5CT specimen is the round bar as it has a

uniform shape. **Table 2.1** shows the required specifications for both strip and round bar specimens. Strip specimens for seamless pipes may be taken from any location about the pipe circumference. For welded pipes, the strip specimen must be taken 90° from the weld. Round bar must be taken from the mid wall of the pipe.

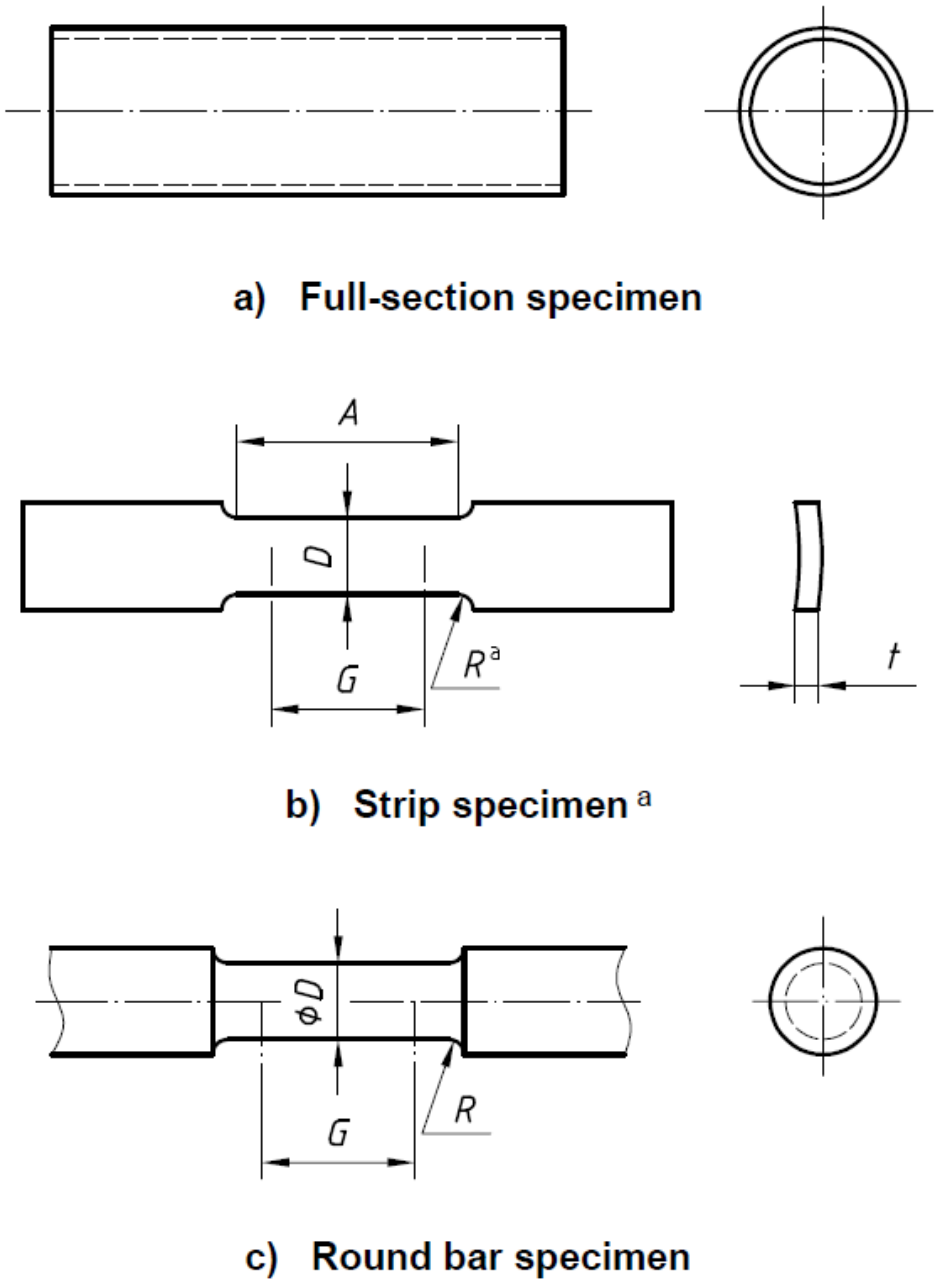

Figure 2.3: Full-section, strip, and round bar test specimen (API 5CT 2006)

Table 2.1: Specifications for strip and round bar specimens (API 5CT 2006)

Dimension	Strip specimen mm (in)	Round bar specimen mm (in)	
		D = 12,7 (0.500)	D = 8,9 (0.350)
Gauge length, G	50,8 ± 0,13 (2.000 ± 0.005)	50,8 ± 0,13 (2.000 ± 0.005)	35,6 ± 0,13 (1.400 ± 0.005)
Diameter or width, D	38,1 (1.500) approx.	12,7 ± 0,25 (0.500 ± 0.010)	8,9 ± 0,18 (0.350 ± 0.007)
Radius of fillet, min., R	25,4 (1.000)	9,5 (0.375)	6,4 (0.250)
Length of reduced section, min., A	57,2 (2.250)	57,2 (2.250)	44,5 (1.750)

2.2.2 Collapse Resistance Testing

The API procedure is found in API 5C3 instead of 5CT and is limited in the scope of testing procedure. The bulletin states that the test specimen must have a length equal to at least twice the outer diameter, the testing apparatus must expose the full specimen length to the test pressure, the apparatus shall not impose radial or axial restraint or axial load on the specimen, and the apparatus shall not apply pressure to the inside surface of the specimen (API 5C3 1994).

The 5C3 bulletin therefore limits collapse testing to external pressure only. Teodoriu and Holzman present two test frames that can test for collapse resistance while also applying axial loads and/or internal pressure (2010). **Figure 2.4** shows the "autoclave" type test frame that uses a piston to apply axial load. The piston works by reacting to the pressure difference between the two chambers. When the pressure in the two chambers is equal, there is no axial load. When the pressure in Chamber 1 is greater than Chamber 2, tension occurs; when the pressure in Chamber 1 is less than Chamber 2, compression occurs. With this test frame it is difficult to apply internal pressure. **Figure 2.5** shows a more common "open" test frame. Axial load is applied with a

hydraulic ram by alternatively pressurizing two chambers, external pressure is applied with the autoclave, and internal pressure is applied with a high volume pneumatic intensifier and high-pressure compressor. The internal gas volume is reduced by the inclusion of a massive bar inside the pipe.

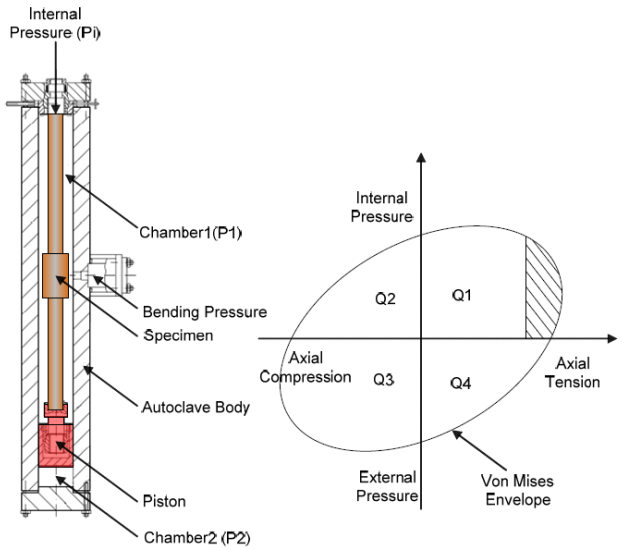

Figure 2.4: "Autoclave" type test frame (Teodoriu and Holzman 2010)

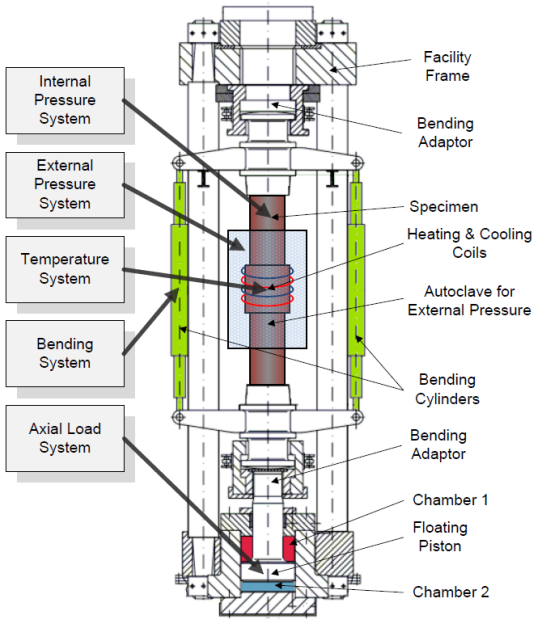

Figure 2.5: "Open" type test frame (Teodoriu and Holzman 2010)

Chapter 3: Classic API Collapse Equations

3.1 Elastic Collapse

The accepted API equation for elastic collapse is rooted in the expression for collapse of long cylinders under external pressure originally developed by M. Levy in 1884 (Clinedinst 1939) as:

$$P = \frac{2E}{1-\nu^2}\frac{1}{(D/t-1)^2} \tag{3.1}$$

where,

$E =$ Young's modulus, psi

$\nu =$ Poisson's ratio

$D =$ Outside diameter, in.

$t =$ Wall thickness, in.

Timoshenko took a similar approach in 1936 with the development of Eq. 3.2 for the elastic collapse of thin-wall tubulars:

$$P = \frac{2E}{1-\nu^2}\xi^3 \tag{3.2}$$

where,

$$\xi = \frac{1}{D/t-1} \tag{3.3}$$

In 1939, Clinedinst pulled from both of these equations to create Eq. 3.4 which assumes a linear stress distribution acting on the outer diameter of the tubular instead of the mean diameter:

$$P = \frac{2E}{1-\nu^2}\frac{1}{D/t\,(D/t-1)^2} \tag{3.4}$$

Later in 1939 the API adopted Eq. 3.4 as the theoretical formula for elastic collapse and took the value for average elastic collapse as 95% of the theoretical formula (API 5C3 1994). Assuming a Young's modulus value of $30x10^6$ psi and Poisson's ratio of 0.3, Eq. 3.5 was accepted as the average elastic collapse pressure:

$$P_{Eavg} = \frac{62.63x10^6}{(D/t)\left((D/t)-1\right)^2} \tag{3.5}$$

At the 1968 API Standardization conference, the minimum elastic collapse pressure was established as 75% of the average value, resulting in 71.25% of the theoretical Clinedinst equation:

$$P_E = \frac{46.95x10^6}{(D/t)\left((D/t)-1\right)^2} \tag{3.6}$$

3.2 Yield Strength Collapse

The API equation for yield strength collapse was calculated by means of the Lamé equation:

$$P_{yp} = 2Y_p\left[\frac{(D/t)-1}{(D/t)^2}\right] \tag{3.7}$$

where,

Y_p = Minimum yield strength, psi

This equation uses the nominal yield strength given by the grade of pipe used (J-55 has nominal yield strength 55,000psi) (API 5C3 1994).

3.3 Plastic Collapse

The equations for plastic collapse were developed by using statistical regression analysis of empirical collapse data. The pool of collapse data used in equation development consisted of 402 collapse tests of K-55 grade pipe, 1440 collapse tests of

N-80 grade pipe, and 646 collapse tests of P-110 grade pipe for a total of 2488 collapse tests. The average plastic collapse formulas are based on Stewart type formulas originally developed by Reid Stewart and published in an ASME paper in May 1906 (API 5C3 1994). Eq. 3.8 shows the standard form for the average plastic collapse pressure equation:

$$P_{pavg} = Y_p \left[\frac{A}{D/t} - B\right] \tag{3.8}$$

where,

$$A = 2.8762 + 0.10679x10^{-5}xY_p + 0.21301x10^{-10}xY_p{}^2 - 0.53132x10^{-16}xY_p{}^3 \tag{3.9}$$

$$B = 0.026233 + 0.50609x10^{-6}xY_p \tag{3.10}$$

To arrive at the minimum plastic collapse pressure, the method adopted in 1968 was to subtract 25% from the value calculated in Eq. 3.8. The updated method for finding minimum plastic collapse pressure is to subtract a constant pressure value determined for each grade. This results in Eq. 3.11:

$$P_p = Y_p \left[\frac{A}{D/t} - B\right] - C \tag{3.11}$$

where,

$$C = -465.93 + 0.030867xY_p - 0.10483x10^{-7}xY_p{}^2 + 0.36989x10^{-13}xY_p{}^3 \tag{3.12}$$

3.4 Transition Collapse

When using average plastic collapse pressure and average elastic collapse pressure, these two curves will intersect, and no transition collapse region is necessary. However, when minimum plastic collapse pressure and minimum elastic collapse pressure are used, the curve for minimum plastic will fall below and not intersect the

minimum elastic curve. The transition curve was developed as a bridge between these two minimum value curves (API 5C3 1994).

The transition curve is made to intersect the D/t value where average plastic collapse is zero and is tangent to minimum elastic collapse resulting in Eq. 3.13:

$$P_T = Y_p \left[\frac{F}{D/t} - G\right] \tag{3.13}$$

where,

$$F = \frac{46.95x10^6 \left[\frac{3B/A}{2 + B/A}\right]^3}{Y_p \left[\frac{3B/A}{2 + (B/A)} - (B/A)\right]\left[1 - \frac{3B/A}{2 + (B/A)}\right]^2} \tag{3.14}$$

$$G = FB/A \tag{3.15}$$

3.5 Delineation of Collapse Mode

Each mode of collapse is associated with a range of D/t values. The following equations give the upper and lower D/t limits for the different regions of the collapse modes. These limits are will differ depending on the associated pipe grade and nominal yield strength.

3.5.1 Yield Strength Collapse Region

The region for yield strength collapse ranges from a D/t value of zero on the low end to the upper limit defined by Eq. 3.16:

$$(D/t)_{yp} = \frac{\sqrt{(A-2)^2 + 8(B + C/Y_p)} + (A-2)}{2(B + C/Y_p)} \tag{3.16}$$

The API Bulletin 5C3 provides a list of the different upper D/t limits for the yield strength collapse region based on pipe grade in **Table 3.1**:

Table 3.1: Yield collapse pressure formula range (API 5C3 1994)

(1) Grade[a]	(2) *D/t* Range[b]
H-40	16.40 and less
-50	15.24 and less
J-K-55	14.81 and less
-60	14.44 and less
-70	13.85 and less
C-E-75	13.60 and less
L-N-80	13.38 and less
C-90	13.01 and less
C-T-X-95	12.85 and less
-100	12.70 and less
P-G-105	12.57 and less
P-110	12.44 and less
-120	12.21 and less
Q-125	12.11 and less
-130	12.02 and less
S-135	11.92 and less
-140	11.84 and less
-150	11.67 and less
-155	11.59 and less
-160	11.52 and less
-170	11.37 and less
-180	11.23 and less

3.5.2 Plastic Collapse Region

The region for minimum plastic collapse ranges from the D/t values calculated with Eq. 3.16 and given in **Table 3.1** as the lower limit, to the upper limit D/t value calculated with Eq. 3.17:

$$(D/t)_{PT} = \frac{Y_p(A - F)}{C + Y_p(B - G)} \tag{3.17}$$

The full range of D/t values for the plastic collapse region for different pipe grades can be seen in **Table 3.2**. This table also gives the values for parameters A, B, and C for use in the calculation of minimum plastic collapse pressure as well as calculating parameters F and G.

Table 3.2: Plastic collapse pressure formula range (API 5C3 1994)

(1)	(2)	(3)	(4)	(5)
	Formula Factor[b]			
Grade[a]	A	B	C	*D/t* Range[b]
H-40	2.950	0.0465	754	16.40 to 27.01
-50	2.976	0.0515	1056	15.24 to 25.63
J-K-55	2.991	0.0541	1206	14.81 to 25.01
-60	3.005	0.0566	1356	14.44 to 24.42
-70	3.037	0.0617	1656	13.85 to 23.38
C-E-75	3.054	0.0642	1806	13.60 to 22.91
L-N-80	3.071	0.0667	1955	13.38 to 22.47
C-90	3.106	0.0718	2254	13.01 to 21.69
C-T-X-95	3.124	0.0743	2404	12.85 to 21.33
-100	3.143	0.0768	2553	12.70 to 21.00
P-G-105	3.162	0.0794	2702	12.57 to 20.70
P-110	3.181	0.0819	2852	12.44 to 20.41
-120	3.219	0.0870	3151	12.21 to 19.88
Q-125	3.239	0.0895	3301	12.11 to 19.63
-130	3.258	0.0920	3451	12.02 to 19.40
S-135	3.278	0.0946	3601	11.92 to 19.18
-140	3.297	0.0971	3751	11.84 to 18.97
-150	3.336	0.1021	4053	11.67 to 18.57
-155	3.356	0.1047	4204	11.59 to 18.37
-160	3.375	0.1072	4356	11.52 to 18.19
-170	3.412	0.1123	4660	11.37 to 17.82
-180	3.449	0.1173	4966	11.23 to 17.47

3.5.3 Transition Collapse Region

The region for transition collapse ranges from the D/t values calculated with Eq. 3.17 and given as the upper limit in **Table 3.2** as the lower limit, to the upper limit D/t value calculated with Eq. 3.18:

$$(D/t)_{TE} = \frac{2 + B/A}{3B/A} \tag{3.18}$$

The full range of D/t values for the transition collapse region for different pipe grades can be seen in **Table 3.3**. This table also gives the values for parameters F and G for use in the calculation of transition collapse pressure.

Table 3.3: Transition collapse pressure formula range (API 5C3 1994)

(1)	(2)	(3)	(4)
	Formula Factors[b]		
Grade[a]	F	G	*D/t* Range[b]
H-40	2.063	0.0325	27.01 to 42.64
-50	2.003	0.0347	25.63 to 38.83
J-K-55	1.989	0.0360	25.01 to 37.21
-60	1.983	0.0373	24.42 to 35.73
-70	1.984	0.0403	23.38 to 33.17
C-E-75	1.990	0.0418	22.91 to 32.05
L-N-80	1.998	0.0434	22.47 to 31.02
C-90	2.017	0.0466	21.69 to 29.18
C-T-X-95	2.029	0.0482	21.33 to 28.36
-100	2.040	0.0499	21.00 to 27.60
P-G-105	2.053	0.0515	20.70 to 26.89
P-110	2.066	0.0532	20.41 to 26.22
-120	2.092	0.0565	19.88 to 25.01
Q-125	2.106	0.0582	19.63 to 24.46
-130	2.119	0.0599	19.40 to 23.94
S-135	2.133	0.0615	19.18 to 23.44
-140	2.146	0.0632	18.97 to 22.98
-150	2.174	0.0666	18.57 to 22.11
-155	2.188	0.0683	18.37 to 21.70
-160	2.202	0.0700	18.19 to 21.32
-170	2.231	0.0734	17.82 to 20.60
-180	2.261	0.0769	17.47 to 19.93

3.5.4 Elastic Collapse Region

The region for minimum elastic collapse ranges from the D/t values calculated with Eq. 3.18 and given as the upper limit in **Table 3.3** as the lower limit, and extends to all D/t values greater than those found in Eq. 3.18.

By looking at the D/t ranges for the different collapse modes in the preceding tables, as the pipe grade and yield strength increases, the points of transition from one collapse mode to the next fall to lower D/t values. This means that with increasing pipe strength, the elastic collapse region starts at lower D/t values and takes up a greater portion of the D/ t range, increasing the likelihood that high strength pipe grades will experience collapse in the elastic region. **Figure 3.1** shows the four collapse mode

curves and resulting overall collapse curve with corresponding collapse mode regions for N-80 grade pipe on the top, and a comparison of the collapse curves of three different pipe grades (J-55, N-80, P-110) on the bottom:

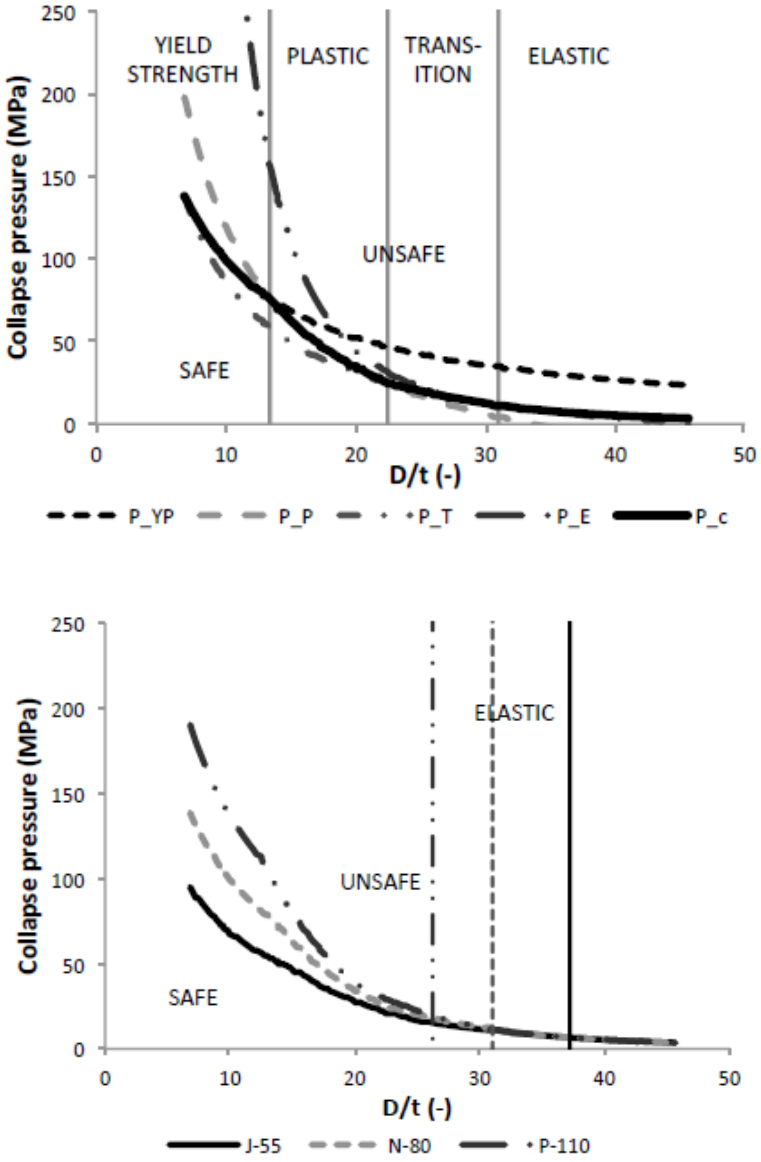

Figure 3.1: Collapse curves for N-80 (top), J-55 vs. N-80 vs. P-110 (bottom) (Staelens et al. 2012)

The bottom half of **Figure 3.1** also gives insight in how varying pipe grades behave in the different collapse regions. The difference in collapse pressure between

pipe grades is greatest in the yield strength collapse and plastic collapse regions. However, as the D/t ratio increases, the elastic collapse pressures tend to converge, resulting in little difference in collapse resistance between pipe grades in the elastic region (Staelens et al. 2012).

3.6 Accounting for Axial Load and Internal Pressure

The API equations can account for the effect of axial load by calculating an equivalent yield strength by using Eq. 3.19:

$$Y_{pa} = \left[\sqrt{1 - 0.75(S_a/Y_p)^2} - 0.5\, S_a/Y_p\right] Y_p \tag{3.19}$$

where,

Y_{pa} = Yield strength of axial stress equivalent grade, psi

S_a = Axial stress, psi

Equation 3.19 is based on the Hencky-von Mises max strain energy of distortion theory of yielding (API 5C3 1994). For tension loads, the value of S_a will be positive, whereas for compression loads, S_a will be negative. Due to the squared value found in Eq. 3.19, this equation does not adequately represent the increase in collapse resistance resulting from compression loads.

To account for the effect of internal pressure, effective pressure is calculated using Eq. 3.20:

$$P_{eq} = P_o - (1 - 2/(D/t))P_i \tag{3.20}$$

Where,

P_o = External pressure, psi

p_i = Internal pressure, psi

As the D/t value increases, the effect of a given internal pressure will also increase. This means pipes in the yield strength collapse region are less susceptible to the effects of internal pressure than pipes in the transition or elastic collapse regions.

Chapter 4: Equations Beyond API

4.1 Shortcomings of API 5C3 Equations

This chapter will show the deficiencies associated with using the API 5C3 equations for calculating collapse pressures and present several new equations that seek to account for those deficiencies. The API equations do a poor job of calculating real collapse pressures. It could be said that the API did not intend to calculate real collapse, but rather to find correlations that could then be coupled with enough safety margin to produce adequately workable casing design programs.

A common misconception exists that the API 5C3 equations reflect a uniform casing failure probability of 0.5% across the entire range of real D/t values. This is untrue due to a number of factors (Kuriyama and Mimaki 1994).

First, the API equations have a safety margins built in directly. They are designed to use the specified minimum yield strength (SYMS) or nominal yield strength in calculations requiring the input of yield strength. This is the yield strength accompanying a specific pipe grade (i.e. N-80 has nominal yield strength 80,000 psi). However, **Table 4.1** from API 5CT shows that for each specific grade, the actual yield strength can exist within a range of 15,000 to 40,000 psi. The inherent safety margin will then be the difference in collapse pressures for real versus nominal yield strength. Additionally, the yield strength collapse pressure calculated by the API 5C3 equation does not actually represent collapse. Rather, it represents the pressure at which yielding

begins at the inner pipe wall (Kuriyama and Mimaki 1994). On top of these built in safety margins, an additional safety factor will be added to the calculations during the design of the casing program which will further exasperate the difference of the calculated value from the real collapse value (Brechan et al. 2018).

Table 4.1: Pipe tensile and hardness requirements (API 5CT 2006)

Group	Grade	Type	Total elongation under load	Yield strength ksi		Tensile strength min.	Hardness [a] max.		Specified wall thickness	Allowable hardness variation [b]
			%	min.	max.	ksi	HRC	HBW	in	HRC
1	*2*	*3*	*4*	*5*	*6*	*7*	*8*	*9*	*10*	*11*
1	H40	—	0.5	40	80	60	—	—	—	—
	J55	—	0.5	55	80	75	—	—	—	—
	K55	—	0.5	55	80	95	—	—	—	—
	N80	1	0.5	80	110	100	—	—	—	—
	N80	Q	0.5	80	110	100	—	—	—	—
2	M65	—	0.5	65	85	85	22	235	—	—
	L80	1	0.5	80	95	95	23	241	—	—
	L80	9Cr	0.5	80	95	95	23	241	—	—
	L80	13Cr	0.5	80	95	95	23	241	—	—
	C90	1, 2	0.5	90	105	100	25.4	255	⩽ 0.500	3.0
	C90	1, 2	0.5	90	105	100	25.4	255	0.501 to 0.749	4.0
	C90	1, 2	0.5	90	105	100	25.4	255	0.750 to 0.999	5.0
	C90	1, 2	0.5	90	105	100	25.4	255	⩾ 1.000	6.0
	C95	—	0.5	95	110	105	—	—	—	—
	T95	1, 2	0.5	95	110	105	25.4	255	⩽ 0.500	3.0
	T95	1, 2	0.5	95	110	105	25.4	255	0.501 to 0.749	4.0
	T95	1, 2	0.5	95	110	105	25.4	255	0.750 to 0.999	5.0
	T95	1, 2	0.5	95	110	105	25.4	255	⩾ 1.000	6.0
3	P110	—	0.6	110	140	125	—	—	—	—
4	Q125	—	0.65	125	150	135	[b]	—	⩽ 0.500	3.0
	Q125	—	0.65	125	150	135	[b]	—	0.501 to 0.749	4.0
	Q125	—	0.65	125	150	135	[b]	—	⩾ 0.750	5.0

[a] In case of dispute, laboratory Rockwell C hardness testing shall be used as the referee method.

[b] No hardness limits are specified, but the maximum variation is restricted as a manufacturing control in accordance with 7.8 and 7.9.

Second, the API is inconsistent with how the minimum collapse values are determined from average collapse values. For elastic collapse, minimum values are achieved by applying a constant 71.25% multiplicative factor across the entire D/t range. However, for minimum plastic collapse, a constant pressure value is subtracted based on pipe grade. The value of plastic collapse pressure will decrease with increasing D/t as shown from the curve in **Figure 3.1**, but because the pressure value subtracted

will stay constant, the percentage of plastic pressure subtracted will increase with increasing D/t (Ju et al. 1998).

Finally, the API equations do not explicitly account for the detrimental effects of pipe imperfections on the collapse resistance, but rather deal with exclusively "ideal" pipes. The ultimate collapse resistance of a real pipe will be affected by ovality, eccentricity, the shape of the stress/strain curve, and the residual stress found in the pipe due to the manufacturing process (Ju et al. 1998, Klever and Tamano 2006).

In order to graphically show the deficiencies of the API equations, Ju et al. plotted observed collapse pressure/API calculated collapse pressure vs a normalized D/t value. To do this, a normalization factor was first defined as shown in Eq. 4.1:

$$r_n = \sqrt{\frac{E}{(1-\nu^2)Y}} - 1 \tag{4.1}$$

where,

r_n = value of D/t where $P_e = P_{yp}$ as seen in **Figure 4.1**

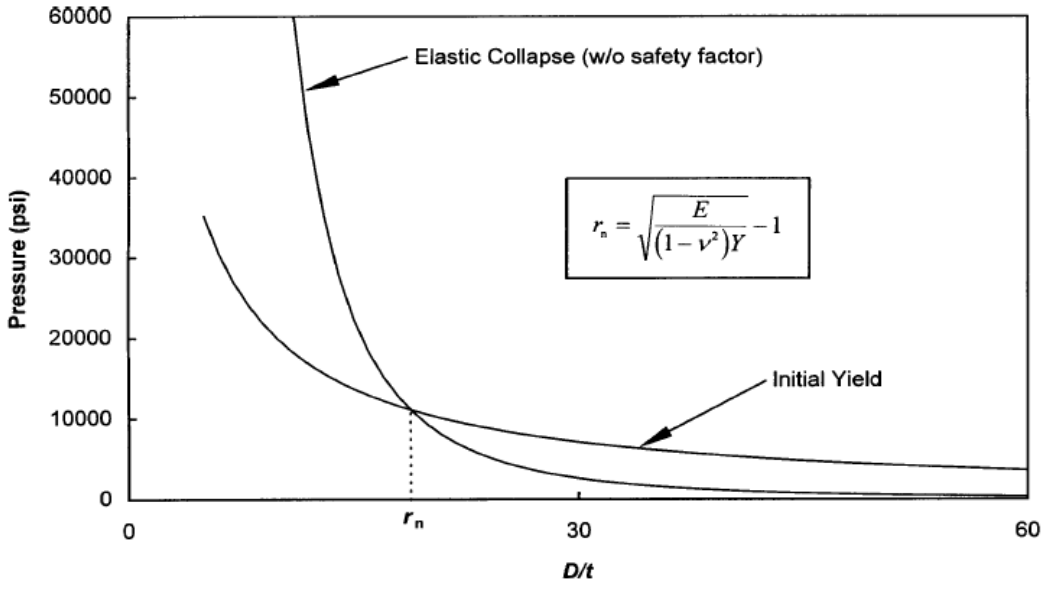

Figure 4.1: Definition of normalization factor r_n (Ju et al 1998)

This normalization factor was then used to define $\overline{D/t}$:

$$\overline{D/t} = \frac{D/t}{r_n} \tag{4.2}$$

The result is shown in **Figures 4.2 and 4.3**.

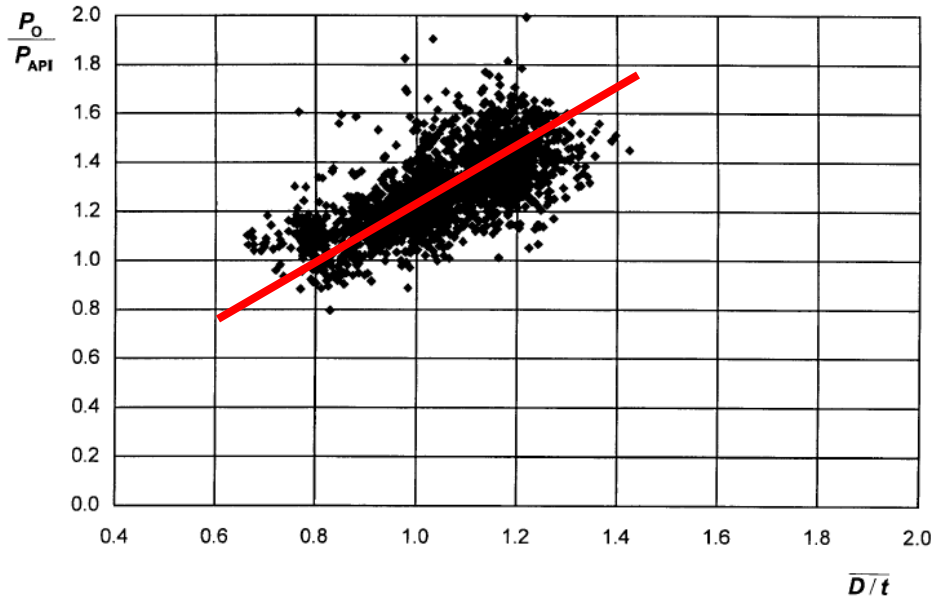

Figure 4.2: Original API database observed collapse pressures normalized by API calculated collapse pressures (Ju et al. 1998)

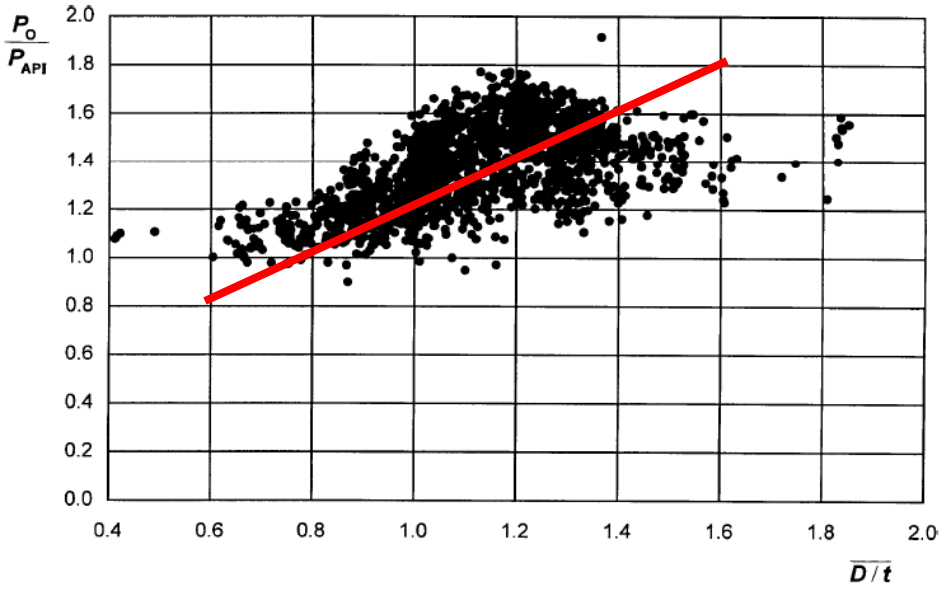

Figure 4.3: Post-1963 database observed collapse pressures normalized by API calculated collapse pressures (Ju et al. 1998)

Best-fit lines applied to **Figures 4.2 and 4.3** show excessive risk for low D/t values and excessive safety for high D/t values. This becomes critical when applied to casing design. Pipe used for surface or intermediate casing will exhibit D/t values greater than 20, whereas pipe used as production liner will exhibit D/t values in between 12 and 15 (Ju et al. 1998, Adams et al. 1998). The production liner will experience greater depths and greater corresponding pressures than the surface or intermediate casing but is at greater risk for collapse when using the API equations for designing the casing program. This can be seen in the following example:

For N-80 grade casing, the value of r_n becomes 19.3. An intermediate casing string with outside diameter of 13 3/8" and wall thickness 0.480" (from API 5CT Table E.1, #68) will have a D/t of 27.86 and $\overline{D/t}$ of 1.44. Based on the best fit lines, the actual collapse pressure will be more than 60% greater than the collapse pressure calculated with the API equations. A production liner with outside 5" and wall thickness 0.362 (from API 5CT Table E.1, #18) will have a D/t of 13.81 and $\overline{D/t}$ of 0.72. Based on the best fit lines, the actual collapse pressure will only be roughly 90% of the collapse pressure predicted by the API equations.

Through this simple example, it can be seen that the intermediate casing string would be greatly over-designed, and the production liner would be under designed when using API equations. The over-designed intermediate string would cost much more and have a great detrimental impact to the economics of the well, whereas the under-designed production liner could result in catastrophic failure in a critical portion of the well. This two-sided design problem is evidence that the classic API equations are in need of improvement.

4.2 New Collapse Equations

The lack of accuracy in the prediction of tubular collapse pressures demonstrated by the example in the previous section exemplifies the need for better methods of collapse pressure calculation. Several methods have been proposed and are detailed in the following sections. Some approaches attempt to develop new equations for each individual collapse mode (yield strength collapse, elastic collapse, plastic collapse), whereas others incorporate the original API equations and attempt to devise a method for fitting the theoretical data to real data. Additionally, some more complete approaches attempt to accomplish both the development of new individual collapse mode equations, and the incorporation of those new equations into a cohesive final design equation.

4.2.1 Yield Strength Collapse

One early equation for yield strength collapse was proposed by Timoshenko for the collapse of thin-wall tubes as seen in Eq. 4.3:

$$p_{thin}^{yc} = 2\sigma_y \xi \tag{4.3}$$

where,

$\xi = \frac{1}{D/t - 1}$ = the characteristic pipe geometry parameter

Another yield strength collapse equation is the Tresca criterion (Klever and Tamano 2006) seen in Eq. 4.4:

$$p_{Tresca}^{yc} = 2\sigma_y \frac{\xi}{1+\xi} \tag{4.4}$$

These two equations are given in a style that is similar to the API equation for yield strength collapse given in Eq. 3.7. That is, each of these three equations takes twice the yield strength value and multiplies it by some ratio of D/t values to calculate

the collapse pressure. However, as has been previously stated, the API yield strength collapse equation is not a true prediction of collapse pressure, but rather a prediction of the pressure at which yielding will occur at the inside wall of the pipe.

In an effort to develop a yield strength collapse equation that would represent real pipes, Tamano et al. developed Eq. 4.5 (1983):

$$p_e^{ycT} = 2\sigma_y \frac{D/t - 1}{(D/t)^2}\left(1 + \frac{fac}{D/t - 1}\right) \tag{4.5}$$

where,

fac = Factor to allow curve fitting to real data

This equation is valid for the case of external pressure only. Development of this equation is an attempt to model the full through-wall yield of the pipe rather than the initial yielding at the inside wall. This is accomplished by taking the original API yield strength collapse equation and adding a multiplicative component with parameter *fac* to allow curve fitting to real data. Tamano et al. (1983) originally used 1.43 as the value of *fac*, but it has since been shown that using a value of 1.5 produces an equation that is second-order correct in t/D (Klever and Tamano 2006).

Building on the original work by Tamano et al, Klever and Tamano proposed Eq. 4.6 for through-wall yield strength collapse for external pressure only:

$$P_e^{yc} = 2\sigma_y \, \xi \left(1 - \frac{1}{2}\xi\right) \tag{4.6}$$

To account for the imperfections found in real pipe, the value σ_y' can be substituted in place of σ_y. σ_y' is given as:

$$\sigma_y' = k_y\left(1 - H_y\right)\sigma_y \tag{4.7}$$

where,

k_y = Yield bias factor

H_y = Yield decrement function

A comparison of the accuracy of prediction of through-wall yield pressure for Eq. 4.5 and Eq. 4.6 can be achieved through scaling with the exact von Mises through-wall yield pressure. Exact von Mises through-wall yield pressure is given as (Klever and Tamano 2006):

$$p_e = -\sigma_y \frac{2}{\sqrt{3}} sin\eta_e \tag{4.8}$$

where,

η_e is a variable whose value results in $G = 0$ for the following equation:

$$G = \int_0^{\eta_e} \frac{2}{\sqrt{3} + tan\eta} d\eta + ln\frac{R_e}{R_i} \tag{4.9}$$

where,

R_e = outside radius, in.

R_i = inside radius, in.

The result of scaling Eq. 4.5 and Eq. 4.6 with the exact von Mises through-wall yield pressure can be seen in **Figure 4.4**. This figure shows the best prediction with Eq. 4.6 for D/t values greater than 12 and adequate prediction with Eq. 4.5 for D/t values greater than 20 when using a *fac* value of 1.5. However, using Eq. 4.5 with *fac* value of 1.47 as originally proposed by Tamano et al. results in an underprediction of through-wall yield pressure throughout the full range of D/t values.

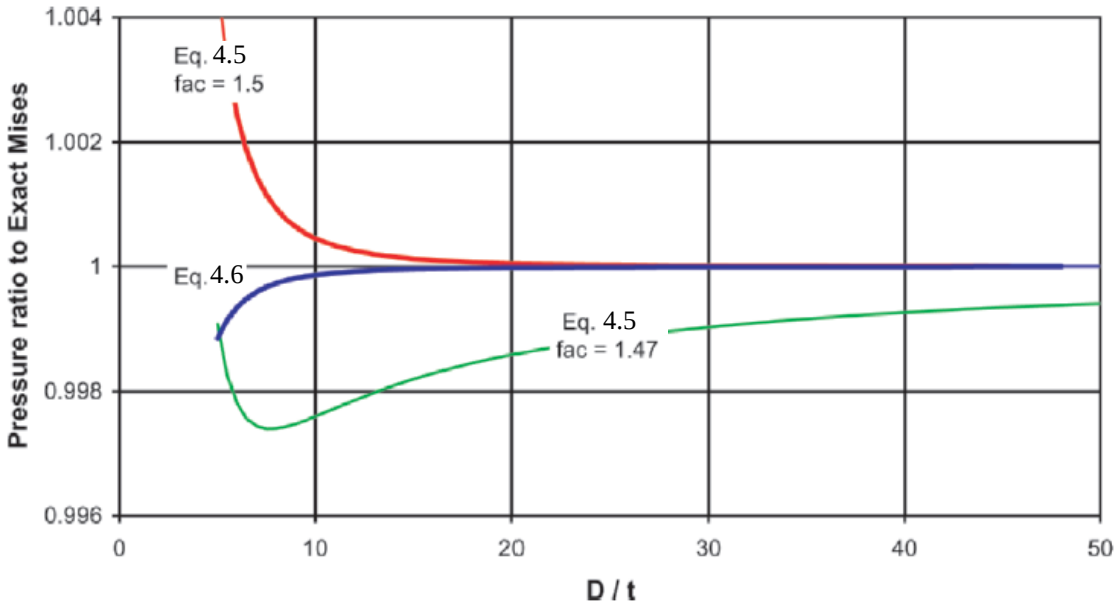

Figure 4.4: Accuracy of Eq. 4.5 and Eq. 4.6 (Klever and Tamano 2006, modified)

To account for the combined effect of axial load, external pressure, and internal pressure, Eq. 4.10 was developed to show the pressure differential between internal and external pressure with the inclusion of an effect axial load at von Mises through-wall yield:

$$\Delta p^{yM} = 2\xi\sigma_y' \frac{2}{\sqrt{3}} \sqrt{1 - \left(\frac{F_{eff}}{2\pi R t \sigma_y'}\right)^2} \tag{4.10}$$

where,

F_{eff} is the effective axial load given by the following equation:

$$F_{eff} = F - p_i A_i + p_e A_e = F + p_i(A_e - A_i) + \Delta p A_e \tag{4.11}$$

where,

A_e = Pipe outside cross-sectional area, in.^{2}

A_i = Pipe inside cross-sectional area, in.^{2}

Given that through-wall yield pressure is a close upper bound to plastic collapse pressure without work hardening, through-wall yield pressure can be used to approximate the yield collapse pressure of thick-wall pipes (Klever and Tamano 2006). As a result, the differential pressure for yield collapse can be taken as the minimum of two values: the average of the von Mises and Tresca, or von Mises alone. This formulation is shown in Eq. 4.12:

$$\Delta p^{yc} = \min\left\{\frac{1}{2}\left(\Delta p^{yM} + 2\xi\sigma_y'\right), \Delta p^{yM}\right\} \tag{4.12}$$

Below the initial yield pressure, the entirety of a pipe wall will be in an elastic mode. As the pressure is increased to and beyond initial yield, the radius of plasticity moves from the inner pipe wall (a) outward. When this radius reaches the outer wall (b), through-wall yield is achieved. The mid-way point between initial yield and through-wall yield is shown in **Figure 4.5** as the radius of plasticity, r_s:

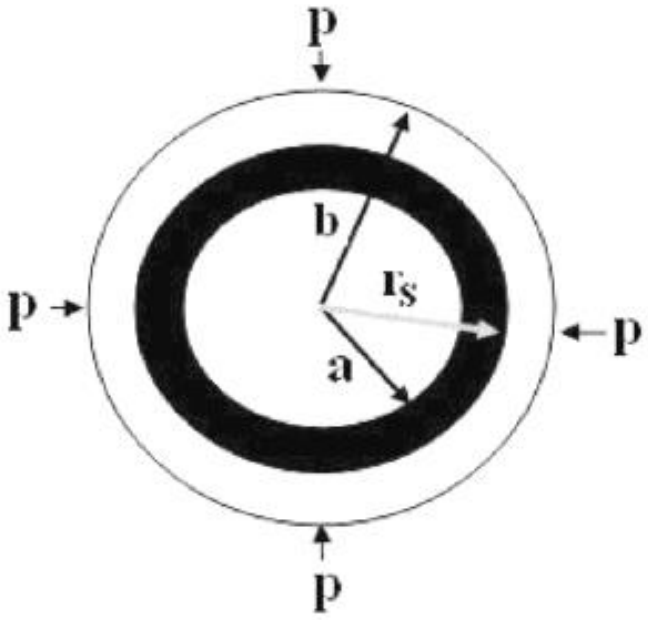

Figure 4.5: Transition from initial to through-wall yield (Sun 2010)

By using elastic and plastic mechanics to find the stresses in the radial and circumferential directions coupled with the von Mises criterion when the radius is at the inner wall, Sun developed an equation for initial yield which differs slightly from the original API formulation:

$$p_{iy} = 2.309\sigma_y \left[\frac{(D/t) - 1}{(D/t)^2}\right] \tag{4.13}$$

The same procedure can be used to develop an equation for through-wall yield by coupling with the von Mises criterion when the radius is at the outside wall:

$$p_{fy} = \frac{2\sigma_y}{\sqrt{3}} \ln\left(\frac{D/t}{D/t - 2}\right) \tag{4.14}$$

Though these equations are updated versions of the classic API equations, their scope is still limited to the theoretical. Without any inclusion of parameters for the correction of imperfections or the ability to provide curve fitting to real data, these equations will suffer the same pitfalls of the original API 5C3 equations.

4.2.2 Elastic Collapse

As discussed previously, the precursor to the Clinedinst elastic collapse equation, which was adopted as the API theoretical collapse pressure, was Eq. 3.2 put forth by Timoshenko to solve for the collapse pressure of thin-wall pipes. Klever and Tamano returned to the Timoshenko when creating a new elastic collapse equation shown in Eq. 4.15:

$$\Delta p^{ec} = \frac{2E'}{1 - \nu^2} \xi^3 (1 + c\xi) \tag{4.15}$$

where,

$c =$ Elastic collapse equation parameter for wall thickness

E' = Factored Young's modulus given by:

$$E' = k_e(1 - H_e)E \tag{4.16}$$

where,

H_e = Elastic decrement function

k_e = Elastic bias factor

It is evident that this is the same as the Timoshenko equation with the addition of a multiplicative factor at the end. Since the original Timoshenko equation was developed for thin-wall pipe, this multiplicative factor is used to incorporate the effect of thick-wall pipe on the elastic collapse pressure.

The value of c in the multiplicative factor will determine how accurate this newly developed elastic collapse equation is compared to the collapse of real pipes. If the value of c is taken to be zero, the original Timoshenko equation will be recovered. Brechan et al. point out that when using the Klever and Tamano elastic collapse pressure, the ISO recommends using c = -1 + t/D. Using this c value, Eq. 4.15 reduces to Eq. 4.17:

$$\Delta p_{ec} = \frac{2k_eE}{(1 - \nu^2)(D/t)(D/t - 1)^2} \tag{4.17}$$

However, when the value of c is taken to be -1 + t/D, c will be less than -0.9 for the entire elastic collapse region. This would effectively result in a reduction of elastic collapse pressure. This is counterintuitive given c was created to account for the effect of thick-wall pipes when using the Timoshenko elastic collapse equation for thin wall pipes (Brechan et al. 2018). **Figure 4.6** shows the comparison of Eq. 4.15 given

different values of c, scaled to the Timoshenko thin-wall elastic collapse equation. The API 5C3 equation for elastic collapse is also included.

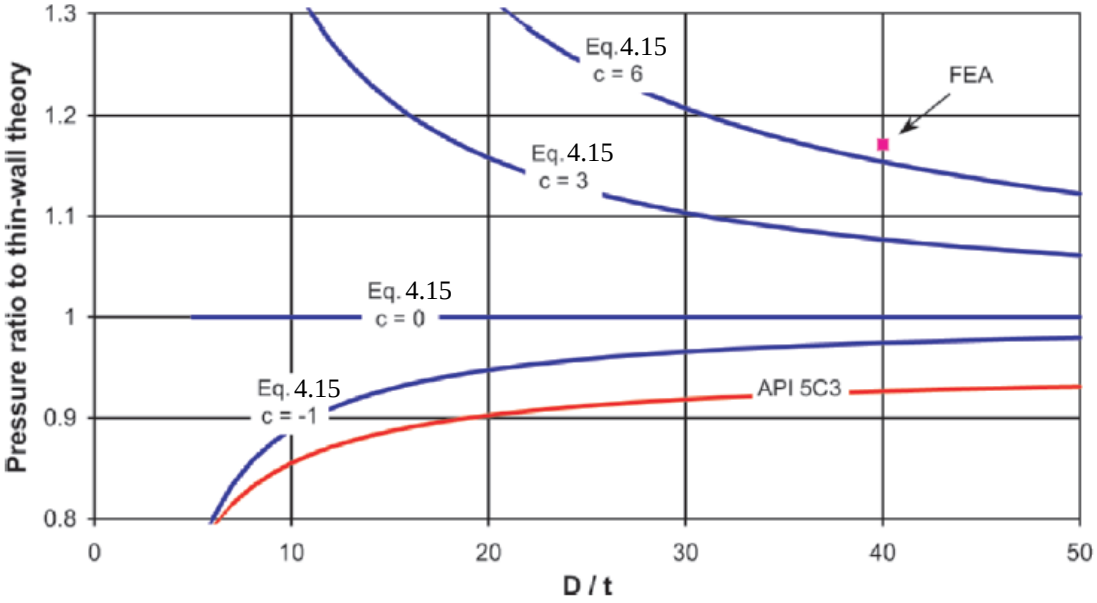

Figure 4.6: Eq. 4.15 comparison given different c values (Klever and Tamano 2006, modified)

By using Finite Element Analysis (FEA) to simulate the collapse pressure of a real pipe with D/t value equal to 40, a determination concerning the appropriate value for c can be made. **Figure 4.6** shows the FEA most closely resembles the value at D/t of 40 for the curve *c* = 6. It is also clear that the ISO value of -0.9 would fall below the elastic collapse pressure given by the Timoshenko equation for the entire D/t range. Therefore, the most appropriate value of c for use in Eq. 4.15 is 6 (Brechan et al 2018).

4.2.3 Combination Elastic/Plastic Collapse

Elastic/plastic combination collapse equations can be used to find collapse pressures by understanding how the material transitions from an elastic state to a plastic state. Eq. 4.18 gives the relationship between the location of the elasto-plastic boundary and the external pressure as proposed by Kuriyama and Mimaki (1994):

$$P_y = \frac{1}{4}\frac{Z(3b^2 + c^2)}{b^2} + \frac{1}{4}\frac{(b^2 - c^2)}{b^2\sqrt{4Y^2 - 3Z^2}} \tag{4.18}$$

where,

a = inner radius, in.

b = outer radius, in.

c = elasto-plastic boundary, in.

P_y = External Pressure, psi

$$Z = -\frac{2}{\sqrt{3}} Y \sin(\frac{\pi}{6} + \theta_c)$$

The collapse pressure of a pipe in the elasto-plastic transition is given by Eq. 4.19:

$$P_c = \frac{24EI}{[(1 - \nu^2)(D - t)^3]} \tag{4.19}$$

where,

I = Geometrical moment of inertia

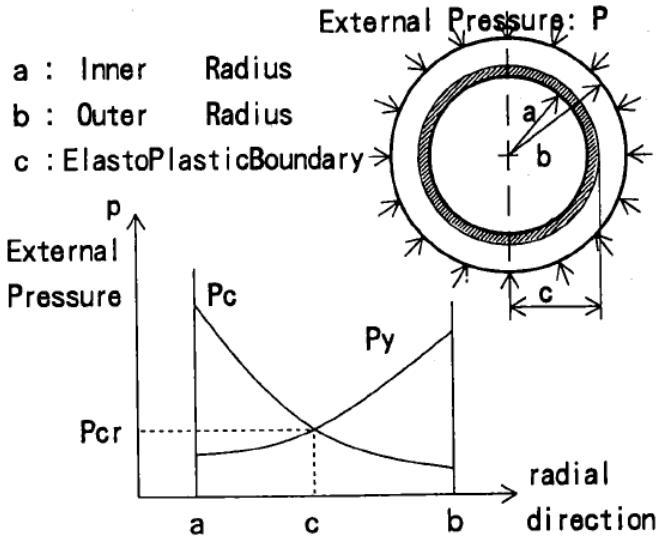

Figure 4.7: Elasto-plastic collapse pressure (Kuriyama and Mimaki 1994)

As the elasto-plastic boundary moves radially away from the inner wall toward the outer wall, the external pressure will increase. Conversely, the collapse pressure will decrease as the elasto-plastic boundary moves toward the outer wall. When the curves cross, $P_y = P_c$, and elasto-plastic collapse occurs at pressure P_{cr} (Kuriyama and Mimaki 1994). This relationship is shown graphically in **Figure 4.7**.

Pipe collapse can also be thought of as a step-wise process involving the mechanics of multiple previously discussed collapse modes. One such mechanism is the 4-hinge collapse model which involves ovalization of the pipe through the elastic stage followed by plastic collapse as seen in **Figures 4.8 and 4.9:**

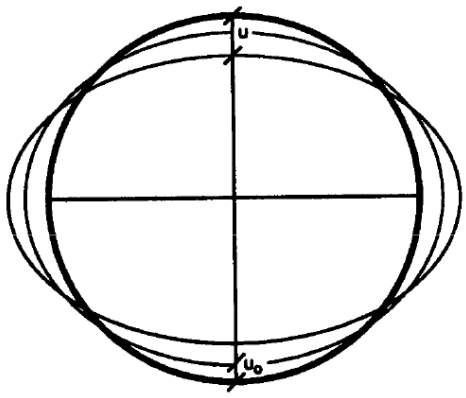

Figure 4.8: Elastic ovalization (Abbassian and Parfitt 1995)

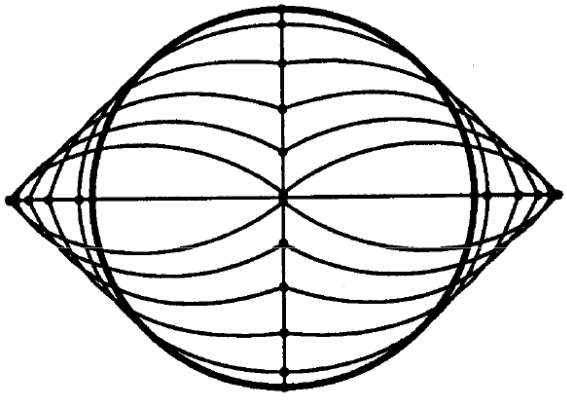

Figure 4.9: 4-hinge mechanism (Abbassian and Parfitt 1995)

Ovalization is an elastic process that involves calculation of the elastic buckling collapse pressure (Eq. 4.20) and the elastic ovalization pressure (Eq. 4.21)(Abbassian and Parfitt 1995):

$$P_{Eb} = \frac{2E}{(1-\nu^2)}\left(\frac{t}{D}\right)^3 \tag{4.20}$$

$$P_{eo} = P_E \frac{u - u_o}{u} \tag{4.21}$$

where,

$u_o =$ Amplitude of original ovality

$u =$ Amplitude of ovality at pressure Peo

The elastic ovalization pressure is a function of the elastic buckling collapse pressure, the ovality of the pipe originally, and the ovality of the pipe at ovalization pressure. The plastic collapse pressure is a function of yield strength, D/t, and ovality amplitude and ovalization pressure given by Eq. 4.22:

$$P_{pc} = \frac{2Yt}{D}\left[-2\frac{D}{t}\left(1-\frac{u}{D}\right)\frac{u}{D} + \sqrt{1+4\frac{D^2}{t^2}\left(1-\frac{u}{D}\right)^2\frac{u^2}{D^2}}\right] \tag{4.22}$$

The initial ovality of the pipe will affect the calculation of the elastic ovalization pressure, the yield strength will affect the calculation of the plastic collapse pressure, and the value of D/t will affect the calculation of both values. In a manner similar to the previous method, when the curves of the elastic ovalization pressure and the plastic collapse pressure cross, true collapse pressure will be found. As pressure increases, the pipe will begin to deform elastically. When the external pressure reaches a critical value, the pipe will have deformed elastically enough that it will jump onto the plastic

collapse curve due to formation of the four hinges (Abbassian and Parfitt 1995). This process can be seen graphically in **Figure 4.10**:

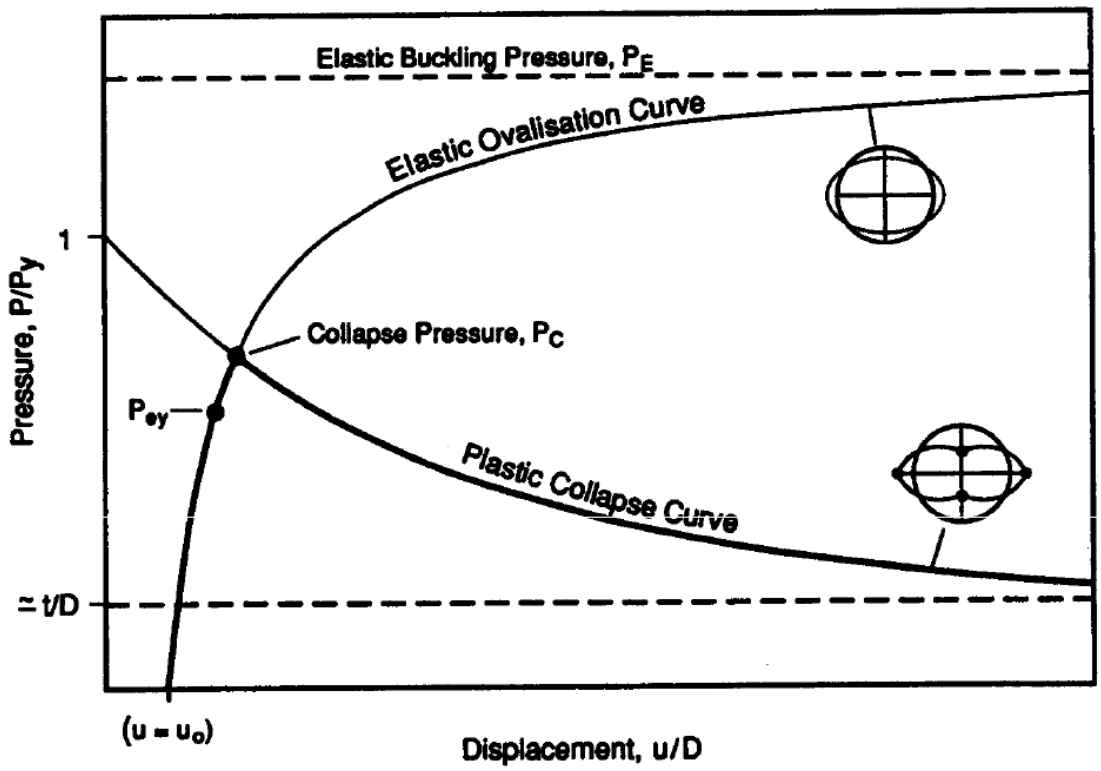

Figure 4.10: Elastic ovalization and plastic collapse curves define collapse pressure (Abbassian and Parfitt 1995)

4.2.4 Design Equations

The design equations pull results from the individual collapse mode equations in an effort to produce one cohesive, user-friendly equation. Some design equations use the new collapse mode equations detailed in earlier sections, whereas others use the API equations and apply different methods to make the results fit real data.

Eq. 4.23 uses the original Clinedinst elastic collapse pressure equation as well as the Tamano et al. yield collapse equation with *fac* set to 1.47 (Adams et al. 1998):

$$p_{c\,ult} = \frac{(p_e + p_y)}{2} - \sqrt{\frac{(p_e - p_y)^2}{4} + p_e p_y H} \tag{4.23}$$

where,

H = decrement function to account for ovality, eccentricity, and residual stress

$$H = 0.0808ov + 0.0114ec - 0.1412rs \tag{4.24}$$

Adams et al. build on the Tamano et al. design equation but also introduce the idea of bias factors k_e and k_y in Eq. 4.25:

$$p_{c\,des} = \frac{(k_e p_e + k_y p_y)}{2} - \sqrt{\frac{(k_e p_e - k_y p_y)^2}{4} + k_e p_e k_y p_y H} \tag{4.25}$$

where,

k_e = Elastic bias factor

k_y = Yield bias factor

Klever and Tamano use the newly developed yield strength collapse equation (Eq. 4.12) and elastic collapse equation (Eq. 4.15) to create a transition equation to bridge between the yield and collapse regions as shown in Eq. 4.26:

$$\Delta p^c = \frac{2\Delta p^{yc}\Delta p^{ec}}{\Delta p^{yc} + \Delta p^{ec} + \sqrt{(\Delta p^{yc} - \Delta p^{ec})^2 + 4H_t \Delta p^{yc}\Delta p^{ec}}} \tag{4.26}$$

where,

H_t = Transition decrement function, $f(\xi, ov, sh, ec, rs)$

From Brechan et al. 2018:

$$H_t = 0.127ov + 0.0039ec + 0.440(rs/\sigma_y) + h_n \tag{4.27}$$

where,

h_n = Correction for the shape of the stress/strain curve

The shape of the stress/strain curve will affect the value of the decrement function H_t and, therefore, will affect the differential collapse pressure calculated in Eq. 4.26. The manufacture and treatment of the pipe will determine the shape of the curve. A hot rotary straightened (HRS), quenched and tempered (Q&T) pipe will exhibit a "sharp-knee" stress/strain curve, whereas a cold rotary straightened (CRS) pipe will exhibit a "round-knee" stress/strain curve. For the calculation of H_t, HRS pipes will have a h_n value of zero and CRS pipes will have a detrimental h_n value of 0.017 (Brechan et al. 2018). CRS pipes may also exhibit work hardening beyond the yield strength. This is the material property of increased strength with increasing strain. The effect of the stress/strain curve shape and work hardening can be seen in **Figure 4.11**:

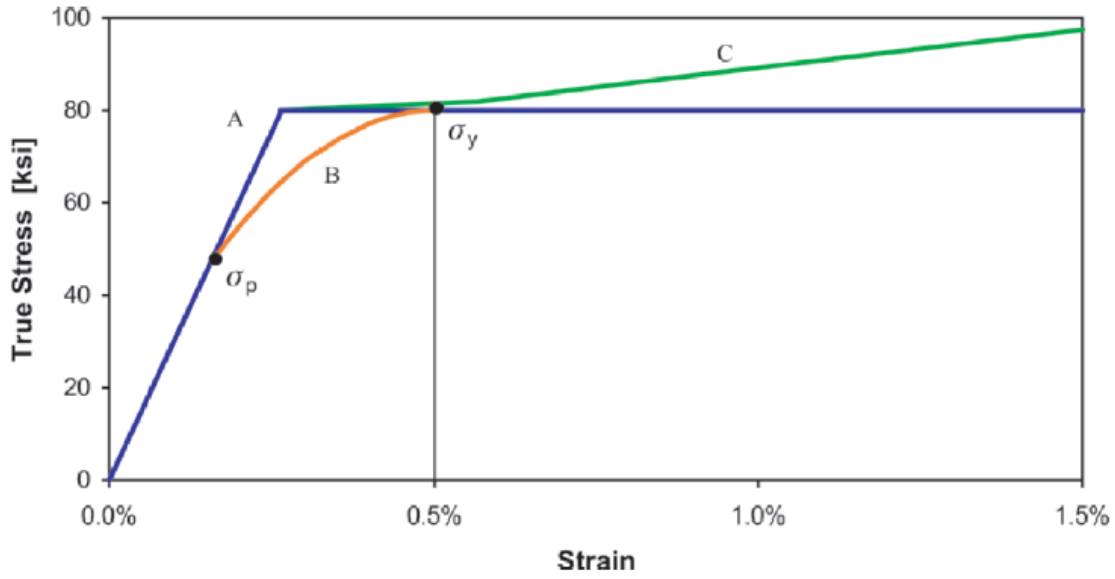

Figure 4.11: Stress/strain curve shape and work hardening (Klever and Tamano 2006)

Figure 4.11 shows the sharp-knee curve (A), round-knee curve (B), and the zone of work hardening (C).

Like API 5C3, Eq. 4.26 can be split into respective collapse modes using a ratio of yield collapse pressure to elastic collapse pressure as seen in Eq. 4.28. The divisions between collapse modes for ratio X are defined in **Table 4.2**.

$$X = \frac{\Delta p^{yc}}{\Delta p^{ec}} \tag{4.28}$$

Table 4.2: Collapse mode (after Klever and Tamano 2006)

Collapse Mode	**Log Ratio**
Yield	Log(X) < -0.3
Transition	-0.3 < log(X) < 0.3
Elastic	Log(X) >0.3

Eq. 4.26 is a design equation because it can be used to find the collapse pressure at any value of D/t. This is made possible by the behavior of the equation at the high-end and low-end values of D/t. At low values of D/t, the elastic collapse pressure will be much greater than the yield strength collapse pressure, and the differential collapse pressure will more closely resemble the yield strength collapse pressure. Conversely, at high D/t values, yield strength collapse pressure will be much greater than elastic collapse pressure, and the differential collapse pressure will more closely resemble the elastic collapse pressure (Klever and Tamano 2006). This can be seen in the statement below:

$$\Delta p^{ec} \gg \Delta p^{yc}, \Delta p^{c} \approx \Delta p^{yc}$$

$$\Delta p^{ec} \ll \Delta p^{yc}, \Delta p^{c} \approx \Delta p^{ec}$$

Other design equations use the API equations with a number of design parameters to attempt to fit the API values to real data. Eq. 4.29 uses the Clinedinst theoretical elastic collapse pressure and API yield strength collapse pressure with a built-in design factor and probability of failure:

$$P_d = \frac{0.76{P_e}^{0.928}{P_{yp}}^{1.072}}{DF\sqrt[3]{{P_e}^3 + {P_{yp}}^3}} \tag{4.29}$$

where,

DF = design factor

Alternatively, if actual values of wall thickness, yield strength, and initial ovality are known, a resistance equation can be calculated to give the best prediction of actual collapse pressure of real pipes as seen in Eq. 4.30:

$$P_R = \frac{{P_e}^{0.928}{P_{yp}}^{1.072}}{\sqrt[5]{{P_e}^5 + {P_{yp}}^5}} F(\Delta) \tag{4.30}$$

where,

$F(\Delta)$ = Ovality correction function

$$F(\Delta) = \left[1 + A_\Delta \left(\overline{D/t}\right)^{B_\Delta} \Delta\right]^{-C_\Delta} \tag{4.31}$$

where,

Δ = Ovality

$$\Delta = \frac{D_{max} - D_{min}}{D_{avg}} \tag{4.32}$$

A_Δ, B_Δ, C_Δ = Constants used in ovality correction

The value of constants A_Δ, B_Δ, and C_Δ depend on the normalized value of D/t calculated in Eq. 4.2 and are summarized in **Table 4.3**:

Table 4.3: Constants for ovality correction (after Ju et al. 1998)

$\overline{D/t} \geq 1$	$\overline{D/t} < 1$
A_Δ = 384.0	A_Δ = 303.6
B_Δ = -2.52	B_Δ = 3.37
C_Δ = 0.257	C_Δ = 0.262

4.2.5 Accounting for Axial Load and Internal Pressure

The API 5C3 Bulletin provides two equations for handling axial load and internal pressure. The first equation calculates an equivalent yield strength and the second equation calculates effective pressure. These equations can be combined into one equation that will account for both at the same time. This modified equivalent yield strength is given by Eq. 4.33 (Brechan et al. 2018):

$$\sigma_e = \sigma_y \left[\sqrt{1 - \frac{3}{4}\left(\frac{\sigma_a + p_i}{\sigma_y}\right)^2} - \frac{1}{2}\frac{(\sigma_a + p_i)}{\sigma_y} \right] \tag{4.33}$$

where,

σ_a = Average axial stress, psi

Axial load is accounted for in the original Tamano et al. model using the same correction factor as Eq. 4.33 but without the inclusion of internal pressure as shown in Eq. 4.34:

$$\Delta p_{yTamano} = 2\sigma_y \frac{D/t - 1}{(D/t)^2}\left(1 + \frac{fac}{D/t - 1}\right)\left[\sqrt{1 - \frac{3}{4}\left(\frac{\sigma_a}{\sigma_y}\right)^2} - \frac{1}{2}\frac{\sigma_a}{\sigma_y} \right] \tag{4.34}$$

Klever and Tamano provided a correction for axial load in the von Mises equation (Eq. 4.10). However, since tension is taken as a positive value and

compression is taken as a negative value, the squared F_{eff} term returns the same value for pipes in tension as pipes in compression. This contradicts the traditional API notion that pipes in tension will show reduced collapse resistance and pipes in compression will show greater collapse resistance (Brechan et al. 2018). Eq. 4.10 can be rewritten so that the beneficial effect of compression is accounted for as seen in Eq. 4.35:

$$\Delta p^{yM} = \xi \sigma_y' \frac{4(1+2\xi)}{3+(1+2\xi)^2}\left[-S_i \pm \sqrt{1+3\frac{1-{S_i}^2}{(1+2\xi)^2}}\right] \tag{4.35}$$

where,

$$S_i = \frac{\sigma_a + p_i}{\sigma_y'} \tag{4.36}$$

4.3 Performance of New Equations

4.3.1 Comparison of Models to API

In order to make a determination about the validity of the individual collapse mode equations and the design equations, their calculated values can be compared to the calculated values of the API equations as well as true collapse pressure data. **Figure 4.12** shows a comparison of Eq. 4.6 (<3D> yield (Mises)) to the Timoshenko thin-wall theory, Tresca criterion, and API 5C3 equation. The Tresca and 5C3 equations both underestimate collapse whereas the thin-wall theory appears to overestimate it. The FEA results show a D/t value of 10 falls on the Eq. 4.6 line and a D/t value of 8 follows the thin-wall theory due to the effect of work hardening.

Figure 4.13 shows a comparison using the Kuriyama and Mimaki elasto-plastic collapse equation. The comparison includes elasto-plastic collapse for an ideal pipe and a pipe with imperfections against the API equations utilizing the SMYS (nominal yield strength). **Figure 4.14** uses the calculated values for an actual pipe and the API equation

from **Figure 4.13** normalized by the values for the ideal pipe. At a D/t value around 13, the margin between the API and actual pipe collapse values is less than 10% of the ideal collapse pressure which indicates an unacceptable risk level. Conversely, the margin between API and actual collapse values for D/t 22.5 is almost 50% of the ideal collapse pressure (Kuriyama and Mimaki 1994). This excessively large margin indicates that the casing design for pipes in this range would be unnecessarily over-designed and expensive.

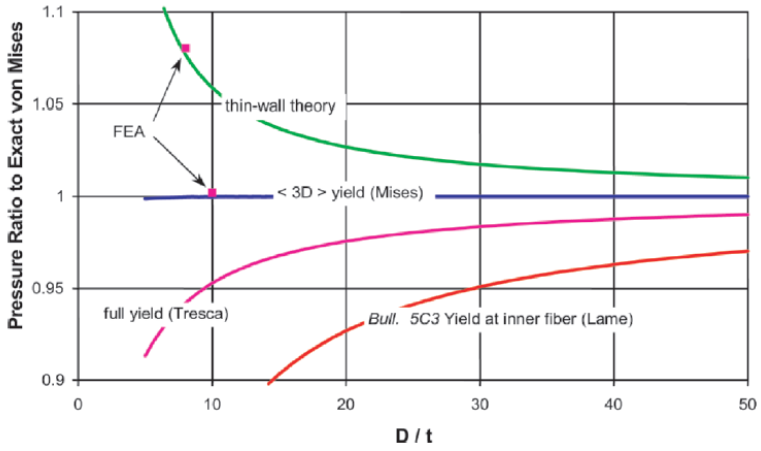

Figure 4.12: Yield strength collapse equation comparison (Klever and Tamano 2006)

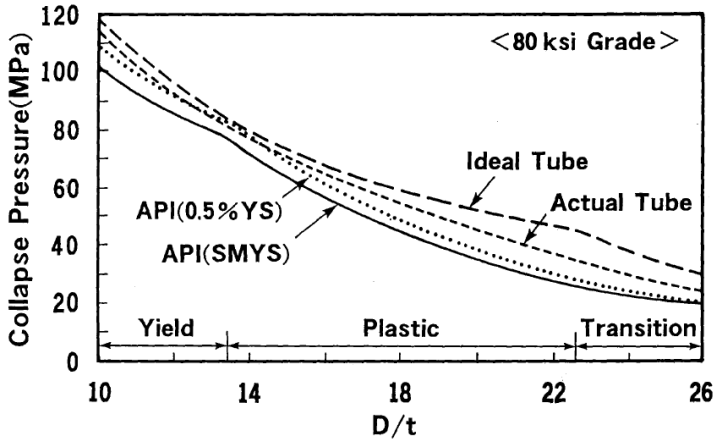

Figure 4.13: Elasto-plastic and API collapse pressure comparison (Kuriyama and Mimaki 1994)

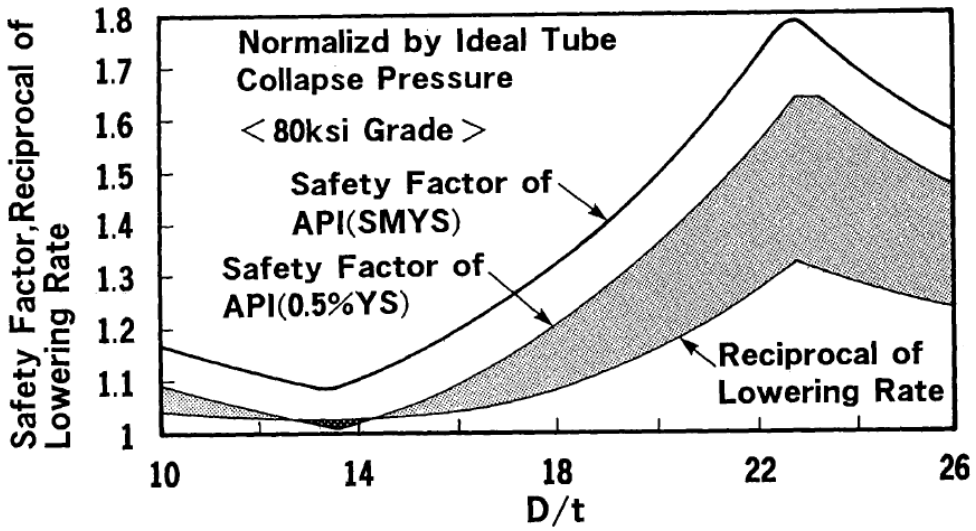

Figure 4.14: Collapse pressure margins normalized by ideal pipe (Kuriyama and Mimaki 1994)

The collapse resistance of a pipe is affected by the original ovality of the pipe, yield strength, and D/t value. In the case of the Abbassian and Parfitt model which is based on pre-collapse ovalization followed by the plastic collapse, the elastic ovalization is affected by the original ovality, plastic collapse is affected by the yield strength, and the D/t value affects both (Abbassian and Parfitt 1995). **Figure 4.15a-c** shows increasing ovality brings down the elastic ovalization curve resulting in a decreased collapse pressure, increasing yield strength raises the plastic collapse curve resulting in an increase in collapse pressure, and increasing D/t reduces both the elastic ovalization and plastic collapse curves resulting in an overall decrease in collapse pressure.

Figure 4.16 shows the comparison of the actual collapse data from full-scale testing to the calculated collapse predictions from the 4-hinge model on the left and the ratio of the calculated collapse prediction/actual collapse data versus the D/t value on

the right. **Figure 4.17** shows the same graphs for the API calculated collapse predictions. The grouping of the test data versus calculated values more closely resembles the trend line for the 4-hinge model compared to the API calculated values. Also, the trend line for the calculated/actual versus D/t value graph is horizontal at a value just above 1 for the 4-hinge model, whereas the trendline slopes downward toward higher D/t values for the API calculated values (Abbassian and Parfitt 1995). This indicates that the 4-hinge model is fairly accurate in predicting real collapse values, but the API calculations over predict collapse resistance for low D/t values and under predict collapse resistance for high D/t values.

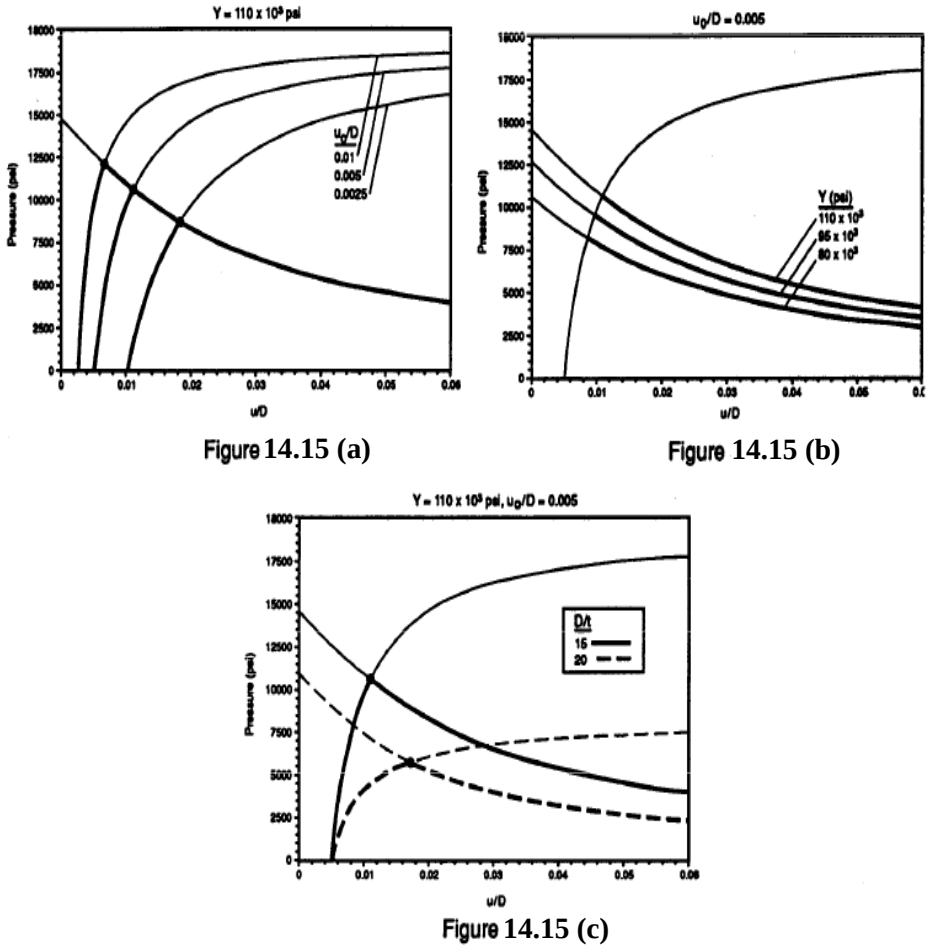

Figure 14.15 (a)

Figure 14.15 (b)

Figure 14.15 (c)

Figure 4.15: Effect of original ovality (a), yield strength (b), and D/t value (c) on collapse pressure (Abbassian and Parfitt 1995)

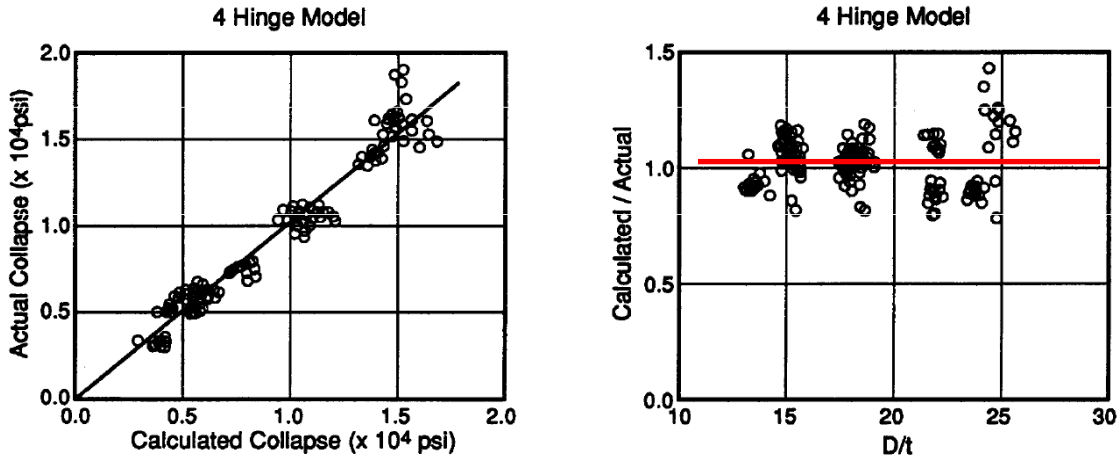

Figure 4.16: 4-hinge model versus test data (Abbassian and Parfitt 1995, modified)

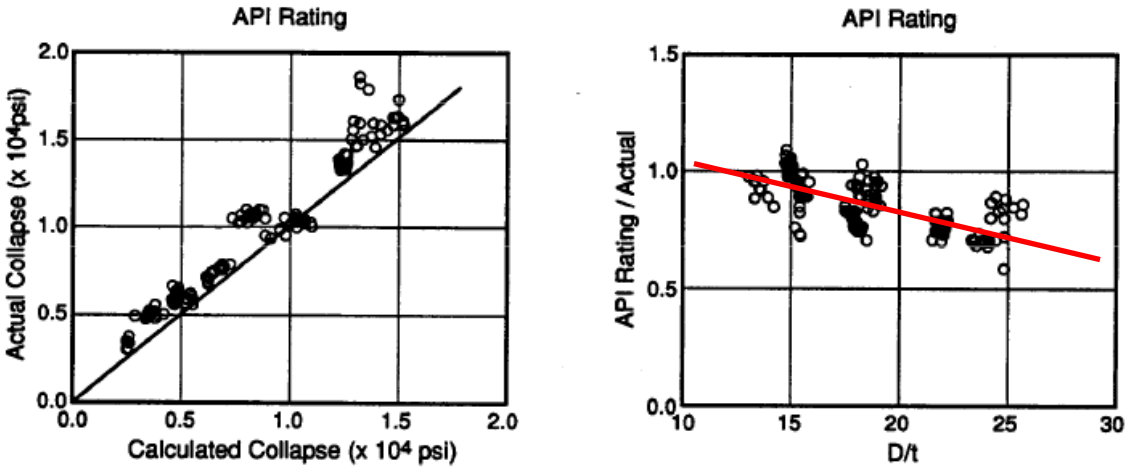

Figure 4.17: API collapse prediction versus test data (Abbassian and Parfitt 1995, modified)

Figure 4.18 shows the observed collapse data normalized by the Ju et al. design equation versus the normalized D/t value. **Figure 4.19** shows the observed collapse data normalized by the Ju et al. resistance equation which takes in to account the actual measurements of wall thickness, yield strength, and initial ovality of a real pipe versus the normalized D/t value (Ju et al. 1998). In both cases, the trendline is horizontal

indicating that the model is accurate for the entire range of applicable D/t values. In the case of the design equation, the trendline sits close to 1.3 revealing a near constant underprediction of real collapse values. For the resistance equation, the trendline sits much closer to 1 which confirms the accuracy of the resistance equation in predicting real collapse values.

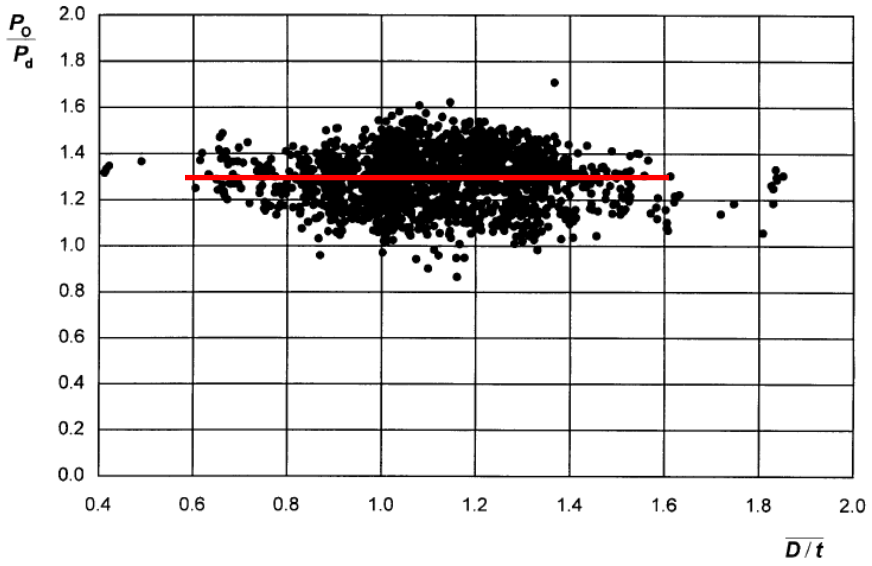

Figure 4.18: Observed collapse data normalized by the design equation (Ju et al. 1998)

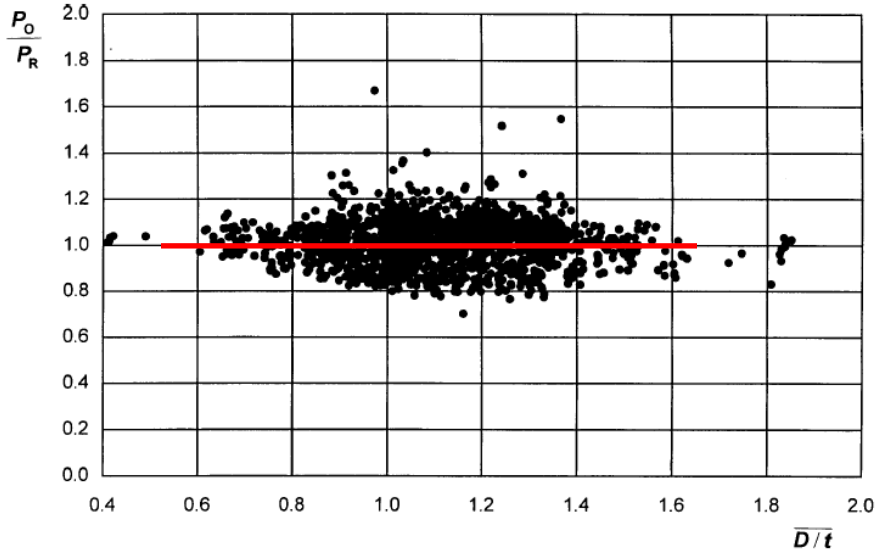

Figure 4.19: Observed collapse data normalized by the resistance equation (Ju et al. 1998)

Figure 4.20 shows the probability of failure given collapse pressure predictions obtained with the API 5C3 equations for four different pipe grades (K-55, L-80, P-110, Q-125). For a D/t value of 12, the probability of failure is roughly 5% on average. This means roughly one in twenty pipes will be expected to fail at this low D/t value, which is unacceptably high. For a D/t value of 40, the probability of failure is only 0.01% (Ju et al. 1998). While a low probability of failure is good for peace of mind for the casing design, such an underprediction of collapse resistance will result in an unnecessarily over-built and costly design.

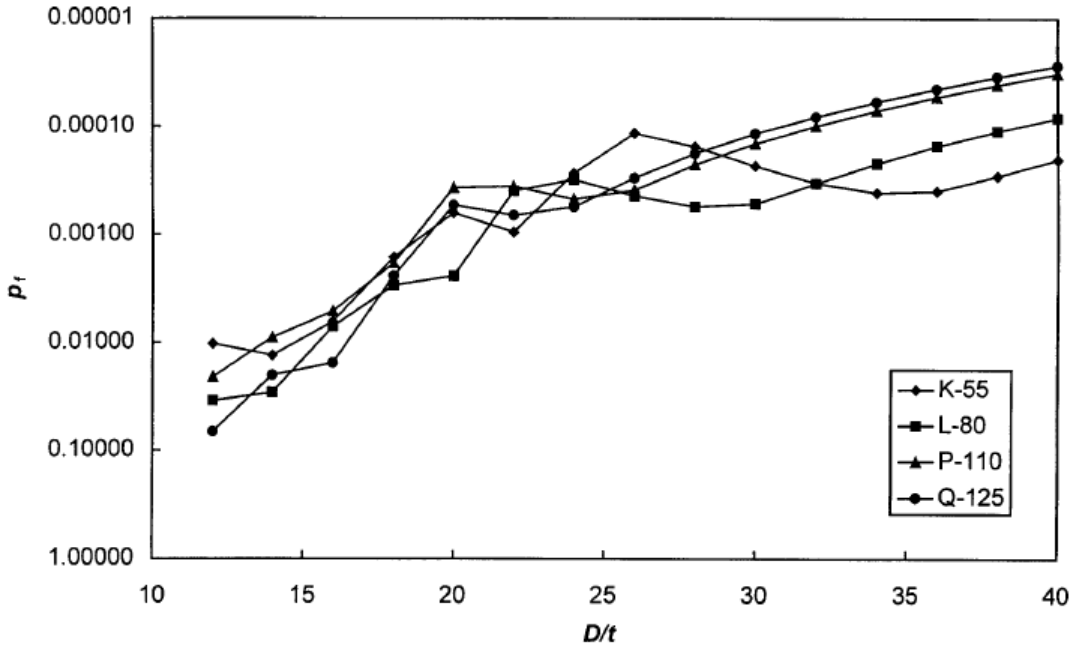

Figure 4.20: Probability of failure for four different pipe grades using API equations (Ju et al. 1998)

Given a design factor (DF) equal to 1, **Figure 4.21** shows the probability of failure for the same four pipe grades shown in **Figure 4.20** using the Ju et al. design equation.

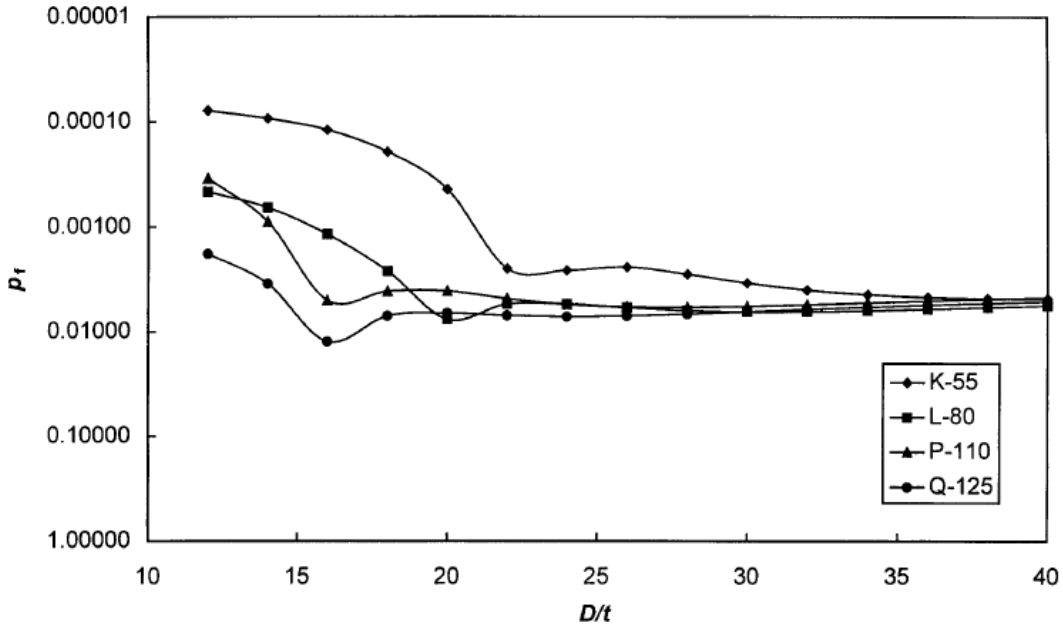

Figure 4.21: Probability of failure for four different pipe grades using the design equation (Ju et al. 1998)

The design equation is more conservative for low D/t values with a range of failure probabilities from 0.01% to 0.1%. For the range of D/t values from 23 to 40, the design equation is fairly consistent in failure probability with a value of 0.8%.

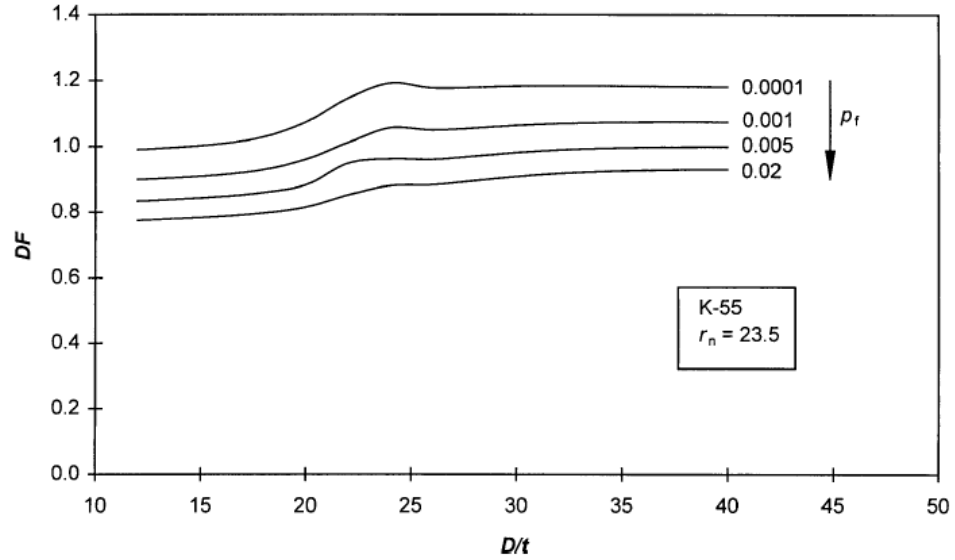

Figure 4.22: Value of DF given desired failure probability, K-55 (Ju et al. 1998)

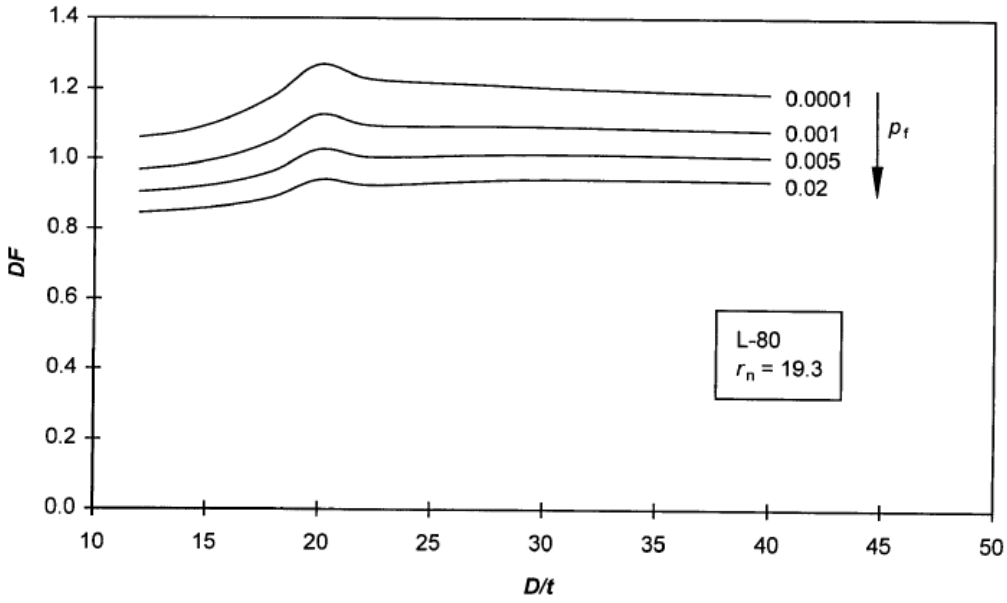

Figure 4.23: Value of DF given desired failure probability, L-80 (Ju et al. 1998)

Figures 4.22 and 4.23 show how a design factor can be chosen for use in the design equation by correlating it to the desired value of failure probability for pipe grades K-55 and L-80, respectively. In both cases, decreasing the probability of failure requires increasing the design factor.

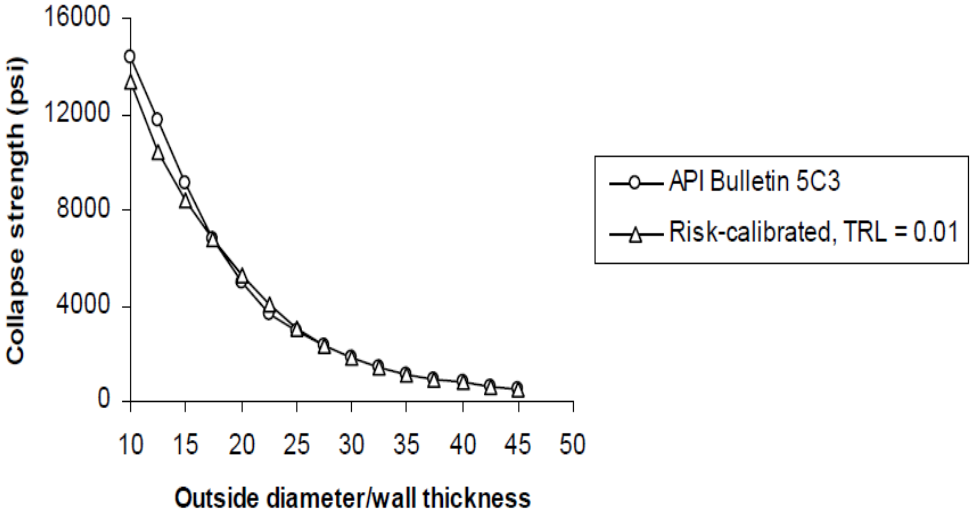

Figure 4.24: Comparison of Adams et al. model and API equations (Adams et al. 1998)

Table 4.4: Down-rating factors (after Adams et al. 1998)

Grade	k_y	k_e
K-55	0.865	0.775
N-80	0.915	0.775
P-110	0.810	0.775

Figure 4.24 shows a comparison of collapse pressures for the Adams et al. model given a constant failure probability of 0.01 and the k_e and k_y values given in **Table 4.4** against the collapse pressure predictions calculated with the API equations. Again this shows the overestimation of collapse resistance for low D/t values by the API equations.

Finite element analysis (FEA) is sometimes used to gauge the accuracy of collapse models against real pipes. **Figure 4.25** shows a comparison of FEA values for D/t value 8, 10, and 40, against the Klever and Tamano collapse model. The FEA values describe the case of both zero axial strain and zero axial load individually:

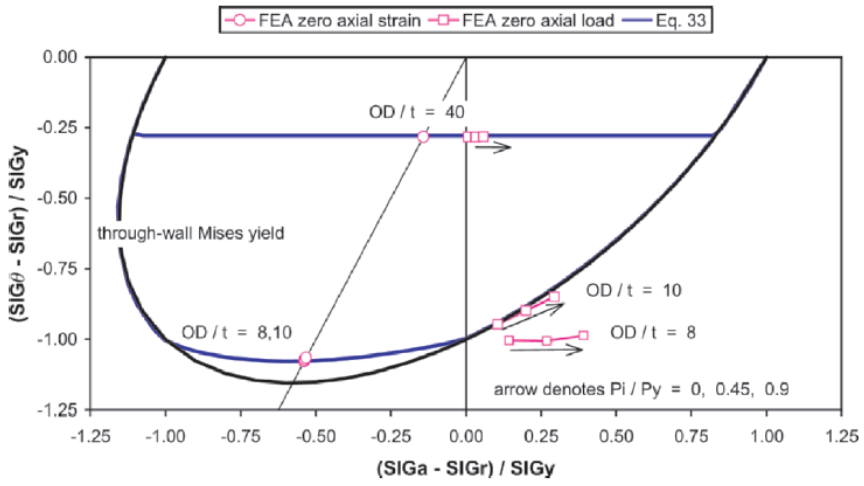

Figure 4.25: FEA compared with model curves (Klever and Tamano 2006)

In the case of zero axial strain, elastic and yield collapse are function of pressure differential only. For D/t values 8 and 10, the FEA predicts collapse pressure just inside the von Mises through-wall yield envelope. This is well modeled by the average between the von Mises and Tresca criteria given by the blue line. For the D/t value of 40, Eq. 4.15 closely matches the FEA when used with a c value of 6 as seen by the blue line (Klever and Tamano 2006). For zero axial load, the effect of internal pressure on yield collapse is a function of the axial load. For D/t value10, the FEA closely follows the von Mises envelope and the pressure differential depends on the internal pressure. FEA predicts the yield collapse resistance of D/t value 8 to be beyond what is predicted by the von Mises envelope with increasing internal pressure. This is a result of the effect of work hardening increasing the material strength beyond yield strength. For D/t value, the collapse pressure differential is independent of axial load, resulting in the horizontal blue line.

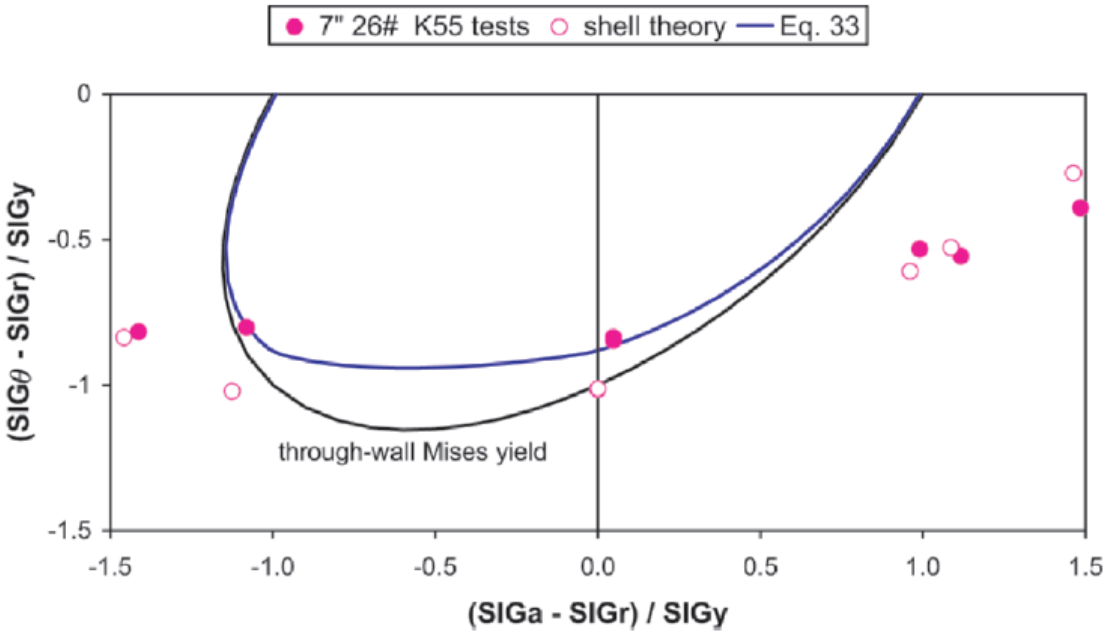

Figure 4.26: Effect of work hardening on collapse resistance (Klever and Tamano 2006)

Figure 4.26 further shows the effect of work hardening on collapse resistance. Inside the yield envelope, the Klever and Tamano collapse model (blue line) accurately predicts real collapse pressures. Beyond the yield envelope in the work hardening regions, the shell-theory model for perfect pipes does an adequate job of predicting true collapse.

An effective method for analyzing the sensitivity of collapse resistance to internal pressure is to examine the derivative to internal pressure of the collapse pressure differential. Eq. 4.37 shows the constant value of this derivative used by the API 5C3 Bulletin:

$$\left.\frac{\partial\, \Delta p^c}{\partial\, p_i}\right|_{API\ Bull.5C3} = -2\frac{t}{D} \tag{4.37}$$

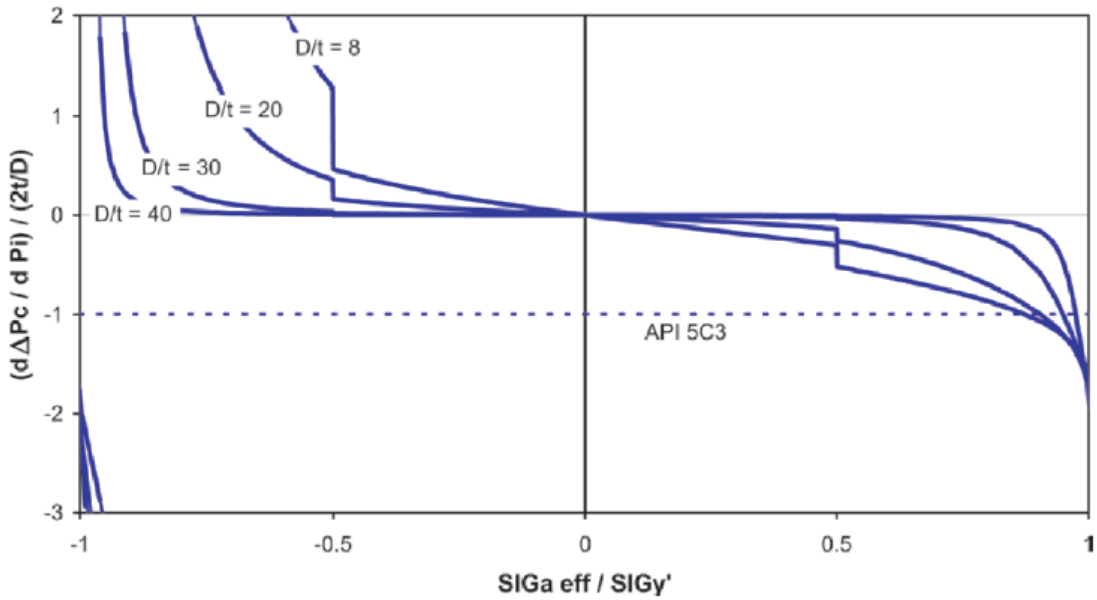

Figure 4.27: Effect of effective axial load on pressure differential gradient (Klever and Tamano 2006)

Effective axial load is given as Eq. 4.38:

$$\sigma_{a\,eff} = F_{eff}/(2\pi Rt) \tag{4.38}$$

Figure 4.27 shows when the pipe is in axial tension, increasing internal pressure decreases the collapse pressure differential. Conversely, when the pipe is in compression, increasing internal pressure increases the collapse pressure differential (Klever and Tamano 2006). This means that although increasing internal pressure will increase collapse resistance, the amount of increase in resistance will not be linearly related to internal pressure increase. The degree to which internal pressure will affect collapse resistance is related to D/t. The effect is great in lower D/t pipes, whereas high D/t pipes are mostly affected by pressure differential only. This characteristic is also well illustrated by **Figure 4.28** where high D/t pipes show little difference in collapse pressure differential throughout the effective axial load range, whereas the collapse pressure differential of low D/t pipes is greatly affected by the effective axial load**.** The discontinuity of the curves in **Figure 4.27** is due to the transition from the average of the von Mises and Tresca criteria to the von Mises value alone (Klever and Tamano 2006).

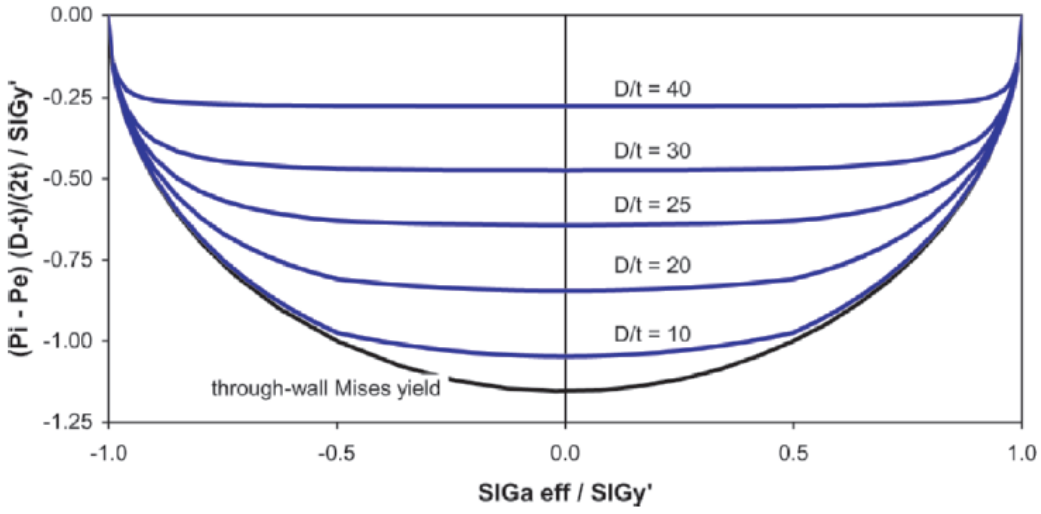

Figure 4.28: Effect of effective axial load on collapse pressure differential (Klever and Tamano 2006)

As in **Figure 4.27**, **Figure 4.28** shows the effect of combined loading (axial load and internal pressure) is greater for low D/t pipes as compared to high D/t pipes.

4.3.2 Model to Model Comparison

The comparison of individual models to one another provides the opportunity to find the best model. Finding the best model involves visual inspection of collapse curves as well as examination of the average predicted collapse values compared to observed data and the standard deviation of the predicted collapse data from the test data. **Figure 4.29** shows a comparison of the Sun equations for initial yield and through-wall yield to the API initial yield and Tamano et al. through wall yield equations:

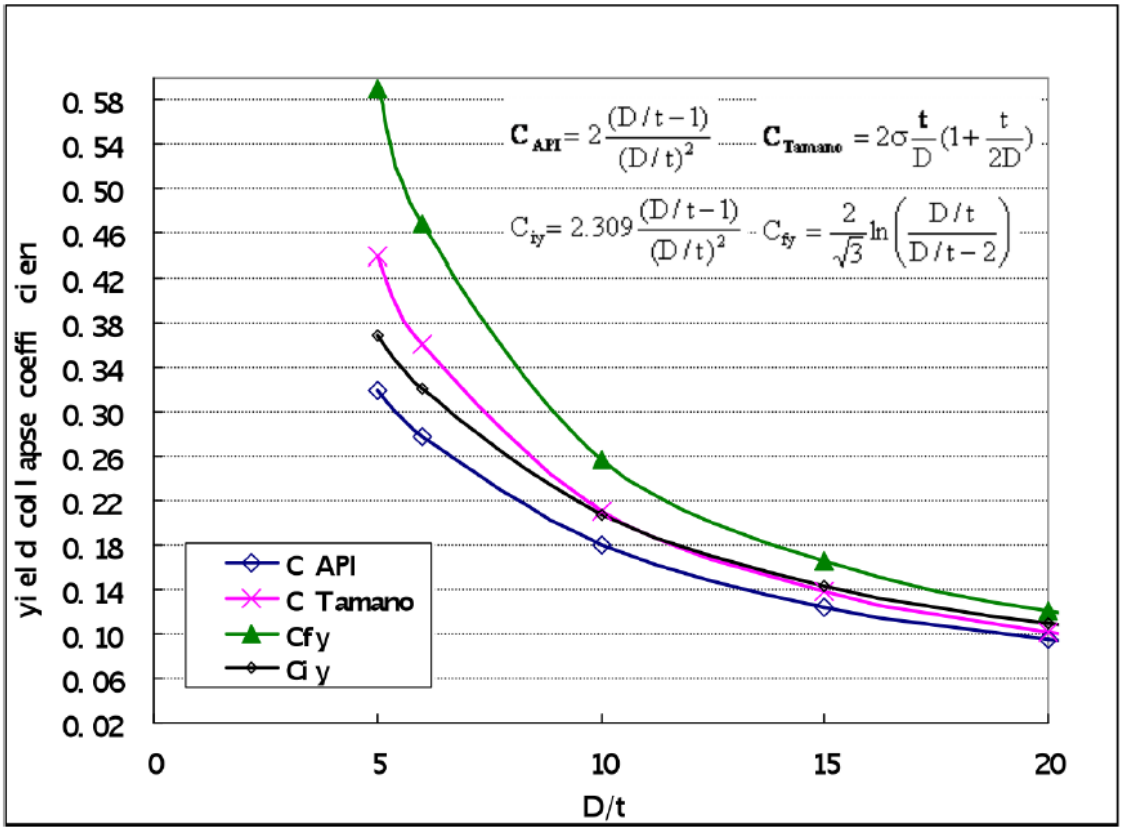

Figure 4.29: Comparison of Sun, API, and Tamano et al. yield equations (Sun 2010)

The equations proposed by Sun show collapse pressures greater than the API and Tamano et al. equations for all applicable values of D/t. Broadly speaking, true increases in collapse resistance would translate to the ability to use lighter or lower grade pipes downhole, resulting in a more economical casing design. However, in this case the proposed equations are based purely on theory and do not have the same ability to account for imperfections or curve fitting to real data as the Tamano equation.

Figure 4.30 shows the comparison of the elasto-plastic collapse model with the theoretical Clinedinst elastic collapse equation (Elastic Collapse), API 5C3 yield strength collapse (Yield Onset), and the Tamano et al. yield collapse with *fac* = 1.47 (General Yield). FEA closely follows the elasto-plastic curve:

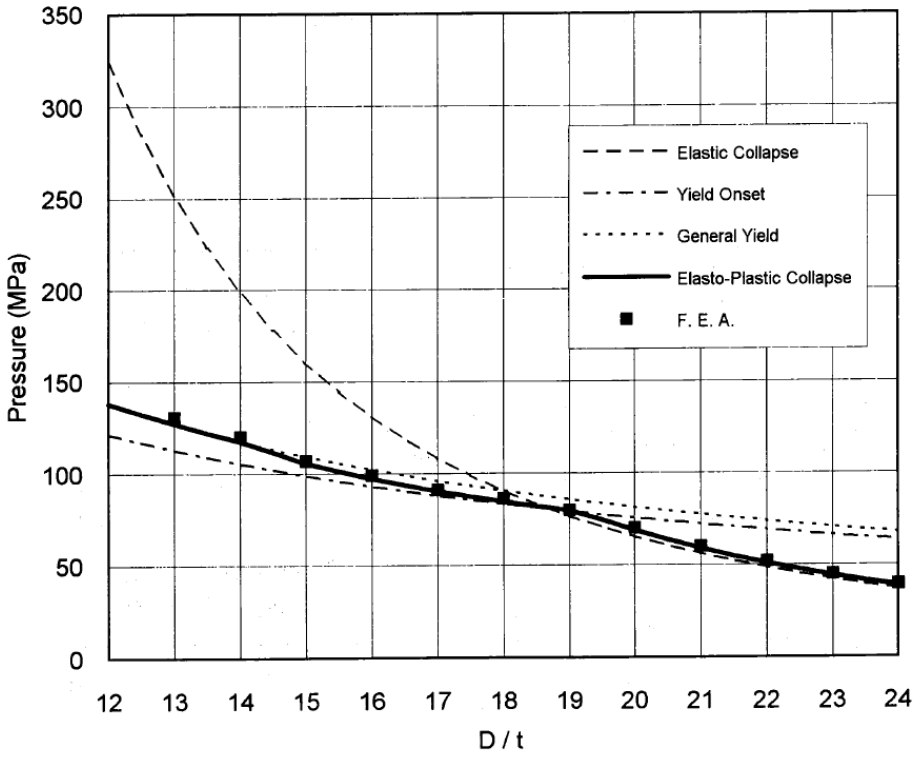

Figure 4.30: Comparison of elasto-plastic collapse with theoretical elastic, API yield, and Tamano et al. yield (Kuriyama and Mimaki 1994)

Figure 4.31 shows four different equations for collapse pressure scaled with the reference pressure found in Eq. 4.39:

$$p^{ref} = 2\xi min\left\{\sigma_y, \frac{E}{1-\nu^2}\xi^2\right\} \tag{4.39}$$

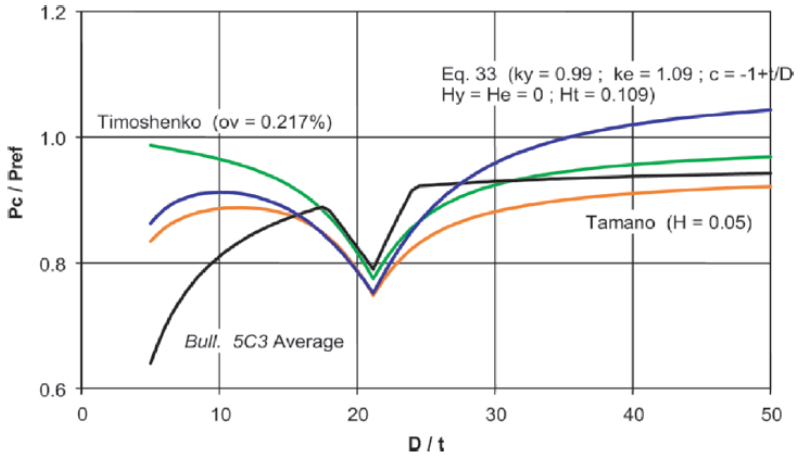

Figure 4.31: Comparison of four collapse pressure models for L-80 pipe (Klever and Tamano 2006)

The four models included in **Figure 4.31** are the Timoshenko model with ovality = 0.217%:

$$(p_e^c)^2 - \left[p_{thin}^{yc} + \left(1 + \frac{3ov}{2\xi}\right)p_{thin}^{ec}\right]p_e^c + p_{thin}^{yc}p_{thin}^{ec} = 0 \tag{4.40}$$

Tamano et al. model with H = 0.05:

$$(p_e^c)^2 - (p^{ycT} + p^{ycT})p_e^c + (1-H)p^{ycT}p^{ecT} = 0 \tag{4.41}$$

Klever and Tamano model with k_y = 0.99, k_e = 1.09, c = -1 + t/D, H_y = H_e = 0, and H_t = 0.109, and the API 5C3 average collapse values. In this comparison, the Klever and Tamano model predicts greater collapse resistance than the other models for high D/t values and falls between Tamano and Timoshenko for low D/t values. For all the models the dip in the middle is due to the increased effect of pipe imperfections on collapse resistance in the transition zone.

Figure 4.32 shows actual strength versus predicted strength for six different collapse pressure models (API 5C3 with mean values, API 5C3 mean/Clinedinst 1985 plastic, Tamano et al. 1983, Tokimasa and Tanaka 1986, Issa and Crawford 1993, Abbassian and Parfitt 1995). This figure shows the Tamano et al. 1983 model has the tightest grouping to the trendline:

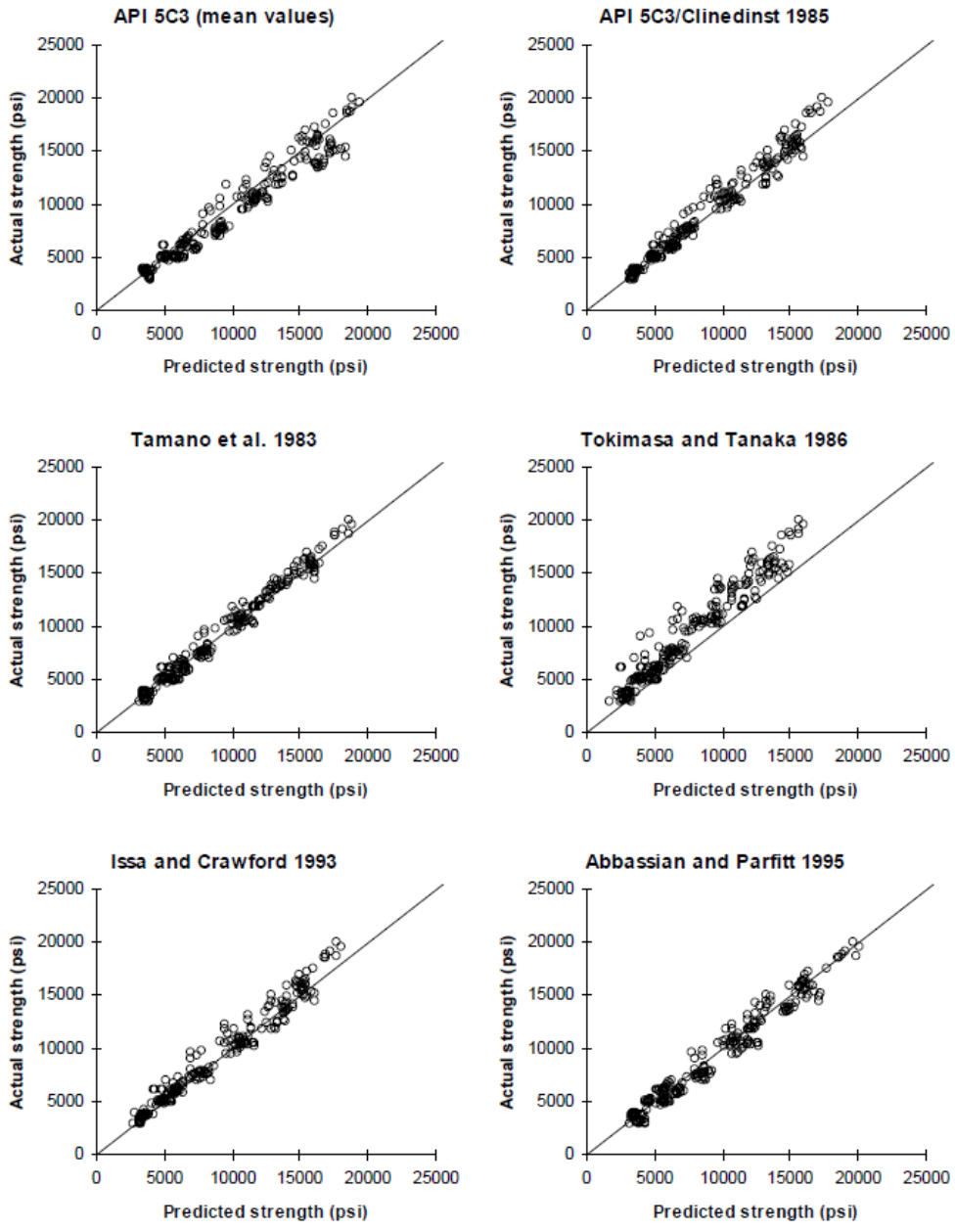

Figure 4.32: Actual versus predicted strength for six models (Adams et al. 1998)

Model comparisons based on the mean and standard deviation for predicted/actual collapse pressure can be seen in **Table 4.5**:

Table 4.5: Model comparison with full-scale test data (Abbassian and Parfitt 1995)

Approaches	Mean (Predicted/Actual)	Standard Dev. (Predicted/Actual)
Present Model	0.998	0.117
Tamano et. al.[15]	0.979	0.088
Clinedinst [4]	0.925	0.081
Tokimasa & Tanaka [3]	0.823	0.087
Issa & Crawford [8]	0.854	0.109

Similar to **Table 4.5**, **Table 4.6** uses the mean of predicted/actual collapse pressure, but instead of standard deviation, the coefficient of variance (COV) is used (Adams et al. 1998). COV = standard deviation/mean.

Table 4.6: Model comparison of predictive accuracies (after Adams et al. 1998)

Model	Mean	COV
API 5C3 (mean values)	1.036	0.133
API 5C3 (mean yield, mean elastic)/Clinedinst 1985 (plastic)	1.028	0.081
Abbassian and Parfitt 1995	0.976	0.105
Tamano et al. 1983	1.002	0.083
Tokimasa and Tanaka 1986	1.244	0.164
Issa and Crawford 1993	1.042	0.094

Based on these comparisons, it is evident that the Tamano et al. 1983 model gives the best combination of near-unity mean and low variance in collapse pressure predictions. By incorporating new decrement functions and bias factors, the Klever and Tamano 2006 model provides the ability to incorporate combined loading and pipe imperfections to make the most accurate prediction of true pipe collapse pressures. Therefore, it can be concluded that the Klever and Tamano model is the best predictive method for collapse pressures to date.

Chapter 5: Yield Strength Acquisition Method

Now that the Klever and Tamano collapse equation has been shown as the most accurate, the second step is to develop a simple, repeatable, and more cost-effective method for finding the yield strength of any given pipe. Beyond the decrement functions and bias factors, yield strength is the biggest factor in determining the true collapse pressure. The API defined pipe grades exist for a range of yield strengths corresponding to a single grade as given in API 5CT, but the nominal yield strength is most often used in collapse resistance calculations. **Tables 5.1, 5.2,** and **5.3** show how the yield strengths of real pipes deviate from the nominal strengths. In each table, "Avg" is the average value of measured yield strength/nominal yield strength.

Table 5.1: Yield strength deviation from nominal, Drilling Engineering Association data set (Brechan et al. 2018)

Grade	J/K-55*	L-80*	N-80*	P-110*	Q-125*	API Seamless* **
Samples	27	15	26	15	9	50
Avg	1.2120	1.0687	1.1808	1.1432	1.1010	1.1322
Std	0.0520	0.0378	0.0642	0.0306	0.0625	0.0618

Table 5.2: Yield strength deviation from nominal, ISO HRS data set (Brechan et al. 2018)

Hot	Grade	J/K-55	L-80	N-80	P-110	Q-125	
Rotary	Avg	–	1.10	1.21	1.10	1.10	
Straightened	Std	–	0.04642	0.049005	0.0396	0.03619	

Table 5.3: Yield strength deviation from nominal, ISO CRS (Brechan et al. 2018)

Cold	Grade	J/K-55	L-80	N-80	P-110	Q-125
Rotary	Avg	1.23	1.10	1.21	1.10	1.10
Straightened	Std	0.08844	0.05819	0.06183	0.05104	0.04752

The deviation from the nominal yield strength can be seen further for P-110 pipe in **Figure 5.1** for the Drilling Engineering Association (DEA) data set and **Figure 5.2** for the ISO data set. These figures show that the real yield strength of these pipes is around 13-15% of the nominal yield strength. Using the nominal yield strength in calculations will consistently under-predict collapse resistance. This results in an excessive safety margin that leads to over the top, sometimes uneconomical casing designs.

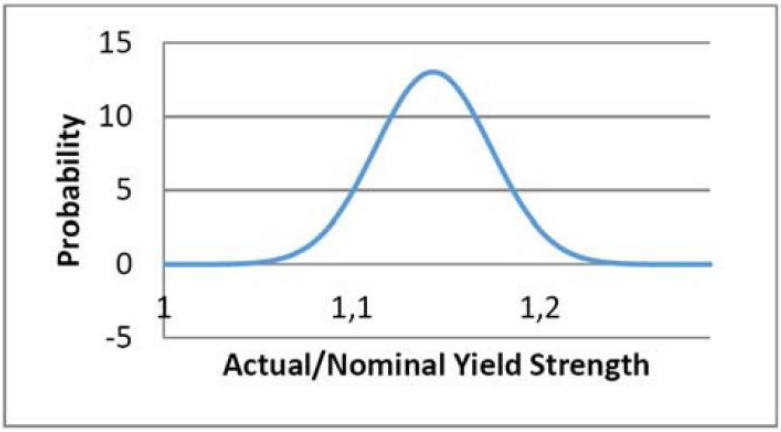

Figure 5.1: Actual/Nominal yield strength, DEA data set (Brechan et al. 2018)

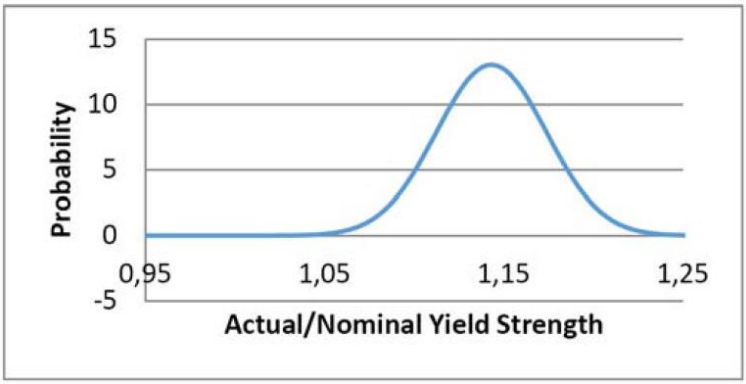

Figure 5.2: Actual/nominal yield strength, ISO data set (Brechan et al. 2018)

It is important to be able to calculate the true collapse resistance of the casing and then apply an appropriate design factor to limit any wasting of excessive strength. The ranges of yield strengths in API grades are the product of the variability in the manufacturing processes of pipes when the standard was adopted in the 1960s, as previously discussed. Improvements in these manufacturing processes enables tighter tolerances to be applied to material properties.

Ideally, the yield strengths of the individual pipes going into the hole would be known before the casing design is made. However, with the infrequency of testing means we are unable to say with much certainty what individual pipe characteristics may be without inherent risk. The infrequency of testing is a result of the large expense that comes with testing. Test specimens must be cut to exact dimensions and then tested axially, or specialized equipment must be used that can handle the curved surfaces of a full section specimen. Additionally, all test specimens are tested for yield strength in the axial direction. As previously discussed, collapse is a function of the yield strength in the hoop direction.

The newly proposed testing method aims to simplify the testing procedure and find yield strength in the hoop direction. Simplifying the test procedure should drive down testing costs and hopefully encourage an increase in the frequency of testing. Finding yield strength in the hoop direction should further increase the accuracy of collapse predictions.

5.1 Experimental Setup

The new yield strength acquisition is based on the simple idea of crushing the pipe and analyzing the force versus displacement curve. The experimental setup started

with a 50-ton hydraulic shop press shown in **Figure 5.3**. To ensure consistent crushing, a steel test apparatus was used, consisting of two steel plates and four steel guide rails as shown in **Figure 5.4**. **Figure 5.5** shows a 3D model of what the apparatus should look like when loaded with a test pipe.

Figure 5.3: Hydraulic shop press

Figure 5.4: Steel test apparatus

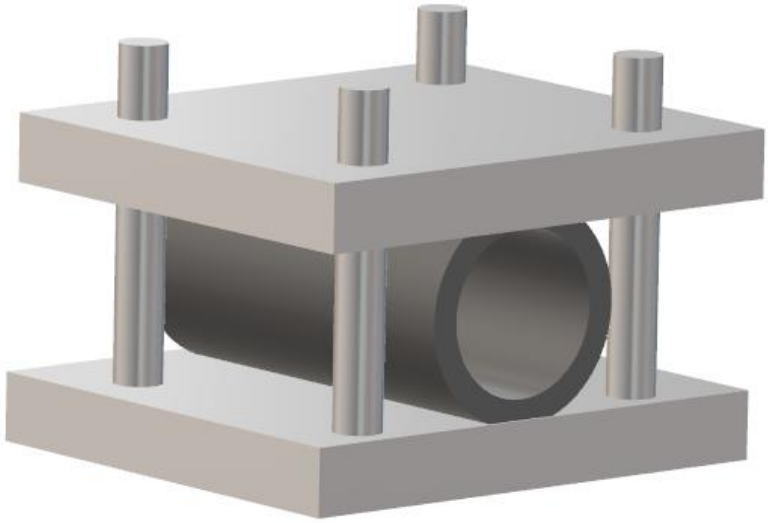

Figure 5.5: Steel test apparatus 3D model

An Omega force gauge with a range of 0-75000 pounds shown in **Figure 5.6** was used to measure the force applied to the pipe. The force gauge was bolted to a circular aluminum plate, so it could then be mounted to the top plate of the test apparatus as shown in **Figure 5.7** and **5.8**.

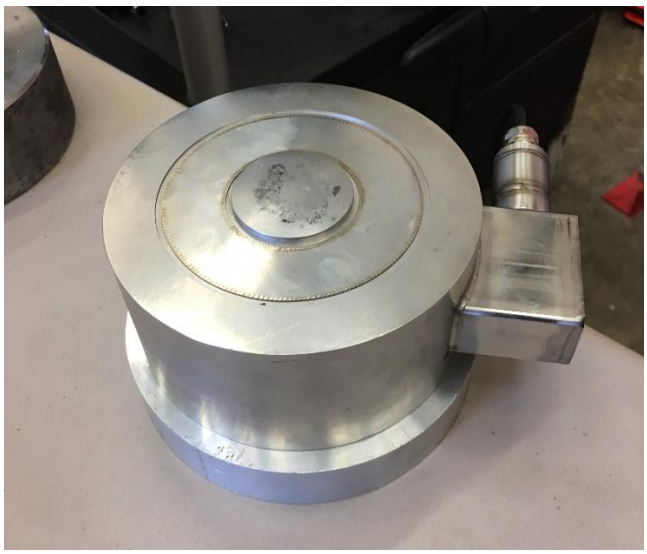

Figure 5.6: Omega force gauge

Figure 5.7: Omega force gauge bolted to aluminum plate

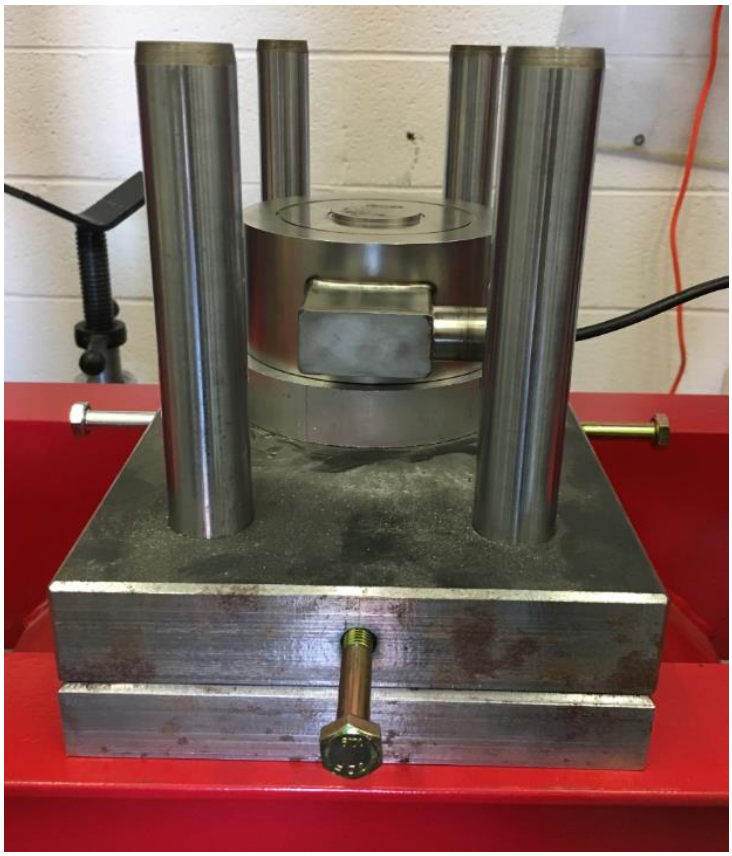

Figure 5.8: Omega force gauge mounted to test apparatus

Holes were then drilled in the support beams of the hydraulic press to incorporate alignment bars as shown in **Figure 5.9** and **Figure 5.10**:

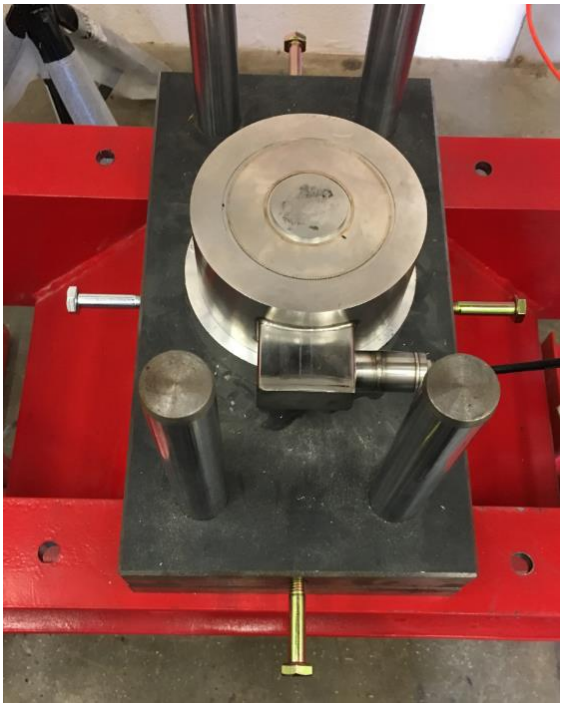

Figure 5.9: Holes drilled in hydraulic press

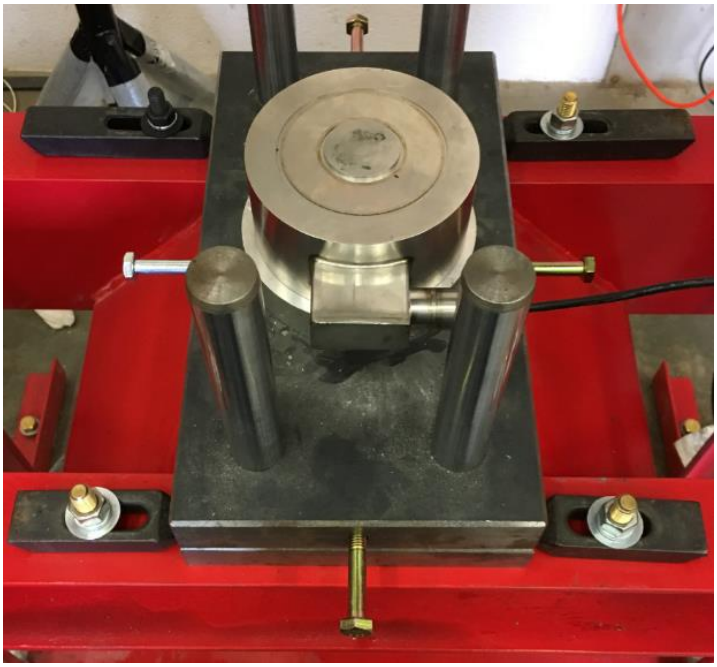

Figure 5.10: Test apparatus with alignment bars

An Omega displacement gauge was used to measure displacement. A cross bar was mounted to the hydraulic ram and the displacement gauge was held in place with clamps so the extensional piece of the gauge stays in contact with the cross bar during the full range of motion of the ram as shown in **Figure 5.11**:

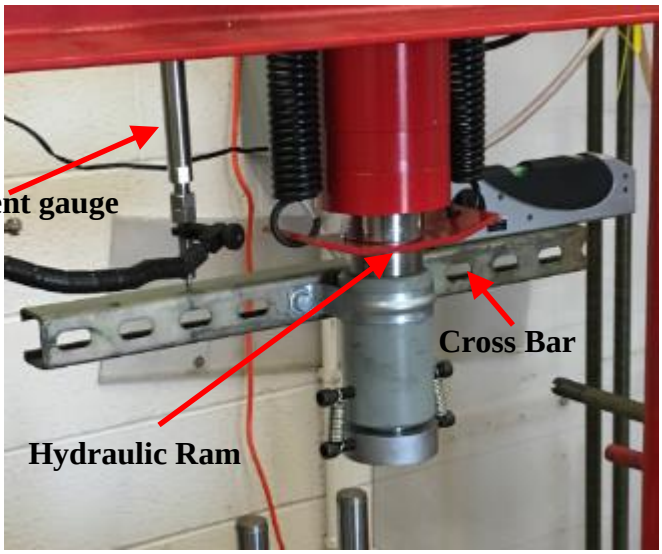

Figure 5.11: Displacement gauge and cross bar

In between tests, the top plate is raised and lowered by using a simple scissor jack mounted to an aluminum plate on top of the press as shown in **Figure 5.12:**

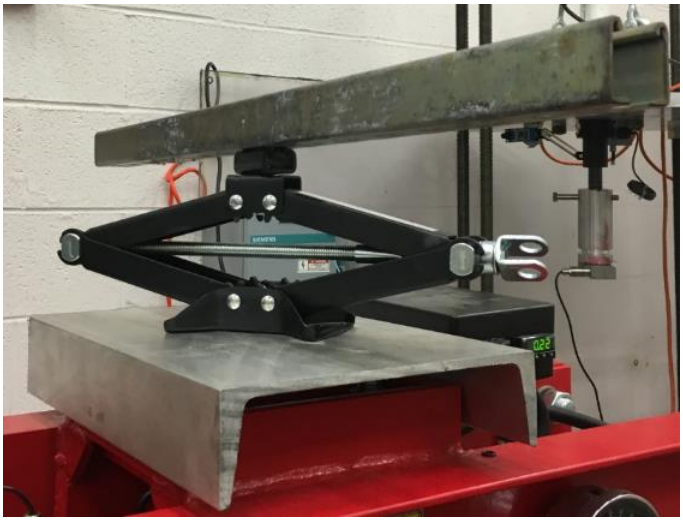

Figure 5.12: Scissor jack on top of the press

Chains are connected from the scissor jack to the top plate of the test apparatus using quick disconnect hooks attached to the bolts in the side of the plate as shown in **Figure 5.13**:

Figure 5.13: Chains attaching top plate to scissor jack

Before testing, the pipe was cut to the appropriate length using a band saw as shown in **Figure 5.14**. For each pipe sample, four test specimens were measured and

cut. Two samples having a length equal to one diameter, and two samples having a length equal to two diameters.

Figure 5.14: Band saw cutting pipe

After cutting, pi tape was used to accurately measure the outer diameter and circumferentially divide the pipe into eight equal sections (A-H) as shown in **Figure 5.15** and **5.16**. A caliper was then used to measure the wall thickness for each of the eight sections at both ends. The caliper was also used to measure outer diameter across the four planes (A-E, B-F-, C-G, D-H). Then, a Positector ultrasonic tool was used to measure wall thickness at multiple points along each of the eight sections as shown in **Figure 5.17**.

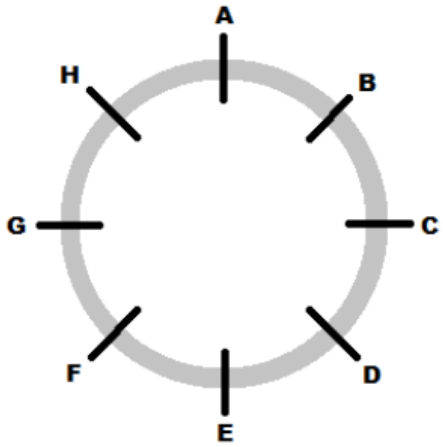

Figure 5.15: Pipe divided into eight equal sections

Figure 5.16: Pipe divided into eight equal sections and marked

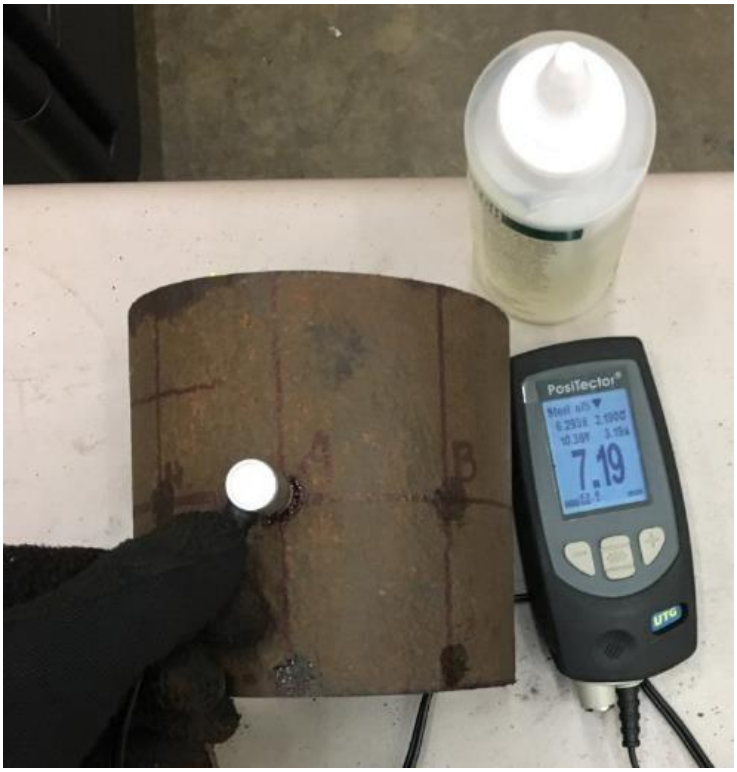

Figure 5.17: Using Positector ultrasonic tool to measure wall thickness

5.2 Test Procedure

1. After initial measurements of the pipe are taken, the pipe is loaded into the test apparatus with the A line pointing up and the E line pointing down in contact with the bottom plate.
2. Using the scissor jack, the top plate is lowered until it is resting on top of the pipe as seen in **Figure 5.18**.
3. Ensure the correct orientation of the pipe (A up, E down) as seen in **Figure 5.19** before lowering the hydraulic ram
4. The hydraulic ram is then lowered until it is just touching the force gauge
5. The Omega data acquisition software is prepared on the laptop with a sampling rate of 5Hz

6. Tare the gauges on the acquisition software to read zero

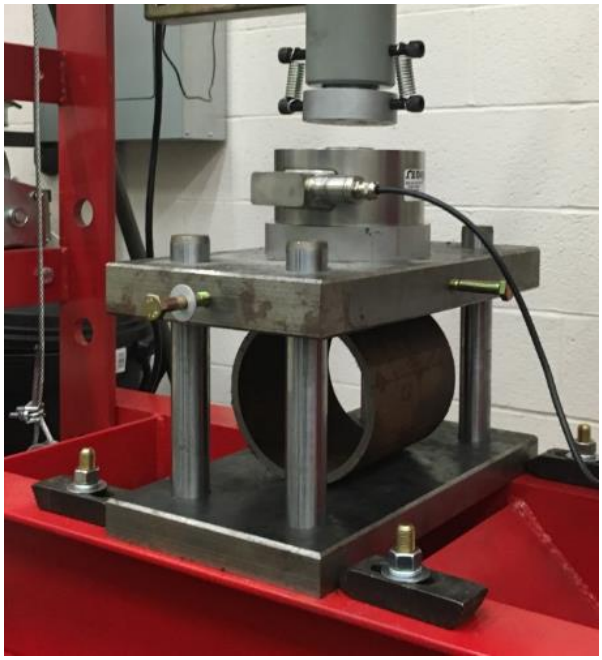

Figure 5.18: Pipe loaded into test apparatus

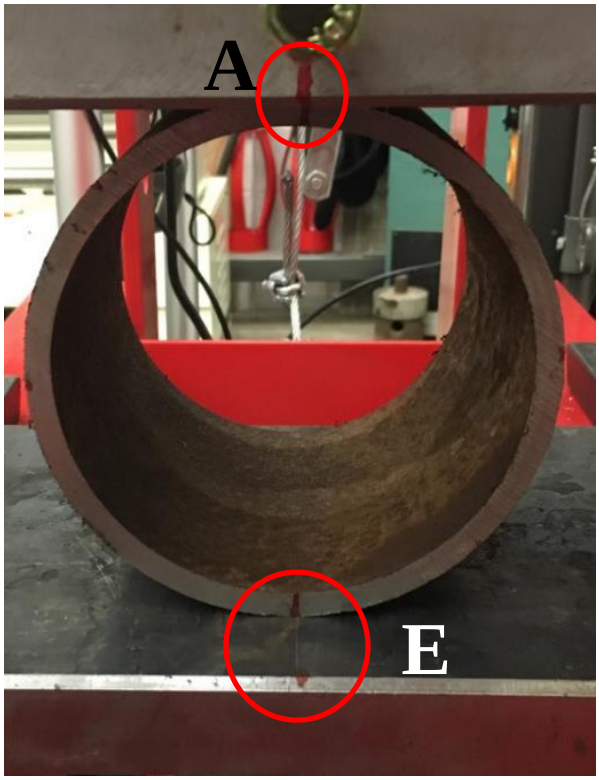

Figure 5.19: Ensure correct pipe orientation

7. Begin collecting data by pressing “Start” on the computer screen
8. Insert the removable handle into the receiver for the small-diameter (slow) plunger on the right-hand side of the pump unit as seen in **Figure 5.20**

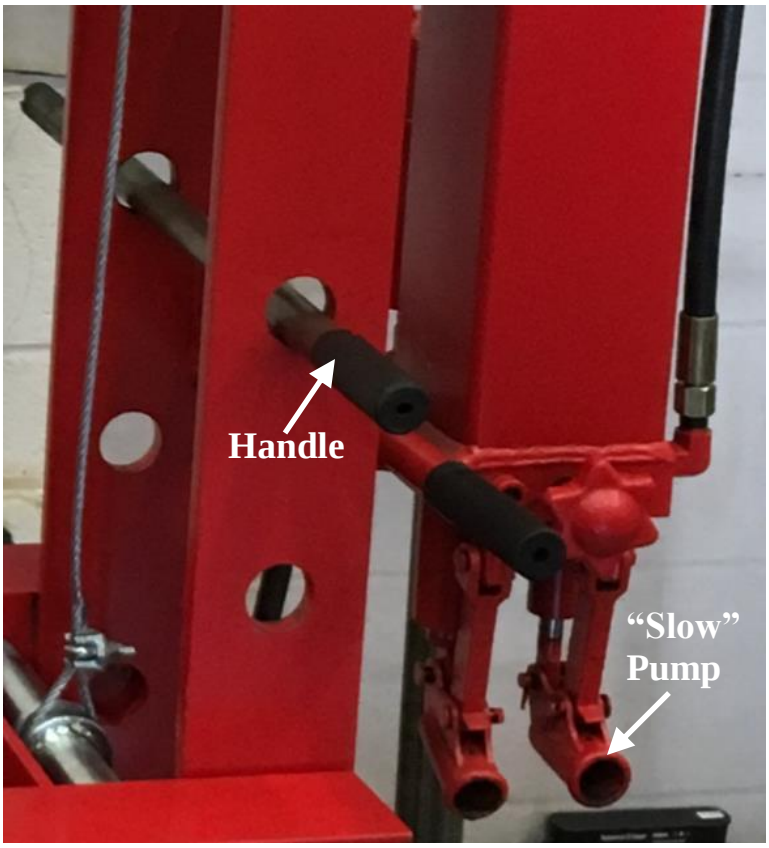

Figure 5.20: Pump layout

9. Begin pumping at a constant rate
10. Pump until the displacement gauge reads 25% of pipe OD
11. Stop pumping, end data collection on the laptop

5.3 Development of the Yield Strength Equation

Initial testing was performed on a 5.5” casing with wall thickness of 0.288”. The initial tests served two purposes: to see if the experimental setup would work and to see if the initial data would provide any clues as how to proceed with the development of

the yield strength equation. The first round of tests was performed using the four specimens with two different lengths (1Da, 1Db, 2Da, 2Db). After testing was completed, it was observed that the force required to crush the 2D samples was roughly twice that needed to crush the 1D samples. The only measured parameter changing from the 1D sample to the 2D sample was the length, which also translates to doubling the cross-sectional area of the pipe.

To find yield strength, a simple model was created to isolate the strain experienced by the pipe to the cross-sectional area of the pipe wall located 90° from the top and bottom plates. This corresponds to sections C and G in **Figure 5.15.** Forces acting at the pipe wall can be thought of as a system of resulting moments acting about a point located at the center of the pipe wall (red dot) as seen in **Figure 5.21**:

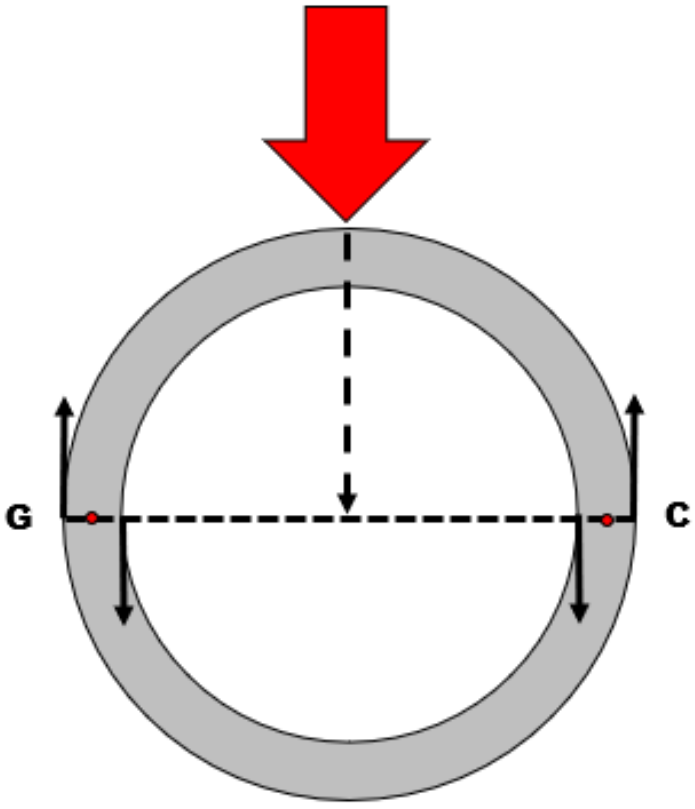

Figure 5.21: Forces occurring at the inner and outer pipe wall

This means the exterior portion of the pipe wall will be in tension, and the interior portion of the pipe wall will be in compression as see in **Figure 5.22:**

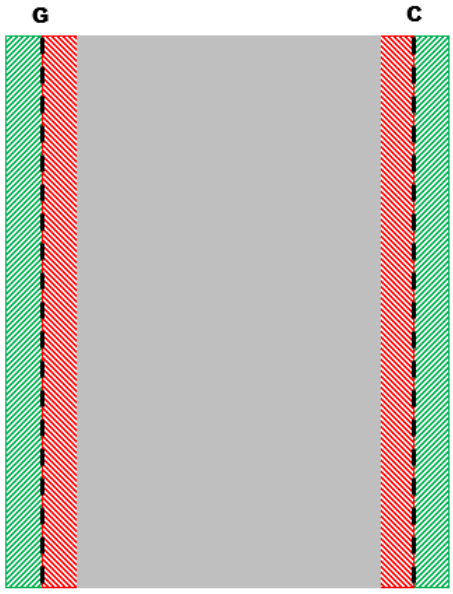

Figure 5.22: Cross-sectional view, pipe wall in tension (green) and compression (red)

A review of moments in the 1990 Bisplinghoff et al. book provides **Figure 5.23:**

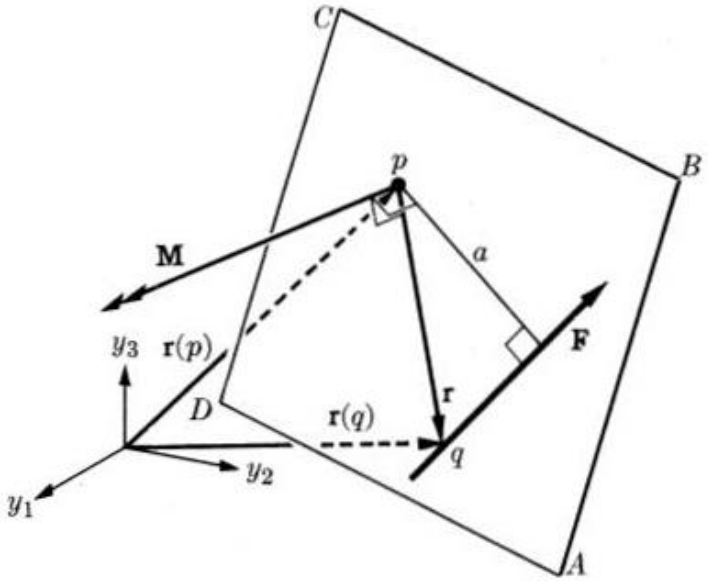

Figure 5.23: Moment of F about point p

From the above figure, the magnitude of the moment of force F about point p can be written as Eq. 5.1:

$$|M| = a|F| \tag{5.1}$$

where,

a = Moment arm

$|F|$ = Force producing the moment about point p

$|M|$ = Magnitude of the moment of F about point p

In the case of the pipe being crushed, the pipe resists strain, so the forces at the interior and exterior wall form a couple moment that is equal and opposite to the moment created by the input force from the press. This can be visualized in **Figure 5.24:**

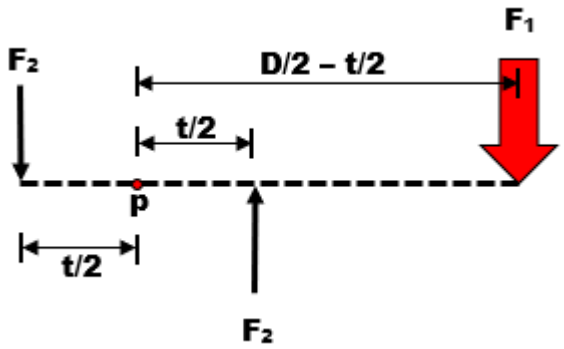

Figure 5.24: Forces associated with pipe crush

In this figure, only one side of the pipe is represented, so F_1 is equal to one half of the input force from the press. F_2 is the force experienced at the interior and exterior surfaces of the pipe wall as a result of the input force. The moment arm for F_1 is D/2-t/2, and the moment arm for each F_2 is t/2. The moments associated with these forces act at point *p*. Using this figure, Eq. 5.2 can be derived in the following manner:

$$0 = {}^{t}/_{2}\,|F_2| + {}^{t}/_{2}\,|F_2| - ({}^{D}/_{2} - {}^{t}/_{2})|F_1|$$

$$({}^{D}/_{2} - {}^{t}/_{2})|F_1| = {}^{t}/_{2}\,|F_2| + {}^{t}/_{2}\,|F_2|$$

$$({}^{D}/_{2} - {}^{t}/_{2})|F_1| = t|F_2|$$

$$|F_2| = \frac{({}^{D}/_{2} - {}^{t}/_{2})|F_1|}{t} \tag{5.2}$$

where,

$|F_1|$ = ½ the force applied to the specimen from the press at the elastic limit, lbs.

$|F_2|$ = Resultant force at the interior and exterior surface of the pipe wall, lbs.

To arrive at the yield strength, the force F_2 must be divided by the appropriate area. In this case, since there is a force present at both the interior and exterior pipe walls, the area should be one half the cross-sectional area of the pipe wall. The result is shown in Eq. 5.3:

$$\sigma_y = \frac{|F_2|}{area/2} \tag{5.3}$$

where,

area = cross sectional area of pipe wall = $l \times t$, in^2

l = length of the test specimen, in

This equation can be simplified further as follows, resulting in Eq. 5.4:

$$\sigma_y = \frac{2({}^{D}/_{2} - {}^{t}/_{2})|F_1|}{lt^2}$$

$$\sigma_y = \frac{(D-t)|F_1|}{lt^2} \tag{5.4}$$

5.4 Results

5.4.1 Finding Yield Strength Empirically

In order to use Eq. 5.4 to find yield strength, we must be able to find the input force from the press at yield. This can be accomplished by finding the force applied at the elastic limit. To do this, the test data from each specimen was plotted on a force versus displacement graph. The linear portion of the graph represents pure elastic deformation. The slope of this linear portion can be thought of as a form of elastic modulus. By finding the point at which the plotted data from the specimen deviates from the straight line, the elastic limit can be found. This means the force of the point at which the data deviates from the elastic modulus line is the force at yield.

Eight different pipe samples were tested, each with four test specimens (1Da, 1Db, 2Da, 2Db). For each test specimen, the data was plotted on a force versus displacement curve with the elastic modulus line. The point of deviation from the line is the elastic limit. The results of this procedure can be seen in **Figure 5.25** through **Figure 5.32**. For simplification, Eq. 5.4 can be applied to create stress versus displacement curves as seen in **Figure 5.33** through **Figure 5.40**.

For the four specimens of the 1.5” pipe, **Figure 5.25** shows the force at yield as 1425 lbs. for both 1D samples, and 2800 and 3000 lbs. for the 2Da and 2Db specimens, respectively. Converted to stress, **Figure 5.33** shows yield stress for specimens 1Da, 1Db, 2Da, and 2Db as 97,033 psi, 94,884 psi, 94,052 psi, and 96,031 psi, respectively.

For the four specimens of the 2 3/8” pipe, **Figure 5.26** shows the force at yield as 6200 and 6600 lbs. for 1Da and 1Db specimens, and 12,400 and 12,800 lbs. for the

2Da and 2Db specimens, respectively. Converted to stress, **Figure 5.34** shows yield stress for specimens 1Da, 1Db, 2Da, and 2Db as 83,360 psi, 79,155 psi, 87,169 psi, and 73,272 psi, respectively.

For the four specimens of the 2 7/8" pipe, **Figure 5.27** shows the force at yield as 5500 lbs. for both 1Da and 1Db specimens, and 11,250 and 11,200 lbs. for the 2Da and 2Db specimens, respectively. Converted to stress, **Figure 5.35** shows yield stress for specimens 1Da, 1Db, 2Da, and 2Db as 55,770 psi, 58,211 psi, 58,005 psi, and 54,978 psi, respectively.

For the four specimens of the 3" pipe, **Figure 5.28** shows the force at yield as 9850 and 10,300 lbs. for 1Da and 1Db specimens, and 20,600 and 19,900 lbs. for the 2Da and 2Db specimens, respectively. Converted to stress, **Figure 5.36** shows yield stress for specimens 1Da, 1Db, 2Da, and 2Db as 73,112 psi, 72,505 psi, 73,410 psi, and 73,116 psi, respectively.

For the four specimens of the 3.5" pipe, **Figure 5.29** shows the force at yield as 3900 and 3800 lbs. for 1Da and 1Db specimens, and 7200 and 7500 lbs. for the 2Da and 2Db specimens, respectively. Converted to stress, **Figure 5.37** shows yield stress for specimens 1Da, 1Db, 2Da, and 2Db as 39,985 psi, 38,867 psi, 37,758 psi, and 38,928 psi, respectively.

For the four specimens of the new 3.5" pipe, **Figure 5.30** shows the force at yield as 5400 and 5450 lbs. for 1Da and 1Db specimens, and 10,950 lbs. for both the 2Da and 2Db specimens. Converted to stress, **Figure 5.38** shows yield stress for specimens 1Da, 1Db, 2Da, and 2Db as 56,489 psi, 57,328 psi, 56,537 psi, and 56,943 psi, respectively.

For the four specimens of the aluminum 3.5” pipe, **Figure 5.31** shows the force at the elastic limit as 5500 lbs. for both the 1Da and 1Db specimens, and 11,000 and 12,000 lbs. for the 2Da and 2Db specimens, respectively. The force at the offset yield point for these specimens is 8600, 8700, 17,900, and 17,800 lbs., respectively. Converted to stress, **Figure 5.39** shows yield stress at the elastic limit for specimens 1Da, 1Db, 2Da, and 2Db as 27,199 psi, 26,865 psi, 26,333 psi, and 28,987 psi. Offset yield strength for these specimens is given as 42,939 psi, 42,503 psi, 42,938 psi, and 42,893 psi respectively.

For the four specimens of the 5.5” pipe, **Figure 5.32** shows the force at yield as 8500 lbs. for both the 1Da and 1Db specimens, and 16,000 and 16,750 lbs. for the 2Da and 2Db specimens, respectively. Converted to stress, **Figure 5.40** shows yield stress for specimens 1Da, 1Db, 2Da, and 2Db as 48,607 psi, 50,272 psi, 51,790 psi, and 51,270 psi, respectively.

In the case of non-ferrous metals, such as aluminum, there will not be a well-defined yield point due to the rounded shape of the stress/strain curve. In this case, an offset yield point must be used. This method uses an offset elastic modulus line shifted some percentage of strain to the right from the original elastic modulus line. Where the offset line intersects the data curve is the actual yield strength. In this case, 5-15% of strain was used as the offset. Further work is required in defining the offset value.

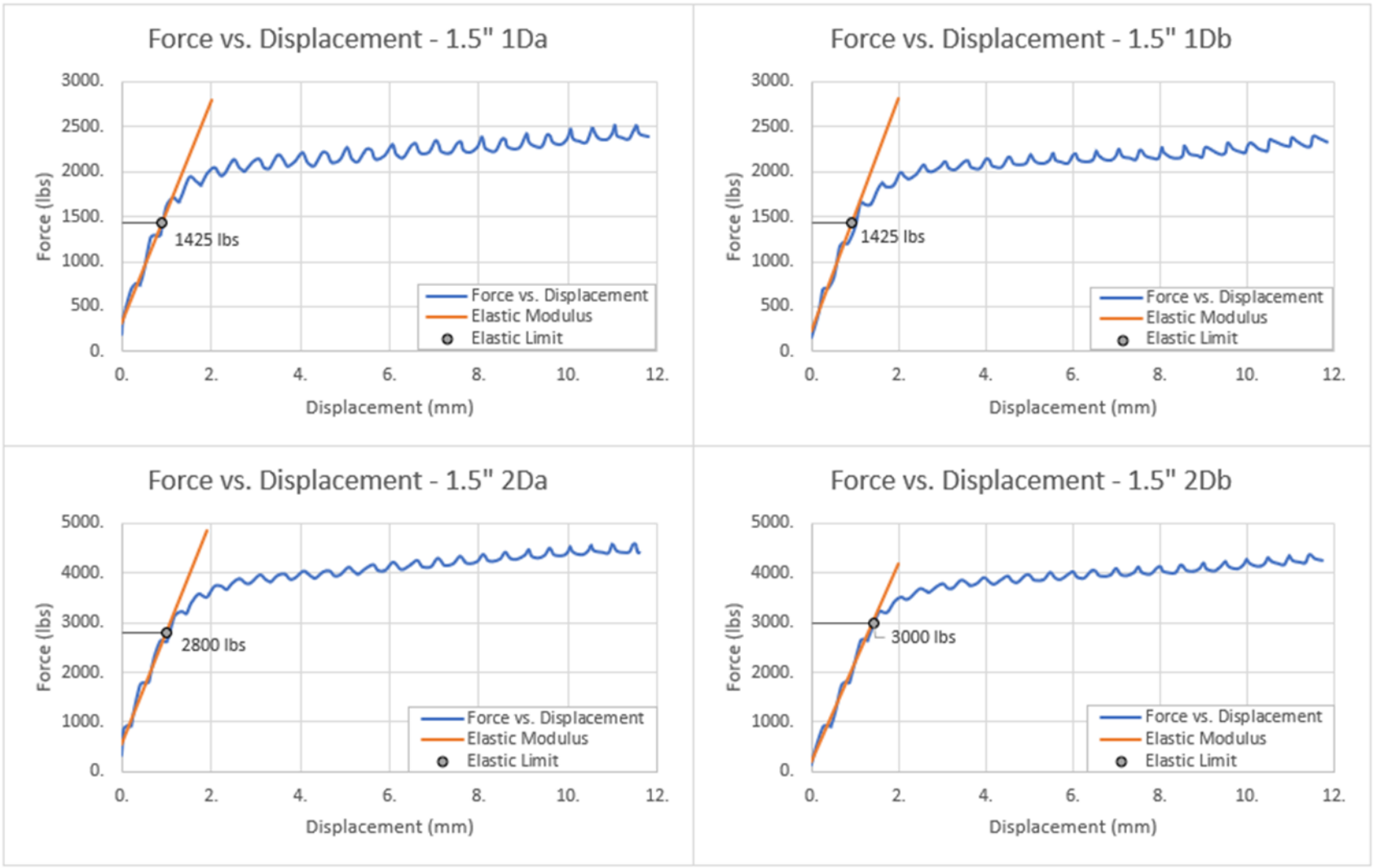

Figure 5.25: 1.5” force vs. displacement curves

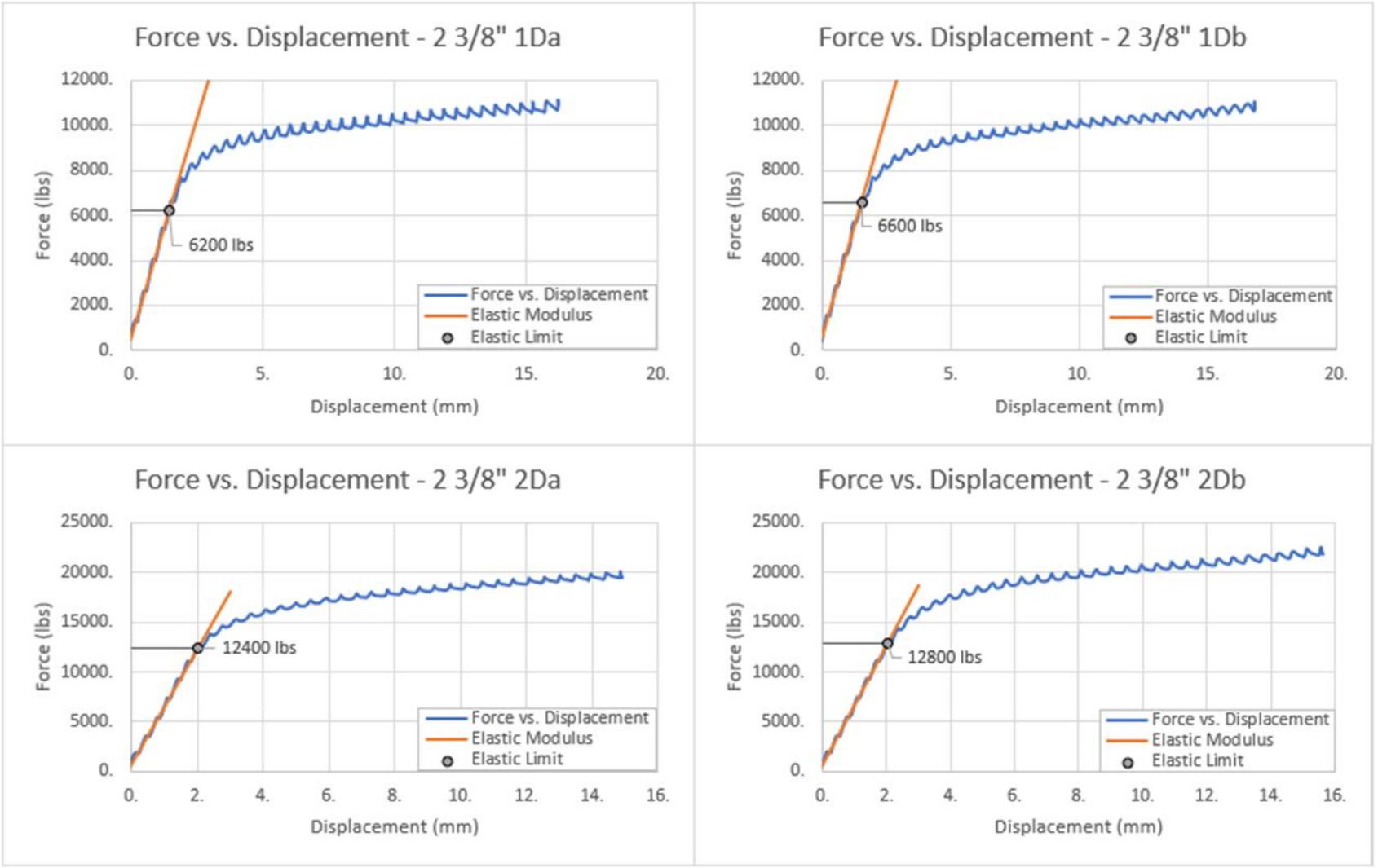

Figure 5.26: 2 3/8" force vs. displacement curves

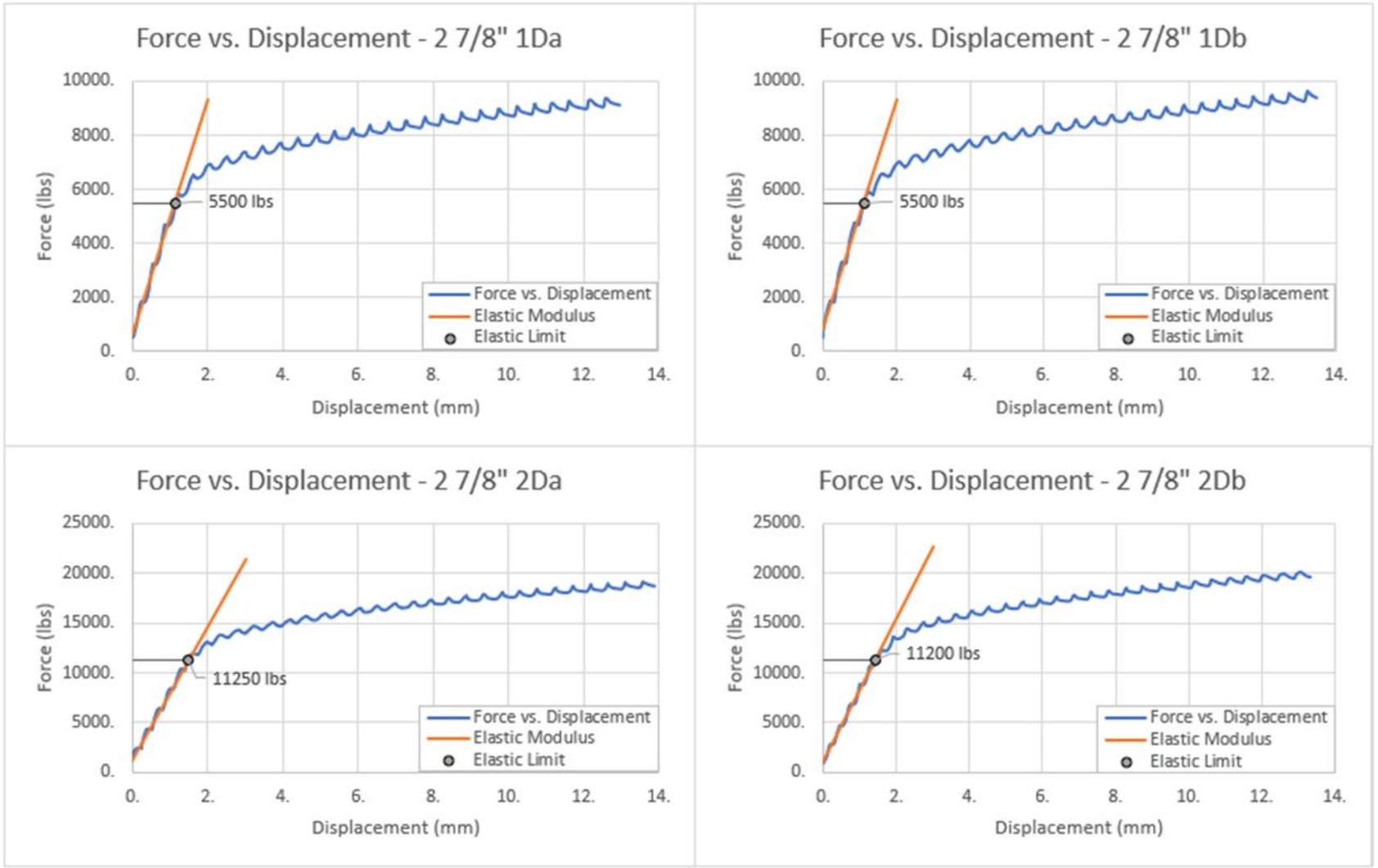

Figure 5.27: 2 7/8” force vs. displacement curves

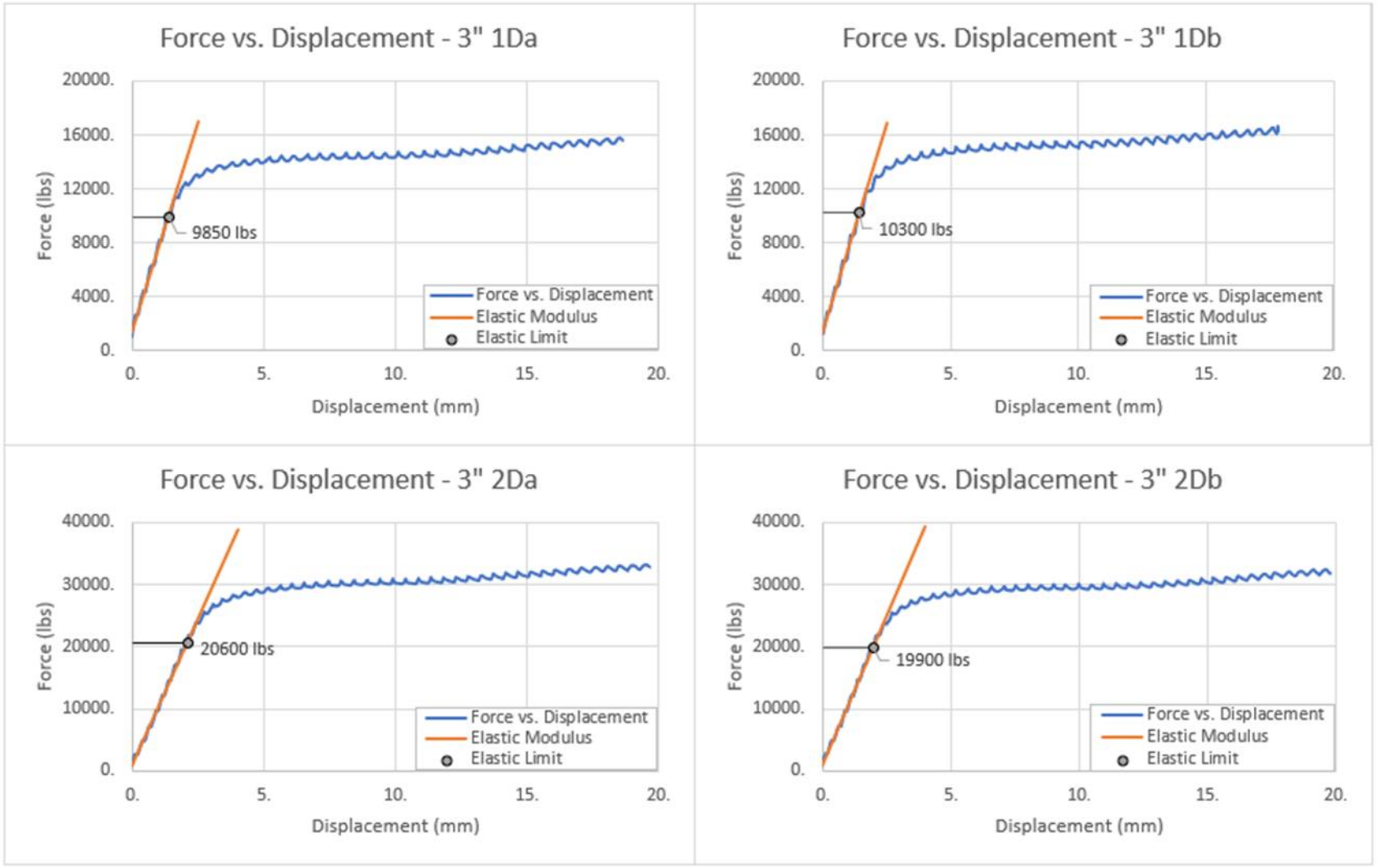

Figure 5.28: 3" force vs. displacement curves

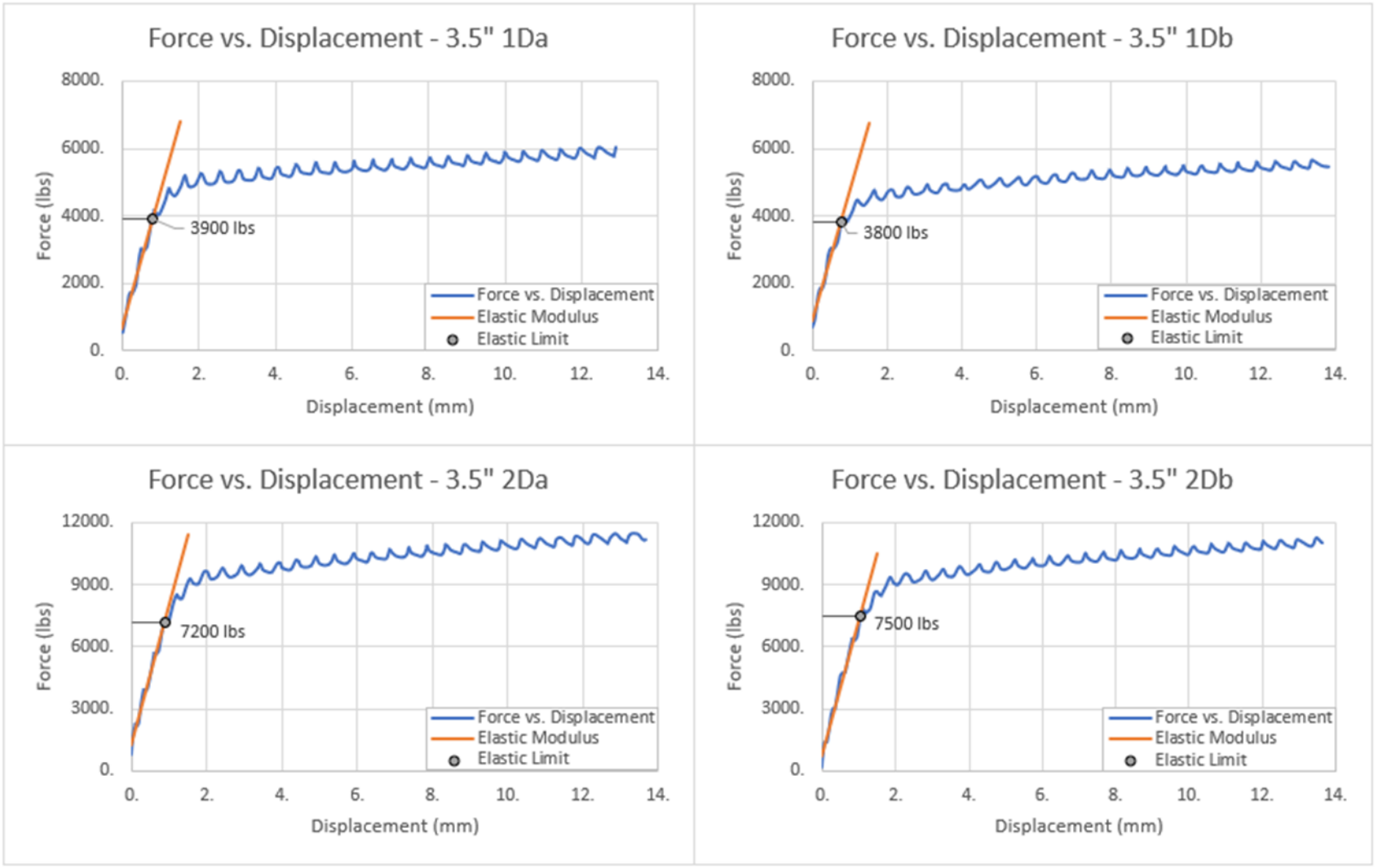

Figure 5.29: 3.5" force vs. displacement curves

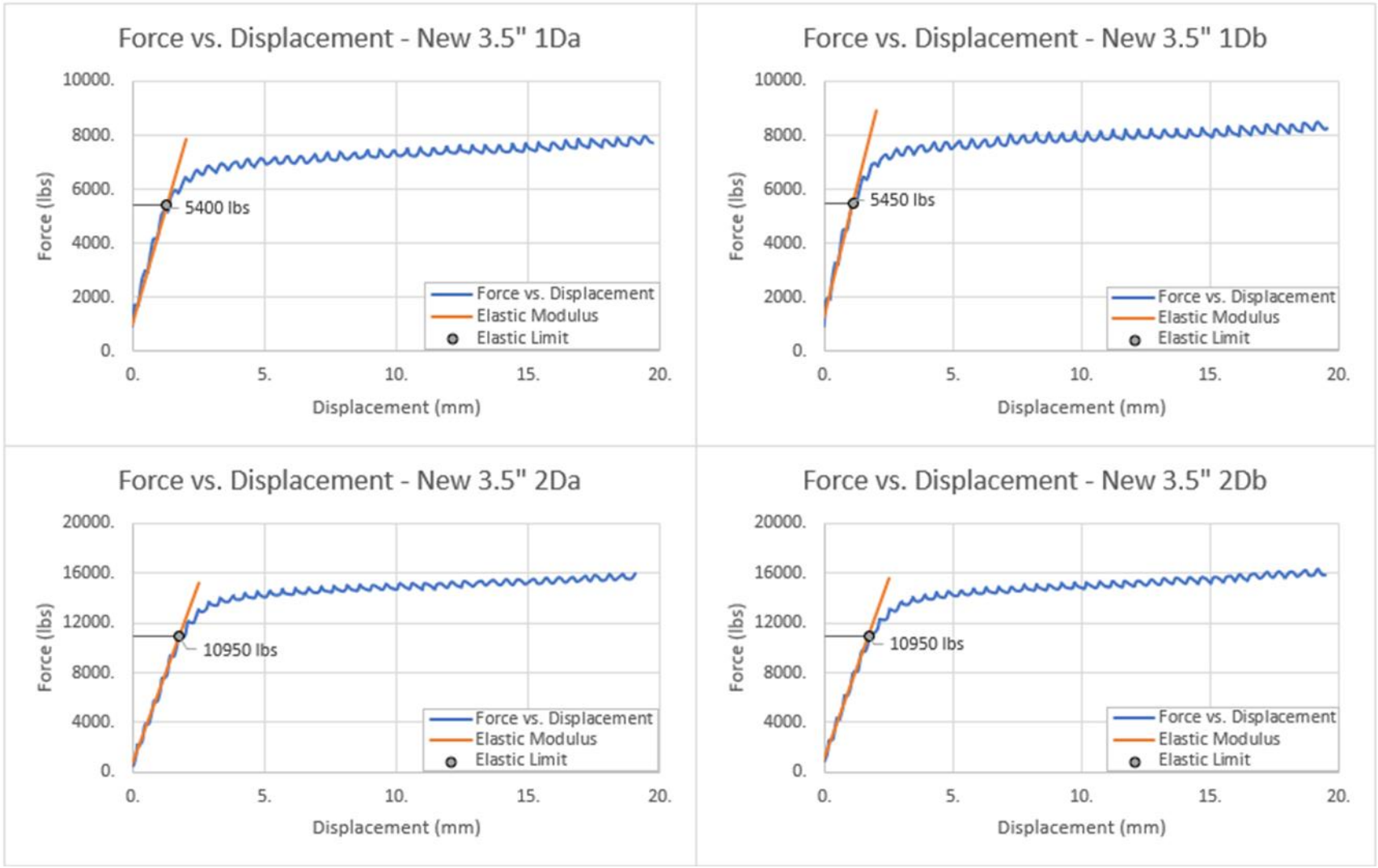

Figure 5.30: New 3.5" force vs. displacement curves

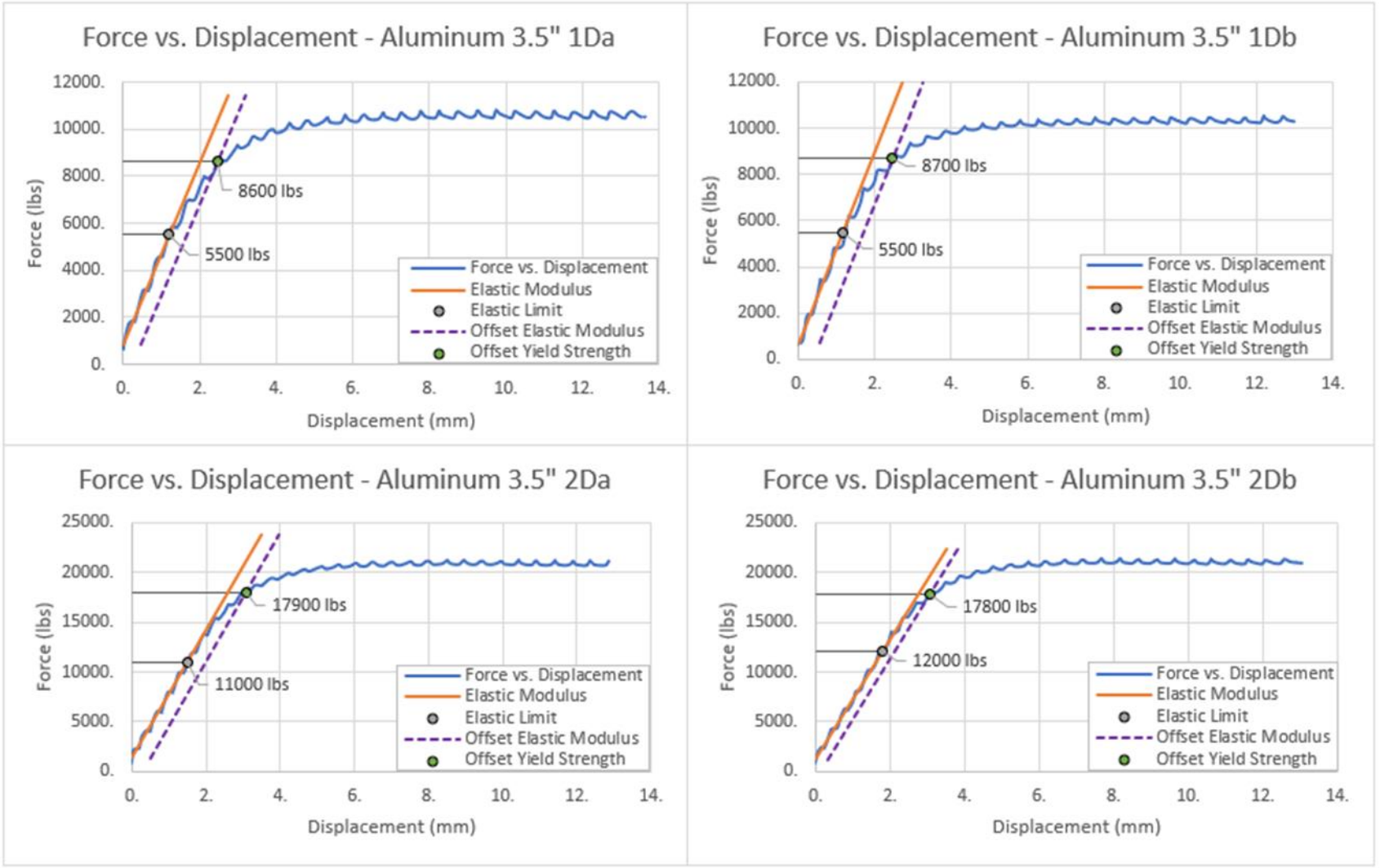

Figure 5.31: Aluminum 3.5” force vs. displacement curves

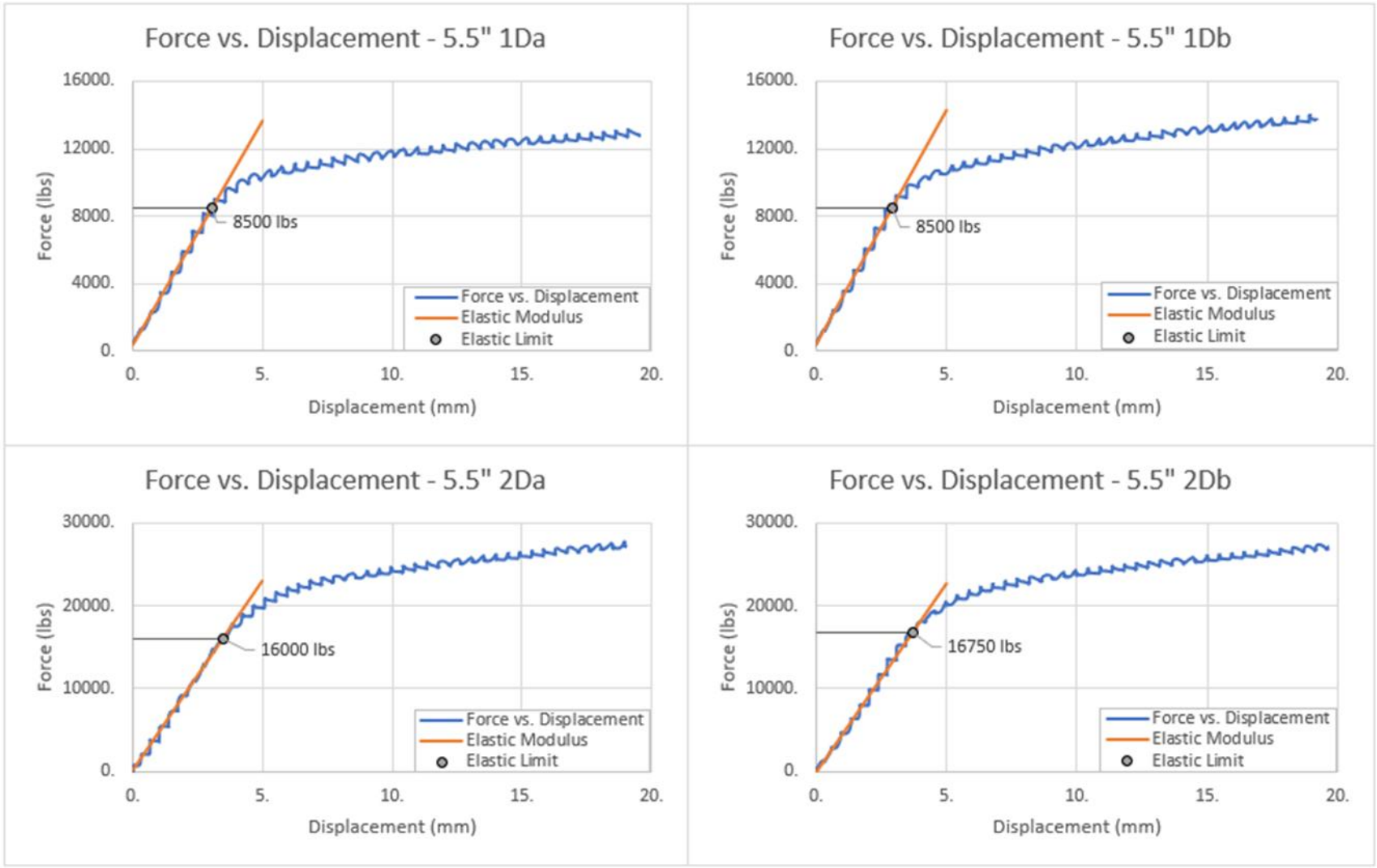

Figure 5.32: 5.5” force vs. displacement curves

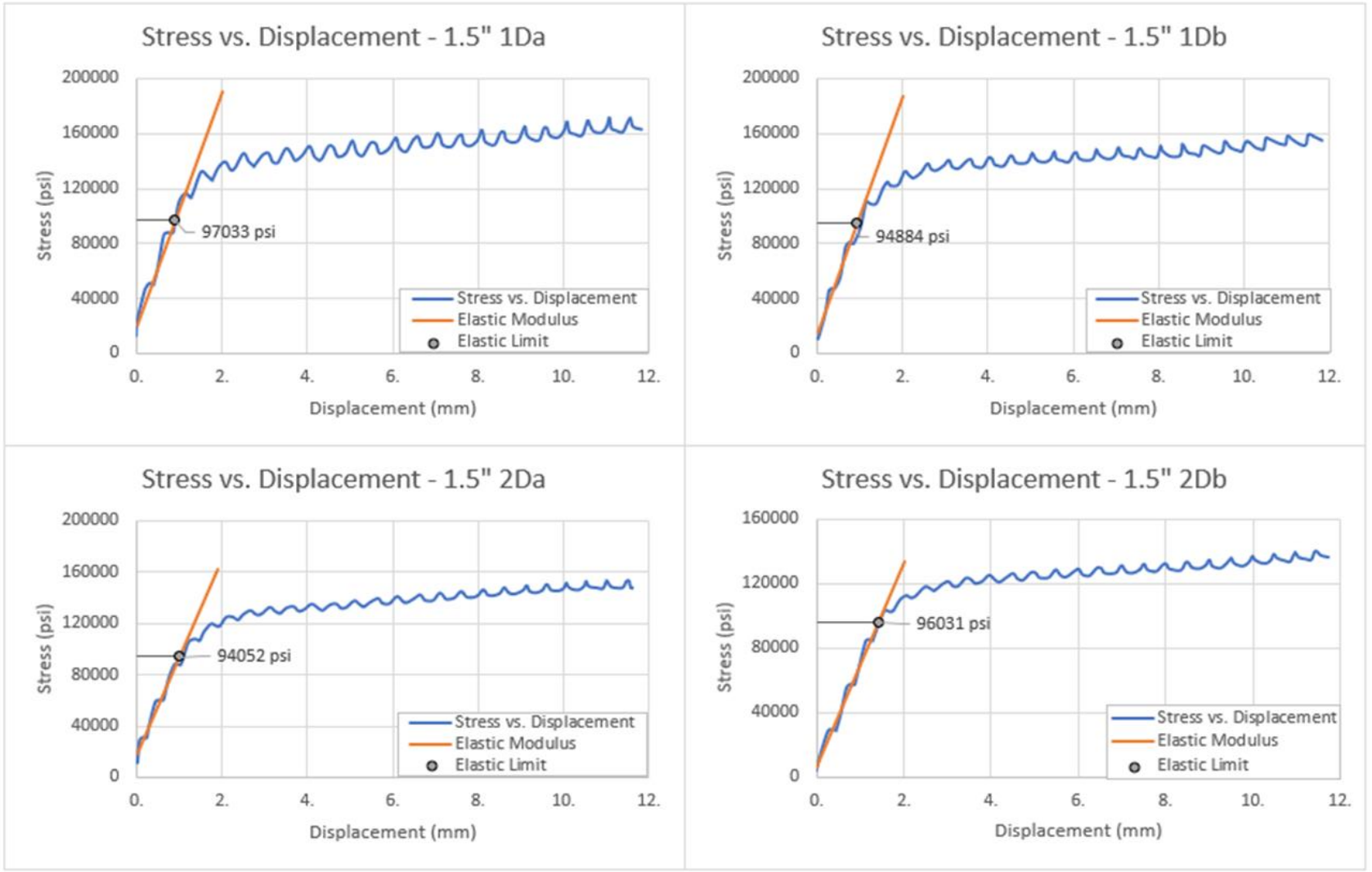

Figure 5.33: 1.5” stress vs. displacement curves

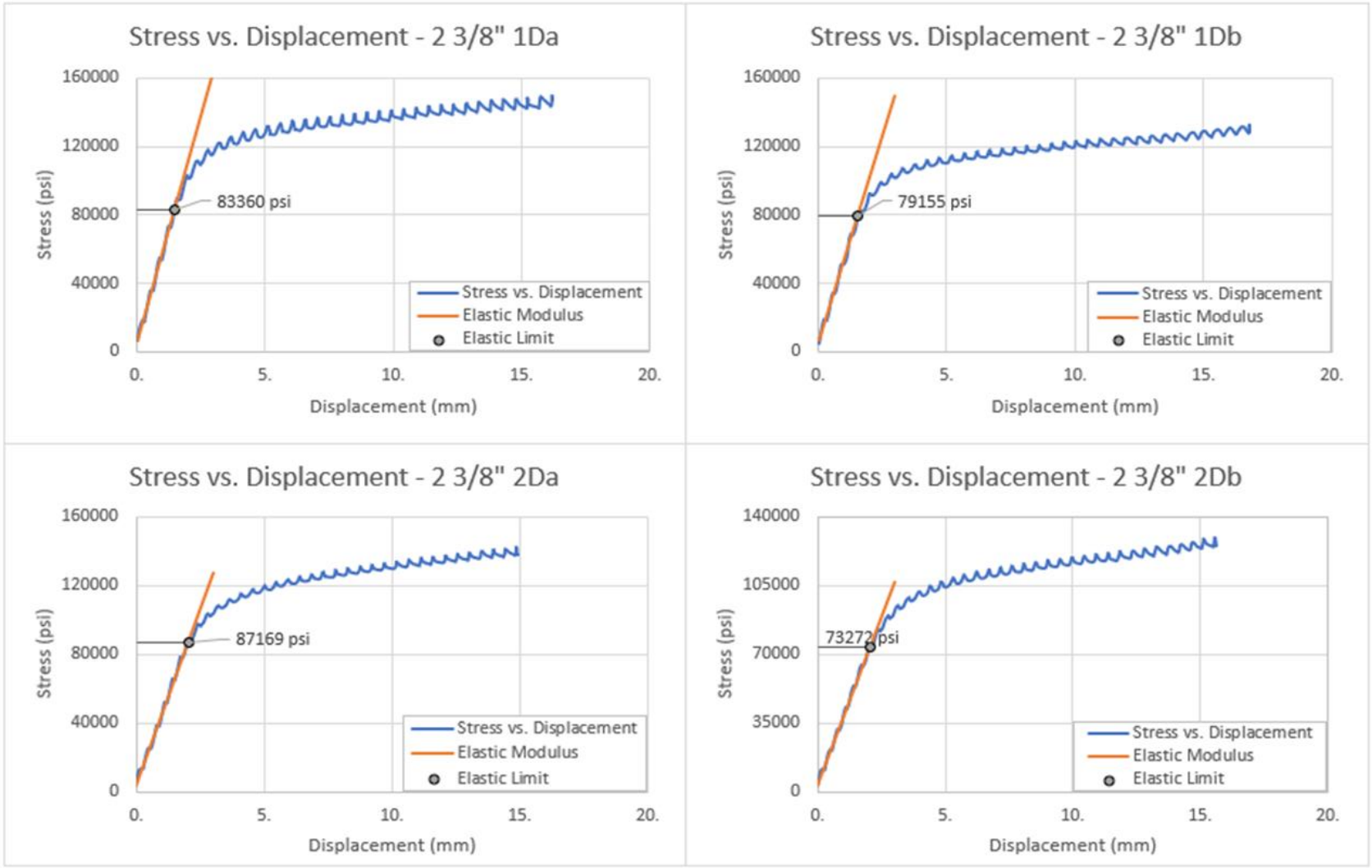

Figure 5.34: 2 3/8” stress vs. displacement curves

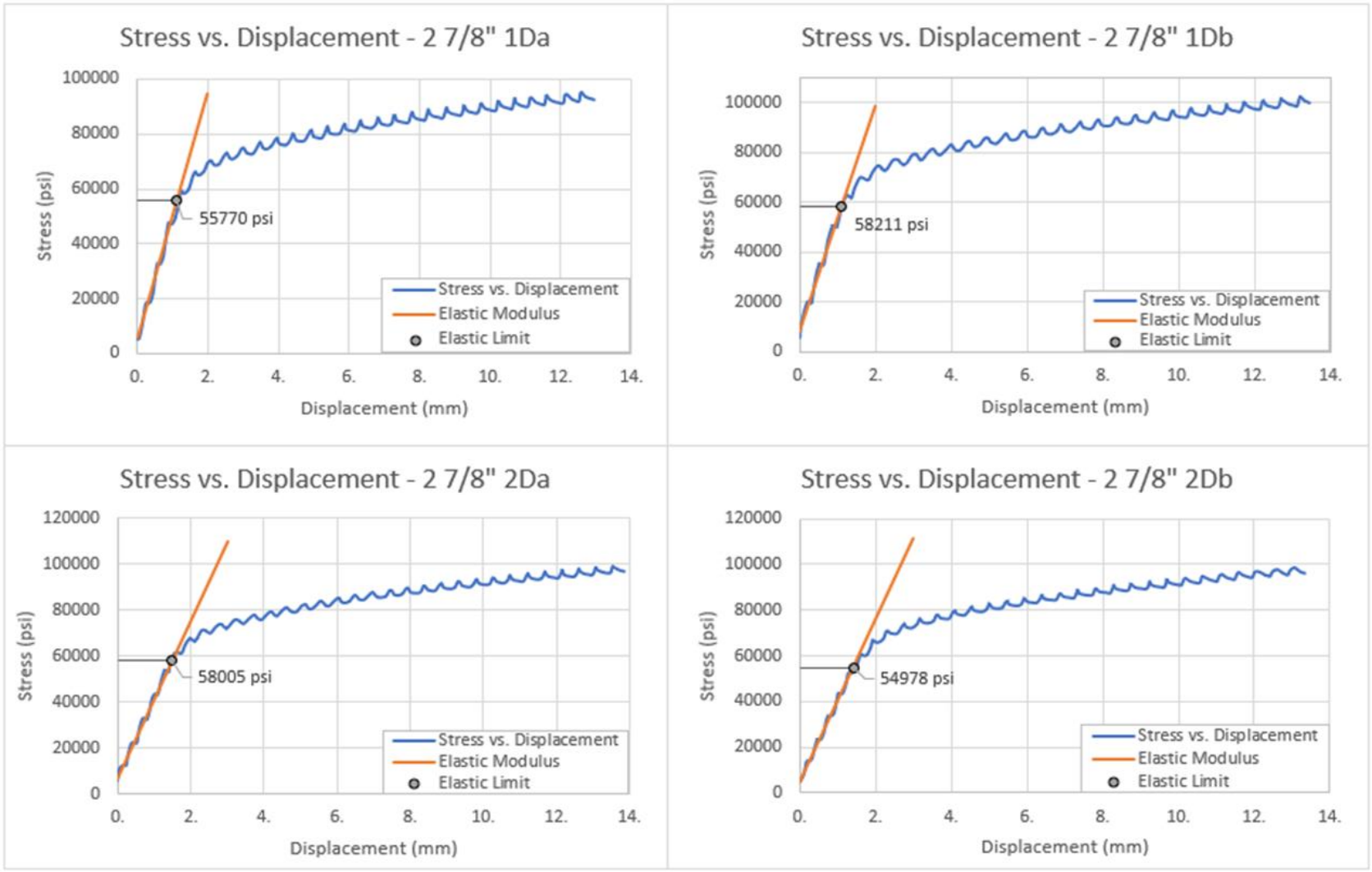

Figure 5.35: 2 7/8” stress vs. displacement curves

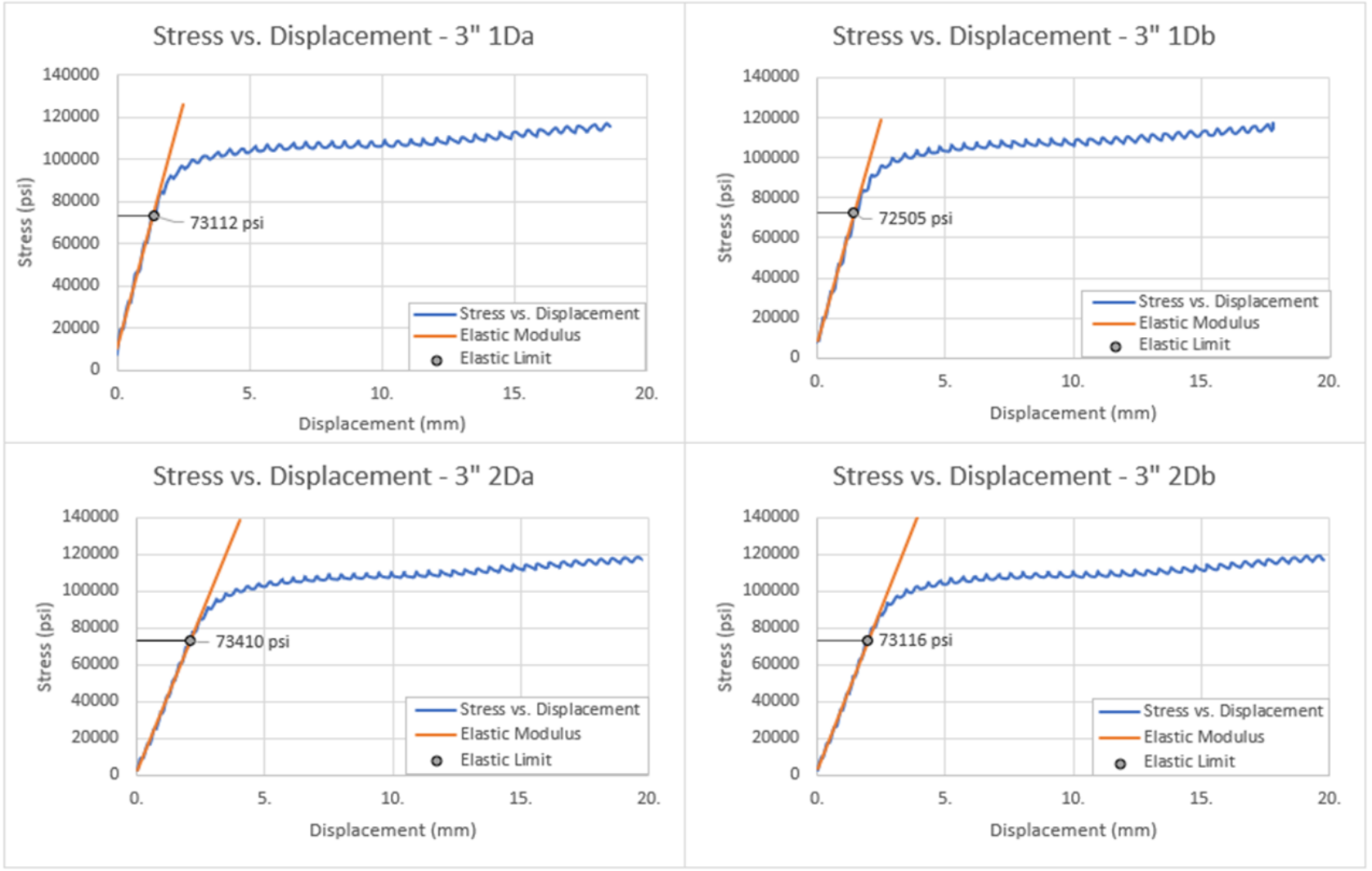

Figure 5.36: 3” stress vs. displacement curves

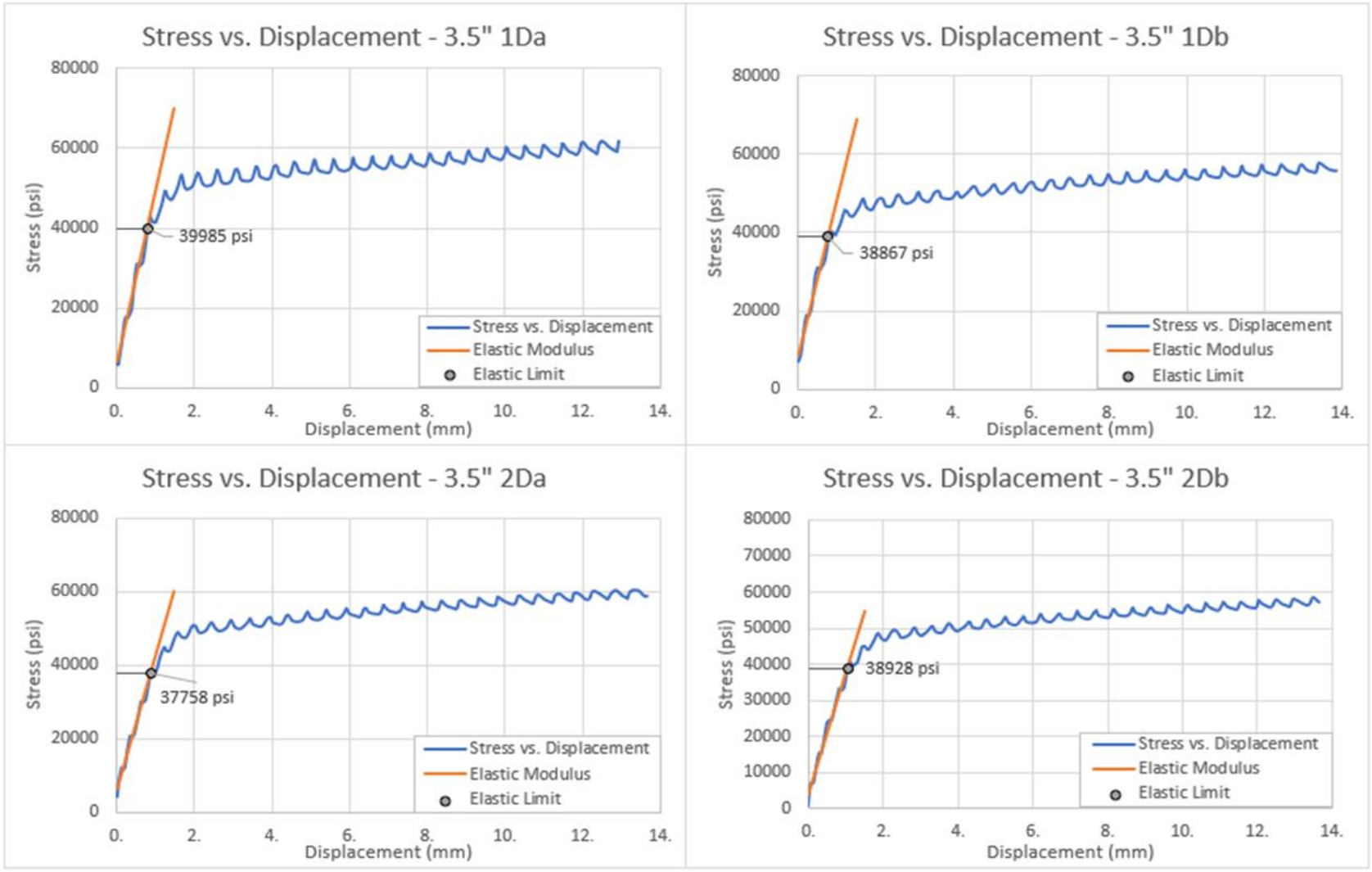

Figure 5.37: 3.5” stress vs. displacement curves

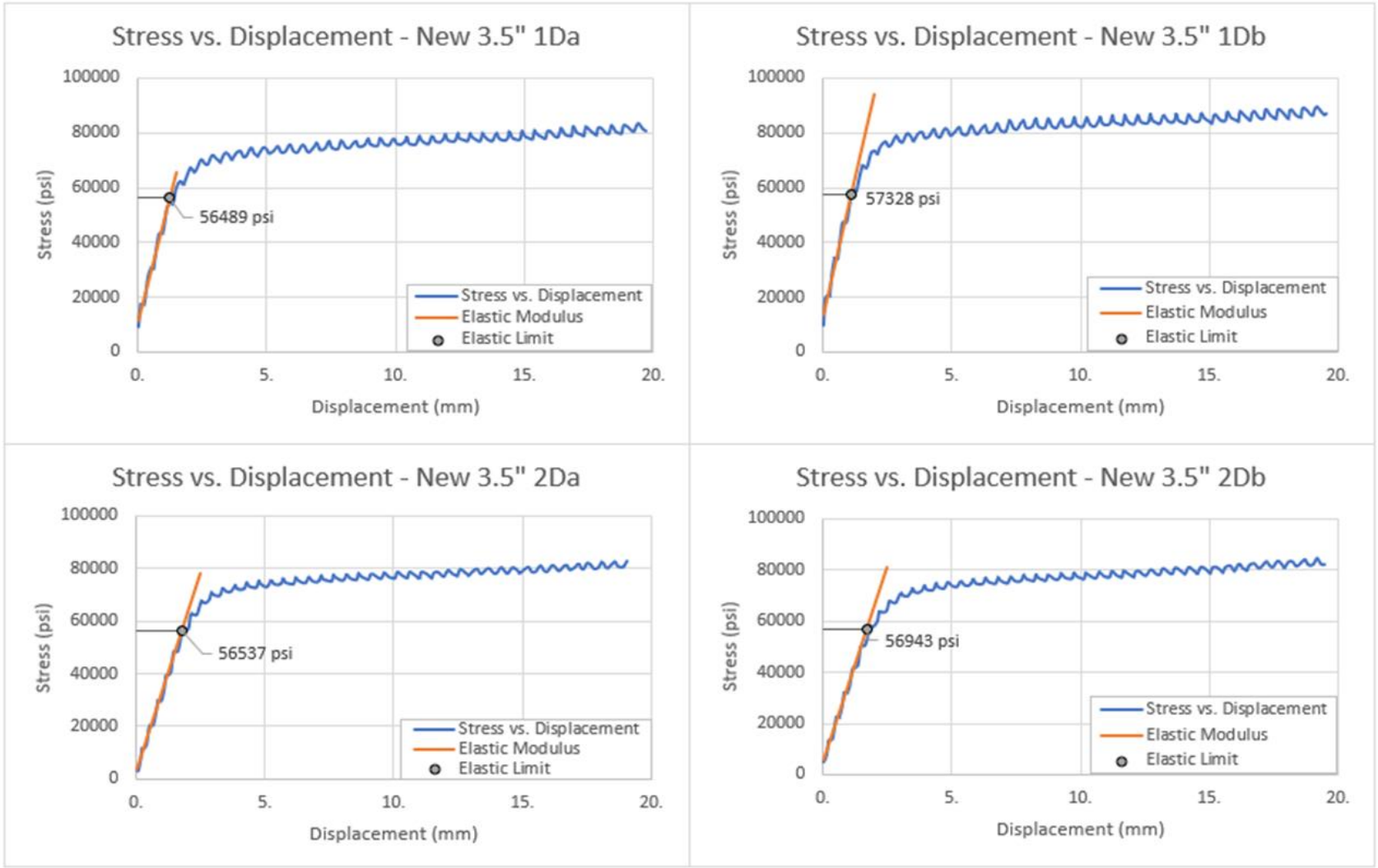

Figure 5.38: New 3.5” stress vs. displacement curves

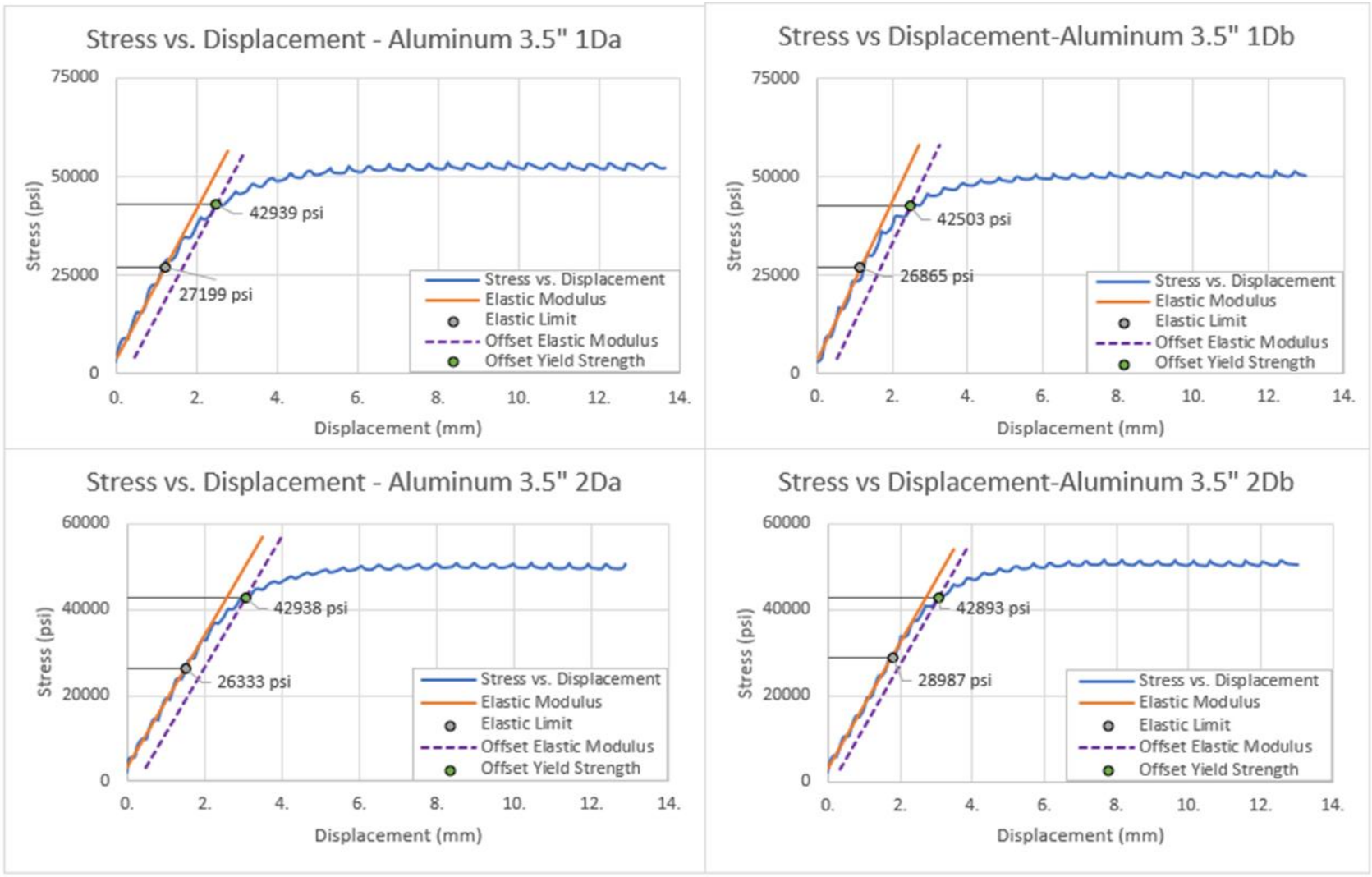

Figure 5.39: Aluminum 3.5” stress vs. displacement curves

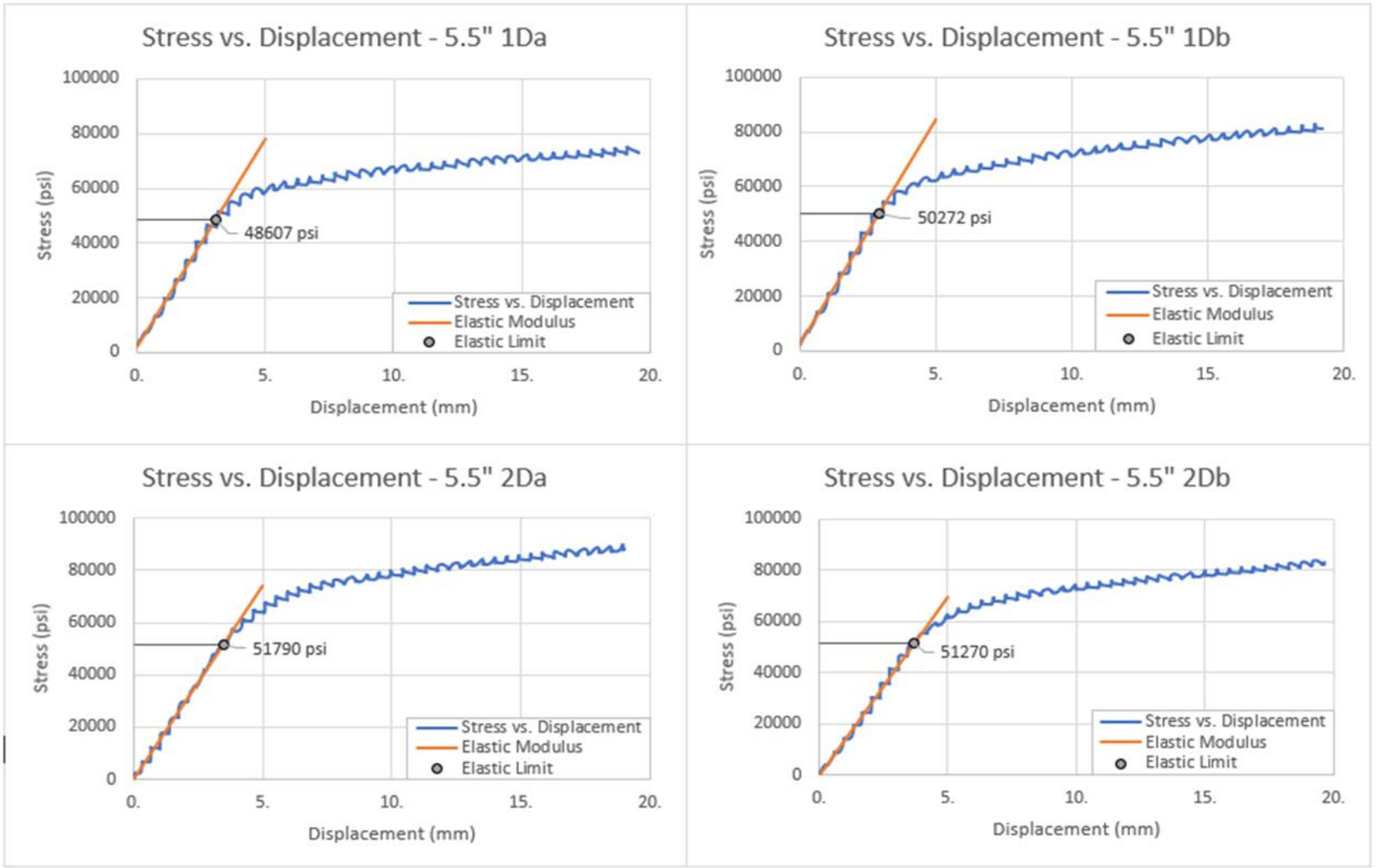

Figure 5.40: 5.5” stress vs. displacement curves

5.4.2 Comparing Empirical Method to Measured Data

Of the eight pipe samples tested, three had a mill test report (MTR) detailing the measured values for yield strength and tensile strength as measured by the manufacturer (1.5”, 3”, new 3.5”). Based on the measured strength values, API pipe grades were assigned to each sample according to the tables in API 5CT. The results of grading are found in **Table 5.4**:

Table 5.4: Resulting API grade for samples with MTR

Outer Diameter, in.	**MTR Measured Yield Strength, psi**	**MTR Measured Tensile Strength, psi**	**Resulting API Pipe Grade**
1.5”	98,000	121,000	T-95
3.0”	73,433	83,880	J-55
3.5”	56,120	65,250	H-40

Comparisons for the empirical yield strength versus API and MTR measured yield strength can be found in **Table 5.5**. The empirical yield strength is significantly greater than API yield strength in the low strength samples (J-55, H-40). However, when compared with the MTR values, the empirical data is quite accurate. Using the sample mean and sample standard deviation of all twelve Empirical/MTR numbers, a statistical confidence interval can be calculated for the true mean of Empirical/MTR values. Using a t-value distribution, it can be said with 99% confidence that the true mean value of Empirical/MTR lies in the interval [0.9957, 1.0045]. That is, it can be said with 99% confidence that the average difference between empirical yield strength values and MTR measured yield strength values is less than 0.5%.

Table 5.5: Empirical yield strength vs. API nominal yield strength vs. MTR yield strength

Outer Diameter, in.	API Grade	Specimen	API Nominal Yield Strength, psi	MTR Measured Yield Strength, psi	Empirical Yield Strength, psi	Empirical / API	Empirical / MTR
1.5"	T-95	1Da	95,000	98,000	98,768	1.040	1.008
		1Db	95,000	98,000	98,119	1.033	1.001
		2Da	95,000	98,000	96,898	1.020	0.989
		2Db	95,000	98,000	97,600	1.027	0.996
3.0"	J-55	1Da	55,000	73,433	73,494	1.336	1.001
		1Db	55,000	73,433	73,420	1.335	1.000
		2Da	55,000	73,433	73,268	1.332	0.998
		2Db	55,000	73,433	73,487	1.336	1.001
3.5"	H-40	1Da	40,000	56,120	56,032	1.401	0.998
		1Db	40,000	56,120	56,524	1.413	1.007
		2Da	40,000	56,120	56,195	1.405	1.001
		2Db	40,000	56,120	56,171	1.404	1.001

5.4.3 Nominal vs. Empirical Yield Strength for K&T Collapse

To further illustrate the effect of yield strength and the importance of using real yield strength in collapse resistance calculations, the three pipe samples with MTR test data were used to compare collapse resistance calculated with the Klever and Tamano equation for API nominal yield strength and the empirically measured yield strength. The results of this comparison appear in **Table 5.6**.

For the 1.5” sample with API pipe grade T-95, the D/t value is 18.08 which places the sample in the transition collapse mode when using the K&T equation. Given the nominal yield strength for this sample is 95ksi and the empirical yield strength is 98.768ksi, the difference in collapse pressures is only 3.1% This is due to the small difference in yield strength and the reduced effect of yield strength on transition zone collapse calculations.

The 3” sample with API grade J-55 has a D/t value of 11.88 which places it in the yield collapse region. The yield strength difference between nominal and empirical is significant for this sample, resulting in a 32.8% difference in collapse pressures. The large difference in yield strength and the significant effect of yield strength on yield collapse are the causes for this wide difference in collapse pressures.

The 3.5” sample has an API grade of H-40 and a D/t value of 16.28, which places it in the yield collapse region. Just like the previous sample, the significant difference between nominal and empirical yield strengths coupled with the heavy influence of yield strength on yield collapse results in a large 38.1% difference in calculated collapse pressures. The difference in collapse pressures for K&T with nominal yield strength and empirical yield strength can be seen in **Figures 5.41** to **5.43**.

Table 5.6: K&T collapse pressures for nominal and empirical yield strengths

Outer Diameter, in.	D/t	Collapse Mode (API, K&T)	API 5C3 Collapse, psi	K&T Collapse, psi (Nominal)	K&T Collapse, psi (Empirical)	K&T (Empirical) / API	K&T (Empirical) / K&T (Nominal)
1.5”	18.08	Plastic, Transition	6,935	8,278	8,532	1.230	1.031
3.0”	11.88	Yield, Yield	8,467	8,440	11,211	1.324	1.328
3.5”	16.28	Yield, Yield	4,607	4,479	6,185	1.343	1.381

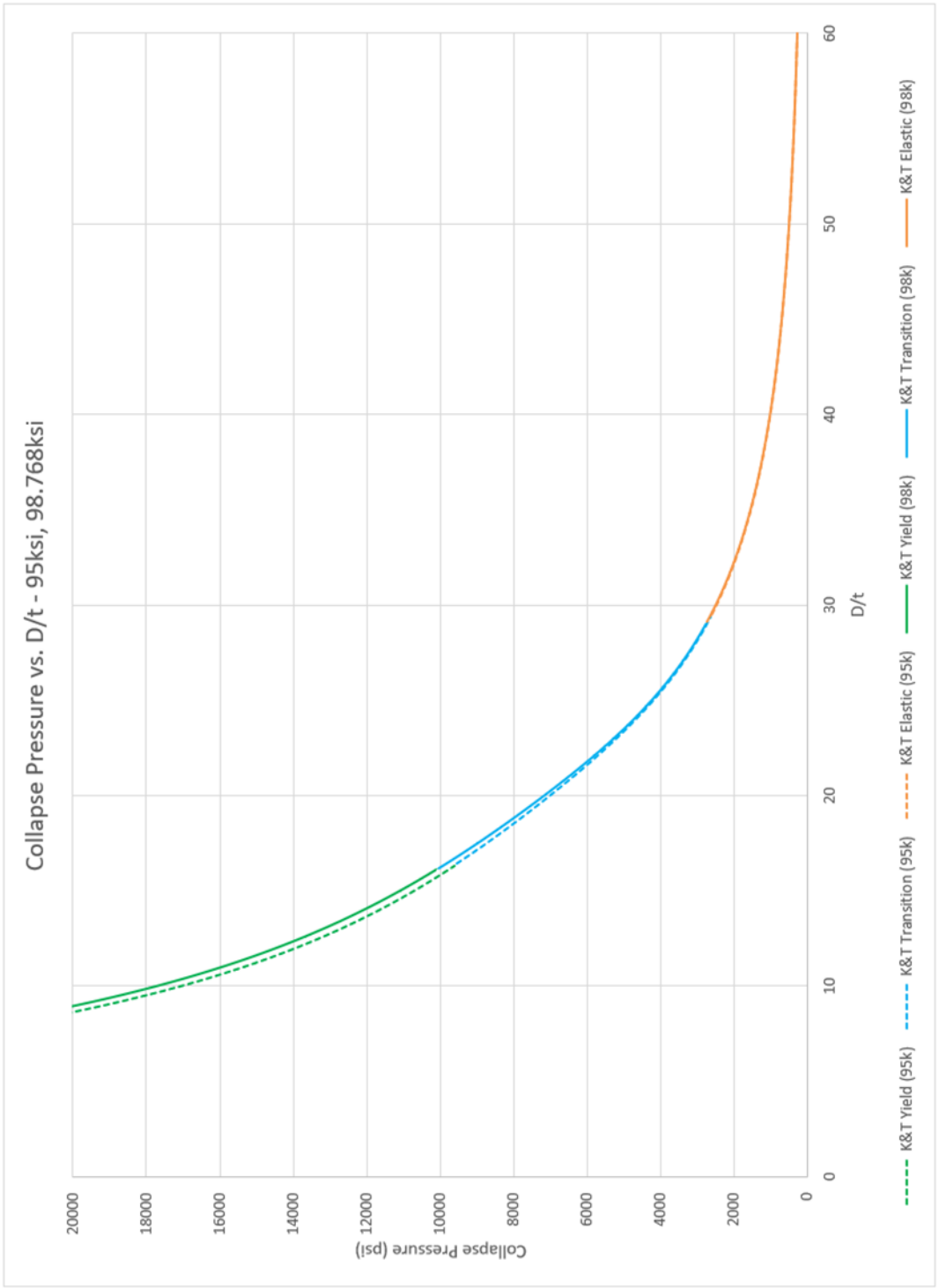

Figure 5.41: K&T collapse pressures for nominal and empirical yield strengths, grade T-95

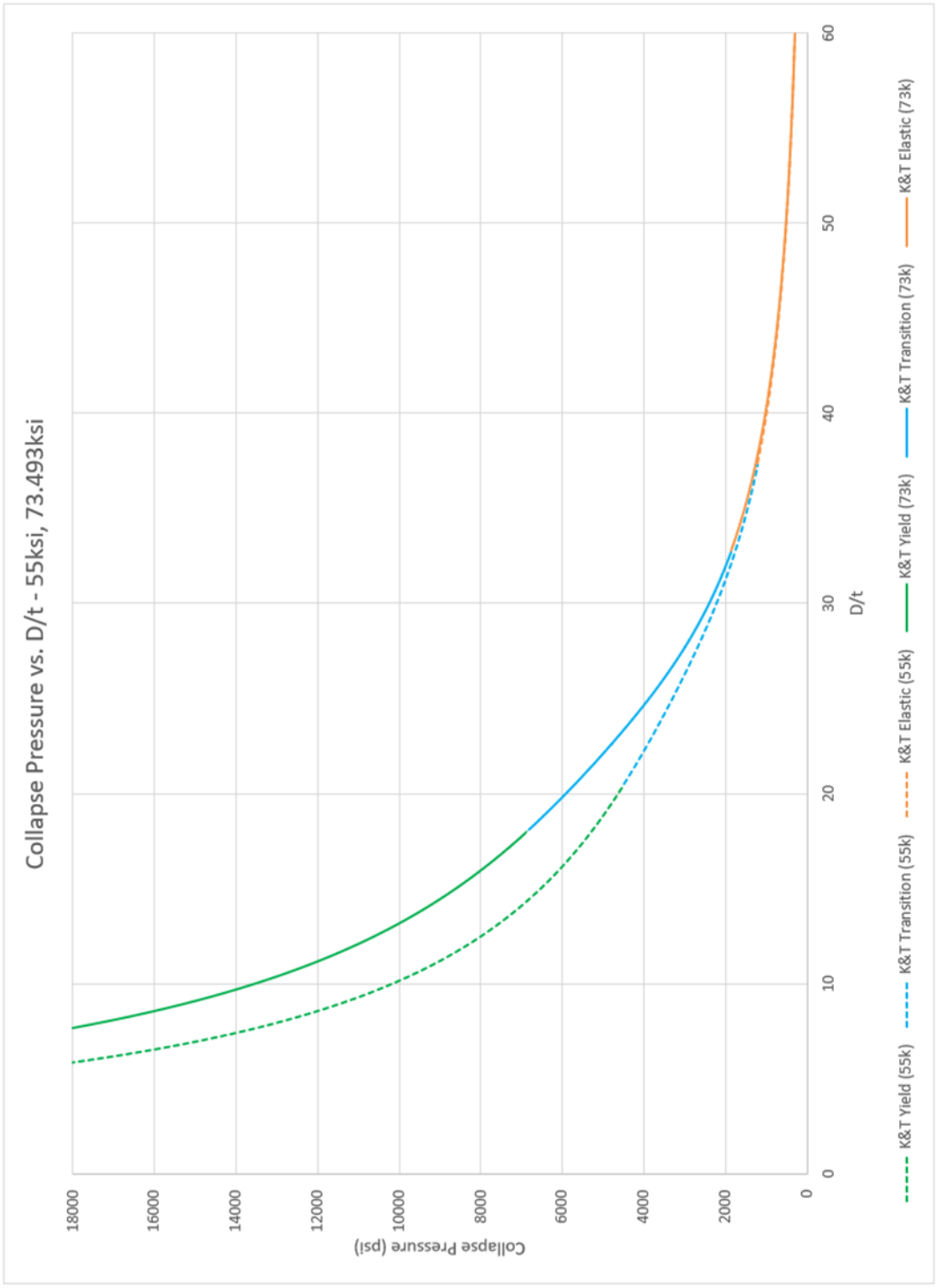

Figure 5.42: K&T collapse pressures for nominal and empirical yield strengths, grade J-55

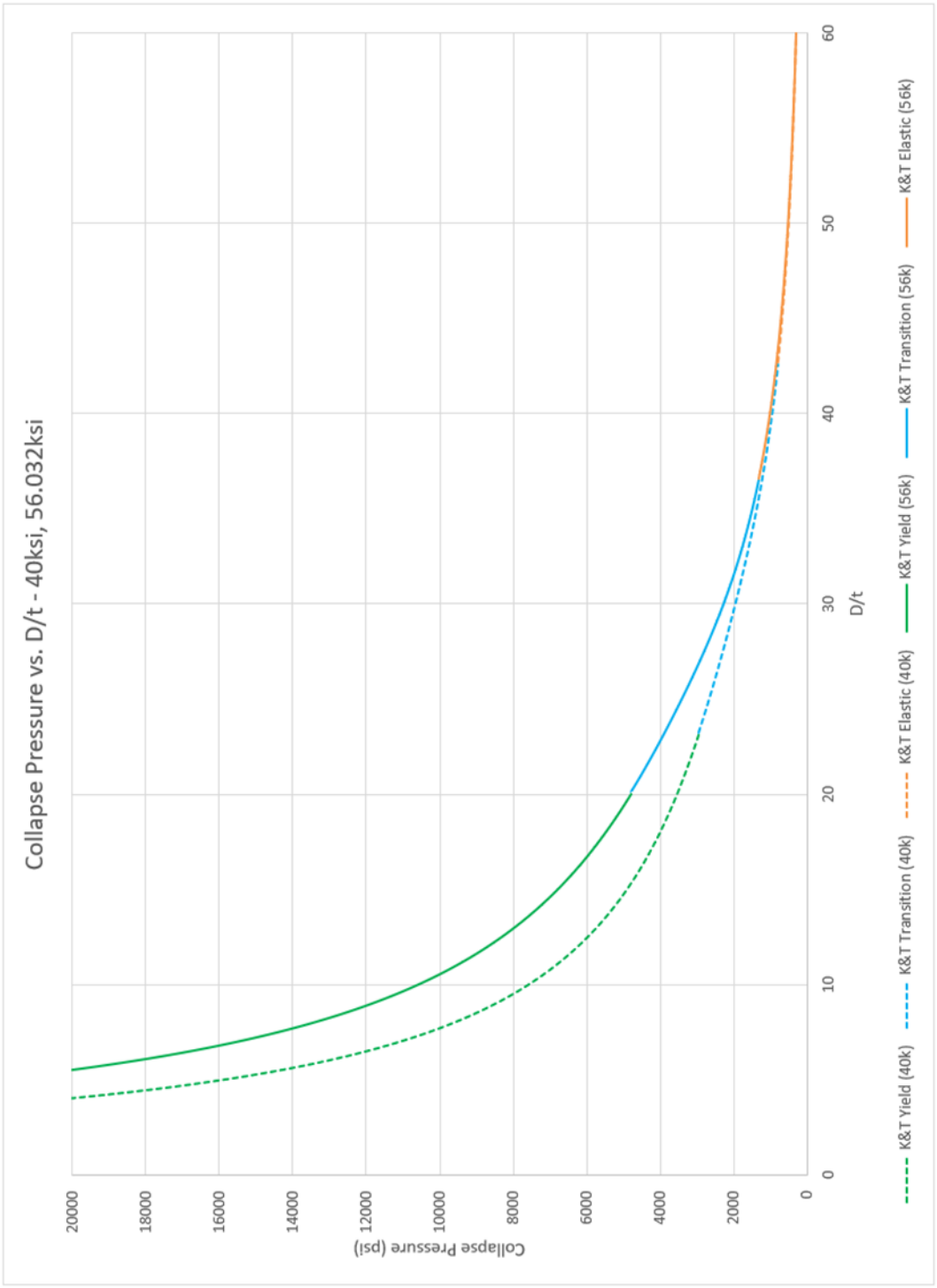

Figure 5.43: K&T collapse pressures for nominal and empirical yield strengths, grade H-40

For **Figure 5.41**, the difference in collapse pressures in minimal because of the small difference between nominal and measured yield strength. The greatest difference in collapse pressure is found in the yield region, with little to no difference in the elastic region. The difference in collapse pressure is greater in **Figure 5.42** due to the greater difference in nominal to measured yield strength. Like the previous figure, the greatest difference in collapse pressure is found in the yield region with a peak around D/t 15, and converges in the elastic region. **Figure 5.43** is much the same showing a peak difference in collapse pressure at D/t 12 in the yield region and converging in the elastic region.

Figure 5.44 provides a visual comparison of collapse pressure calculated with the API equations using nominal yield strength and the Klever and Tamano equation using the empirical yield strength. This is an extension of the values previously provided in **Table 5.5** and **Table 5.6**. The red line in the figure is the line of equality where the collapse values calculated by the two methods are equal. The points for each of the twelve specimens tested fall below this line indicating the values calculated with the empirical yield strength and Klever and Tamano equation is greater than the values calculated with nominal yield strength and API equations. The figure also lists the D/t value for each group of specimens. It can be seen that decreasing D/t increases the distance of the group away from the red line. This means that specimens with low D/t values with show a greater difference between API and K&T than specimens with high D/t values. This confirms the trend of the greatest difference in collapse values in the yield region, decreasing in the plastic region, and converging in the elastic region as seen in **Figures 5.41 – 5.43.**

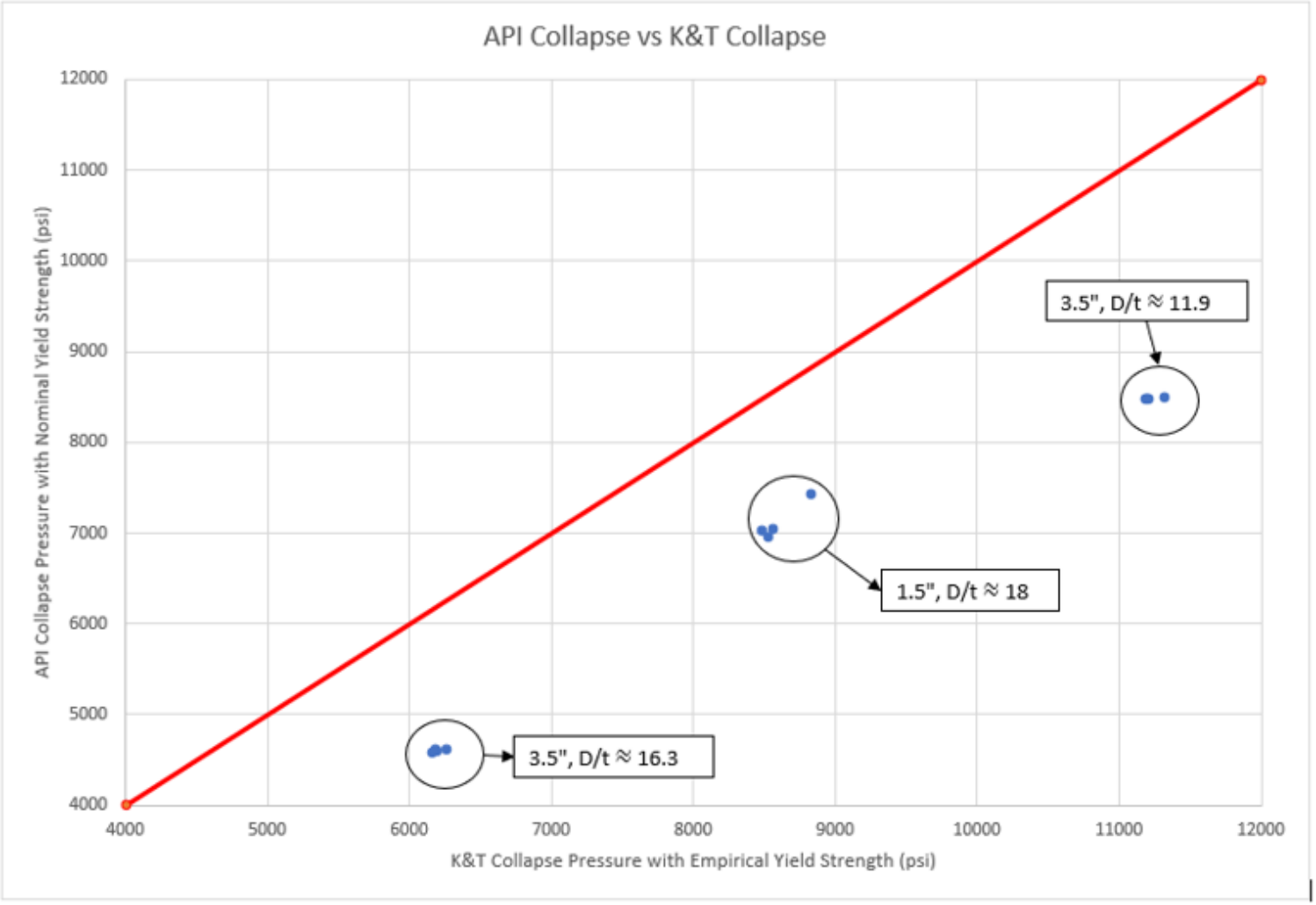

Figure 5.44: API collapse with nominal yield strength versus K&T collapse with empirical yield strength

Chapter 6: Conclusion and Recommendations

6.1 Conclusion

1. The Klever and Tamano equation uses decrement functions, bias factors, and curve fitting parameters to account for the imperfections in real pipe to create what was found to be the best-performing prediction of true collapse resistance
2. With a more accurate equation for predicting collapse resistance, knowing the real yield strength becomes the biggest factor in accurately calculating true collapse resistance
3. The high expense of pipe testing results in infrequent testing and uncertainty in the material properties of any given pipe
4. Proposed a completely new method to find the yield strength of pipe using a crush test
5. Developed an equation to convert input crush force to the yield strength of the pipe wall
6. Yield strength found by plotting a stress versus displacement graph and finding where the test curve deviates from the elastic deformation region
7. Comparing empirical yield strength obtained through crush tests to the yield strength supplied by the pipe manufacturer reveals remarkable accuracy in the new acquisition method
8. Applying newly acquired yield strength to the Klever and Tamano equation gives best estimate of true collapse resistance

6.2 Recommendations

1. The testing procedure may potentially be improved by increasing sampling frequency and developing a new method for operating the hydraulic ram. Hand pumping the hydraulic press creates a jagged curve which makes it difficult to accurately determine the force at the elastic limit. Applying the force in a more consistent manner could smooth out the data curve and aid in interpretation.
2. A new testing apparatus should be developed to apply tension or compression to the pipe being tested. This could reveal whether or not this method can be used to predict the collapse resistance calculated by the modified equations accounting for axial load.
3. Further testing with a larger sample size as well as more specimen lengths could help to refine the accuracy of this method.

Nomenclature

$a =$ Inner radius, in.

a = Moment arm (Bisplinghoff et al.)

A_e = Pipe outside cross-sectional area, in.^{2}

A_i = Pipe inside cross-sectional area, in.^{2}

A_Δ, B_Δ, C_Δ = Constants used in ovality correction

API = American Petroleum Institute

$b =$ Outer radius, in.

$c =$ Elastic collapse equation parameter

$c =$ Elasto-plastic boundary, in. (Kuriyama and Mimaki)

CRS = cold rotary straightened

$D =$ Outside diameter, in.

$DF =$ Design factor

$D_{avg} =$ Average measured outside diameter, in.

$D_{max} =$ Maximum measured outside diameter, in.

$D_{min} =$ Minimum measured outside diameter, in.

$\overline{D/t} =$ Normalized D/t

$(D/t)_{yp}$ = D/t intersection between yield strength collapse and plastic collapse

$(D/t)_{PT}$ = D/t intersection between plastic collapse and transition collapse

$(D/t)_{TE}$ = D/t intersection between transition collapse and elastic collapse

$ec = (t_{max} - t_{min})/t_{av} =$ eccentricity

$E =$ Young's modulus

E' = Factored Young's modulus

fac = Factor to allow curve fitting to real data

F = Axial load, lbs.

F_{eff} = Effective axial load, lbs.

$F(\Delta)$ = Ovality correction function

$|F|$ = Force producing the moment about point p

$|F_1|$ = ½ the force applied to the specimen from the press at the elastic limit, lbs.

$|F_2|$ = Resultant force at the interior and exterior surface of the pipe wall, lbs.

h_n = Correction for the shape of the stress/strain curve

H = Decrement function, $f(\xi, ov, ec, rs)$

H_e = Elastic decrement function, $f(\xi, ov, sh, ec, rs)$

H_t = Transition decrement function, $f(\xi, ov, sh, ec, rs)$

H_y = Yield decrement function, $f(\xi, ov, sh, ec, rs)$

HRS = hot rotary straightened

I = Geometrical moment of inertia

k_e = Elastic bias factor

k_y = Yield bias factor

l = length of test specimen, in.

$|M|$ = Magnitude of the moment of F about point p

MTR = Mill Test Report

$ov = (D_{max} - D_{min})/D_{av}$ = ovality

p_{API} = P_{yp}, psi

$p_{c\,des}$ = Design collapse pressure, psi

$p_{c\,ult}$ = Ultimate collapse pressure, psi

p_e = External pressure, psi

p_e^{ycT} = Tamano yield collapse pressure (external pressure only), psi

p_{fy} = Through-wall yield collapse, psi

p_i = Internal pressure, psi

p_{iy} = Initial yield collapse, psi

p_{Tamano} = p_e^{ycT}, psi

$p_{Tamano,fac=1.5}$ = P_e^{yc}, psi

p_{Tresca}^{yc} = Exact through-wall Tresca yield pressure, psi

P_c = Elasto-plastic collapse pressure, psi

P_d = Design equation collapse pressure, psi

P_e = Theoretical elastic collapse pressure, psi

P_e^{yc} = Yield collapse pressure (external pressure only), psi

P_{eo} = Elastic ovalization pressure, psi

P_{eq} = Equivalent external pressure, psi

P_E = Minimum elastic collapse pressure, psi

P_{Eavg} = Average elastic collapse pressure, psi

P_{Eb} = Elastic buckling collapse pressure, psi

P_o = External pressure, psi

P_p = Minimum plastic collapse pressure, psi

P_{pavg} = Average plastic collapse pressure, psi

P_{pc} = Plastic collapse pressure, psi

P_R = Resistance equation collapse pressure, psi

P_T = Minimum plastic/elastic transition collapse pressure, psi

P_y = External Pressure, psi

P_{yp} = Pressure associated with initial yield at the interior wall of the tubular, psi

P_Y = Minimum yield strength collapse pressure, psi

$Q\&T$ = quenched and tempered

r_n = Value of D/t where $P_e = P_{yp}$

$rs = \sigma_{res}/\sigma_y$ = residual stress over yield stress

R = Midwall pipe radius, in.

R_e = outside radius, in.

R_i = inside radius, in.

sh = Parameter characterizing stress/strain-curve shape

S_a = Axial stress, psi

S_i = Combined loading parameter in yield collapse

t = Wall thickness, in.

u = Amplitude of ovality at pressure Peo

u_o = Amplitude of original ovality

X = Collapse characterization parameter

Y = Yield strength, psi

Y_p = Minimum yield strength, psi

Y_{pa} = Yield strength of axial stress equivalent grade, psi

$$Z = -\frac{2}{\sqrt{3}} Y \sin(\frac{\pi}{6} + \theta_c)$$

Δ = Ovality

Δp = Pressure differential = $p_e - p_i$, psi

Δp^c = Collapse pressure differential, psi

Δp^{ec} = Elastic collapse pressure differential, psi

Δp_{ec} = Elastic collapse pressure differential (for c = -1+t/D), psi

Δp_{thin}^{ec} = Elastic collapse pressure differential for thin-walled pipe, psi

Δp^{yc} = Yield collapse pressure differential, psi

Δp_{thin}^{yc} = Yield collapse pressure differential for thin-walled pipe, psi

Δp^{yM} = von Mises yield pressure differential, psi

$\Delta p_{yTamano}$ = Yield collapse pressure differential with axial stress, psi

$\left|\frac{d\,\Delta p^c}{d\,p_i}\right|$ = Collapse pressure differential gradient

η_e = variable whose value results in $G = 0$

$\theta_c =$ Auxiliary angle for von Mises yield criterion

$\nu =$ Poisson's ratio

ξ = Characteristic pipe geometry parameter

σ_a = Average axial stress, psi

σ_e = Equivalent yield strength, psi

σ_y = Yield stress, psi

σ_y' = Factored yield stress, psi

References

Abbassian, F., and Parfitt, S.H.L. 1995. Collapse and Post Collapse Behaviour of Tubulars: a simple approach. Paper SPE 29458 presented at the SPE Production Operations Symposium, Oklahoma City, Oklahoma, 2-4 April.

Adams, A.J., Warren, A.V.R., and Masson, P.C. 1998. On the Development of Reliability-Based Design Rules for Casing Collapse. Paper SPE 48331 presented at the SPE Applied Technology Workshop on Risk Based Design of Well Casing and Tubing, The Woodlands, Texas, 7-8 May.

American Petroleum Institute. *Bull. 5C2.* 1999. Bulletin on Performance Properties of Casing, Tubing, and Drill Pipe. 21st edition. Washington, DC: API (October).

American Petroleum Institute. *Bull. 5C3.* 1994. Bulletin on Formulas and Calculations for Casing, Tubing, Drill Pipe, and Line Pipe Properties. Sixth edition. Washington, DC: API (October).

American Petroleum Institute. *Spec. 5CT.* 2006. Specification for Casing and Tubing. Eighth edition. Washington, DC: API (January).

Bisplinghoff, R.L., Mar, J.W., and Pian, T.H.H. 1990. *Statics of Deformable Solids.* Dover edition. 58-61. Mineola, New York: Dover Publications, Inc.

Bourgoyne Jr., A.T., Millheim, K.K., Chenevert, M.E., and Young Jr., F.S. 1986. *Applied Drilling Engineering.* SPE Textbook Series Vol. 2. 300-324. Richardson, Texas: Society of Petroleum Engineers.

Brechan, B., Kornberg, E., Sangesland, S., and Dale, S.E. 2018. Well Integrity Model – Klever & Tamano Collapse. Paper SPE 189395 presented at the SPE/IADC Middle East Drilling Technology Conference and Exhibition, Abu Dhabi, UAE, 29-31 January.

Clinedinst, W.O. 1939. A Rational Expression for the Critical Collapsing Pressure of Pipe under External Pressure. Presented at the API Twentieth Annual Meeting, Chicago, Illinois, 16 November.

Greenip, J.F. 2016. Collapse Strength of Casing Subjected to Combined Load. Paper SPE 178806 presented at the IADC/SPE Drilling Conference and Exhibition, Fort Worth, Texas, 1-3 March.

Ju, G.T., Power, T.L., and Tallin, A.G. 1998. A Reliability Approach to the Design of OCTG Tubulars Against Collapse. Paper SPE 48332 presented at the SPE Applied Technology Workshop on Risk Based Design of Well Casing and Tubing, The Woodlands, Texas, 7-8 May.

Klever, F.J. and Tamano, T. 2006. A New OCTG Strength Equation for Collapse Under Combined Loads. Paper SPE 90904 presented at 2004 SPE Annual Technical Conference and Exhibition, Houston, Texas, 26-29 September.

Kuriyama, Y. and Mimaki, T. 1994. A New Formula for Elasto-Plastic Collapse Strength of Thick-Walled Casing. Paper SPE 28327 presented at the SPE 69th Annual Technical Conference and Exhibition, New Orleans, Louisiana, 25-28 September.

Staelens, S., Galle, T., De Waele, W., and De Baets, P. 2012. Analysis of API 5C3 Failure Prediction Formulae for Casing and Tubing. *Sustainable Construction and Design* 3:80-88. Ghent, Belgium: Ghent University, Laboratory Soete.

Sun, Y. 2010. Equation for Calculation Casing Through-Wall Yield Collapse Pressure. Paper SPE 126580 provided to SPE for distribution and possible publication in an SPE Journal.

Tamano, T., Mimaki, T., and Yanagimoto, S. 1983. A New Empirical Formula for Collapse Resistance of Commercial Casing. Transactions of the ASME, *Journal of Energy Resource Technology:* 489-495.

Teodoriu, C., and Holzman, J. 2010. Pushing to the Limits: How Oil Country Tubular Goods Evolution Affects the Testing Facilities Requirements? *Underground Storage of CO2 and Energy.* 353-359. Boca Raton, Florida: CRC Press.

Timoshenko, S. 1936. *Theory of Elastic Stability.* First edition. 222-224. Columbus, Ohio: McGraw-Hill.